IMPACT OF HILLSLOPE THERMOKARST ON THE NEARSHORE CARBON BUDGET ALONG THE YUKON COAST, CANADA

Justine Lucille Ramage

Thesis presented for the degree of
Doctorate of Natural Sciences
(doctor rerum naturalium)
In the field of "Geomorphology"

Cumulative Dissertation
Presented at the Faculty of Science
Institute of Earth- and Environmental Science
University of Potsdam

prepared at

The Alfred-Wegener Institute
Helmholtz Centre for Polar- and Marine Research
Potsdam, Germany

Place and date of the defense: University of Potsdam, 2018.10.11
Main Supervisor: Prof. Hugues Lantuit, University of Potsdam
Second Supervisor: Prof. Peter Kuhry, Stockholm University
Mentor: Dr. Anne Morgenstern, Alfred Wegener Institute

Published online at the
Institutional Repository of the University of Potsdam:
URN urn:nbn:de:kobv:517-opus4-421867
https://nbn-resolving.org/urn:nbn:de:kobv:517-opus4-421867

En mémoire de Marie-Laure.

Is this the real life?
Is this just fantasy?
Caught in a landslide
No escape from reality

Bohemian Rhapsody, Queen
Freddie Mercury, 1975

Acknowledgements

The adventure started on a post-it: "I am looking for a PhD position! If you have something in mind related to permafrost please contact me". I would like to thank my supervisors; Hugues Lantuit and Anne Morgenstern for their sober answer "Talk to us after session 525B" and the exciting meeting that followed. Thank you for your trust, patience, endless support and scientific discussions during the past years.
I would also like to thank the members of my PhD committee, Peter Kuhry and Guido Grosse, who followed the progress of this project, and contributed to shaping it with their advice and comments.

This PhD would not have been possible without the help of the Swedish National Board of Student Aid (Centrala studiestödsnämnden, CSN) who provided me with financial support during the first year and thus allowed me to start working on this project. I would like to acknowledge the University of Potsdam who funded the remaining of the project through a 2-years PhD stipend, and provided me with funding to attend conferences in Canada and Russia.
Fieldworks, courses and conferences were funded by the ÅForsk foundation, the COPER Young Investigator Group, the Alfred Wegener Institute for Polar and Marine Research (AWI), the Potsdam Graduate School, and the Helmholtz Graduate School for Polar and Marine Research. I would like to thank the AWI Potsdam administrative staff as well as Claudia Sprengel and Claudia Hanfland who provided me with the opportunity to attend advanced trainings and to develop international networking.

I owe a part of my thesis to my colleagues who helped me collect samples on Herschel Island (Canada) and in the Lena Delta (Russia): Samuel Stettner, Jan Kahl, George Tanski, Gustaf Huguelius, Hugues Lantuit, Sebastian Wetterich, Georgy Maximov, Anne Morgenstern, Guido Grosse, Anna Irrgang, Isabel Eischeid, Frank Günther and Lydia Stolpmann. Thank you for the pits and sorry for the mud!
Stefanie Hohberg, Nadja Kuhl, Dyke Scheideman and Patrick Lahouette, most of my samples would still be in a freezer without your help, thank you for your patience in the lab.

This PhD time would not have been as nice without my colleagues and friends at AWI Potsdam with whom I shared lively moments around the coffee machine and in the commuting trains. Anna, thank you for all your support throughout the PhD, until the last translation of my abstract into German.

I am grateful to Daniel Fortier for enriching my knowledge in geomorphology, and to the students at the Geocryolab for the scientific discussions during my stay at Montreal University.
During this time as a PhD student, I was involved in the Permafrost Young Researcher Network (PYRN). I would like to thank all co-2016-2018 ExCom with whom I enjoyed working and networking.

I should also acknowledge all the places (cafes, houses, libraries, trains, planes and cars) that hosted me and inspired me while writing this thesis: Potsdam, Berlin, Stockholm, Paris, Val-André, Chișinău, Marseille, Saint-Brice, Montréal, Ingonish, Lugano. Friends and family you were there; thank you for your distractions, laughs and inspiration. August, Jules, Nava, and Maïa, I look forward to spending more time with you.
Papa, Maman, merci de m'avoir fait voyager en dehors des sentiers battus aux quatre coins d'Europe et de m'avoir appris à mélanger les couleurs pour enrichir mes palettes. Nenette et Antoine, merci pour le bazar, pour votre inspiration en musique et vos rires euphoriques. Nico, your positive energy helps me wake up everyday. Thank you for bringing the concrete to my life and help me shape the most implausible ideas. Many more to come!

Stockholm, 23.03.2018

Abstract

In ice-rich permafrost regions, changes in the permafrost thermal regime cause surface disturbances. These changes are amplified by the increase in air temperatures recorded in the Arctic in the past decades. Thermokarst is a process that leads to surface subsidence and formation of characteristic landforms following thawing of ice-rich permafrost or melting of massive ice. Thermokarst is widespread on hillslopes and the number of associated landforms is increasing in the Arctic. Through this process large amounts of material are eroded and transported to the sea or accumulate along hillslopes. While hillslope thermokarst modifies terrestrial and aquatic ecosystems, there is limited understanding of its environmental impact at a regional scale.

In this thesis we quantify the environmental impacts of hillslope thermokarst on the valley and nearshore ecosystems along the Yukon Coast, Canada. Using supervised machine learning, we identified geomorphic factors that favour the development of coastal retrogressive thaw slump (RTS), one of the most dynamic hillslope thermokarst landform. Coastal geomorphology and ground ice type and content play a major role in RTS occurrence. Using aerial photographs and satellite imagery, we traced the evolution of RTSs between 1952 and 2011. During this time, the number and areal coverage of RTSs increased by 73%. RTSs eroded and partly released to the nearshore zone organic carbon contained in millions of cubic meters of material. Our results show that 56% of the RTSs identified along the coast in 2011 have eroded 16.6×10^6 m^3 of material; a large part (45%) was transported alongshore due to coastal processes. Moreover, we show that RTSs are a major contributor to the carbon budget in the nearshore ecosystem: 17% of the coastal RTSs identified in 2011 contributed annually up to 0.6% of the organic carbon released by coastal retreat along the Yukon Coast. To assess the impact of hillslope thermokarst on the terrestrial ecosystem, we measured the spatial distribution of soil organic carbon (SOC) and total nitrogen (TN) along hillslopes in three Arctic valleys. We highlight the high spatial variability in the distribution of SOC and TN in the valleys. This distribution is caused by complex soil processes occurring along the hillslopes. Hillslope thermokarst impacts the degradation of organic matter and affects the storage of SOC and TN.

Zusammenfassung

Veränderungen im thermalen Regime des Permafrosts verursachen Störungen der Erdoberfläche. Diese Veränderungen werden durch die in der Arktis seit Jahrzehnten ansteigenden Temperaturen verstärkt. Thermokarst ist ein Prozess, welcher die Erdoberfläche durch Schmelzen von Grundeis, oder Auftauen von Permafrost absacken lässt, wodurch charakteristische Landformen entstehen. Thermokarst ist vor allem entlang von Hängen weit verbreitet und die Anzahl der damit verbundenen Landformen in der Arktis steigt stetig an. Dieser Prozess mobilisiert große Mengen an Material, welche in Richtung Meer transportiert oder entlang von Hängen akkumuliert werden. Während entlang von Hängen auftretender Thermokarst terrestrische sowie aquatische Ökosysteme stark verändert, ist dessen Einfluss auf regionaler Skala zurzeit noch Gegenstand der Forschung.

In dieser Arbeit quantifizieren wir die Auswirkungen von Thermokarstprozessen entlang von Hängen auf die umliegenden Ökosysteme der küstennahen Täler und Nahküstenbereiche entlang der Yukon Küste in Kanada. Mittels überwachtem maschinellen Lernen haben wir geomorphische Faktoren identifiziert, welche die Entwicklung von retrogressiven Auftaurutschungen (RTS) begünstigen. RTS sind eine Erscheinungsform von Thermokarst entlang von Hängen. Die Küstengeomorphologie, sowie der Grundeistyp und -inhalt sind die wesentlichen bestimmenden Faktoren für das Auftreten von RTS. Wir haben Luftbildaufnahmen und Satellitenbilder genutzt, um die Evolution von RTS im Zeitraum von 1952 bis 2011 zu verfolgen. Während dieser Zeit ist die Anzahl und Ausdehnung von RTS linear angestiegen. Wir zeigen, dass 56% der RTS welche entlang der Küste in 2011 identifiziert wurden, 16.6×10^6 m^3 an Material erodiert haben. Hiervon wurden 45% durch Küstenprozesse entlang der Küste transportiert. RTS tragen wesentlich zu dem Kohlenstoff-Budget des Nahküstenbereiches bei: 17% der in 2011 identifizierten RTS, haben 0.6% des organischen Kohlenstoffes transportiert, welcher durch Küstenerosion entlang der Yukon Küste jährlich freigesetzt wird. Um den Einfluss von Thermokarst entlang von Hängen auf das terrestrische Ökosystem zu beurteilen, haben wir die räumliche Verteilung von organischem Bodenkohlenstoff und Stickstoff (SOC, TN) entlang von Hangprofilen in drei arktischen Tälern analysiert. Wir weisen auf eine hohe räumliche Variabilität in der Verteilung von SOC und TN hin, welche auf komplexe Bodenprozesse zurückzuführen ist, welche entlang von Hängen auftreten. Thermokarst entlang von Hängen hat einen großen Einfluss auf die Degradierung von organischem Material und die Speicherung von SOC und TN.

Résumé

Le changement climatique est la cause de la dégradation rapide du pergélisol à travers les régions arctiques et subarctiques. Cette dégradation s'exprime par des changements dans la taille, l'abondance et la structure des glissements rétrogressifs dus au dégel (GRD) et autres processus de pente thermokarstiques. Ces processus d'érosion des pentes contribuent au transport de sédiments vers l'Océan Arctique. Bien que l'impact des processus thermokarstiques sur les écosystèmes terrestres et aquatiques soit reconnu, il n'y a toujours pas d'étude qui quantifie leurs impacts sur les écosystèmes côtiers de l'Arctique. Dans cette thèse, nous quantifions les impacts des thermokarstes de pente dans les vallées et le long de la côte du Yukon, Canada. Nous avons utilisé des méthodes statistiques telles que les arbres de classification et les régressions logistiques pour identifier les facteurs qui favorisent le développement des GRD, un des modelés de dégradation du pergélisol le plus actif. La géomorphologie côtière ainsi que la nature et la quantité de glace dans le sol jouent un rôle prépondérant dans le développement des GRD. En utilisant des images satellite et des photos aériennes, nous avons suivi l'évolution des glissements rétrogressifs dus au dégel entre 1952 et 2011. Sur cette période, le nombre et l'étendue des GRD ont augmenté de 73% le long de la côte du Yukon. Les GRD ont érodé et partiellement relâché dans l'océan du carbon organic contenu dans des millions de mètres cubes de sédiments. Nos résultats montrent que 56% des GRD identifiés le long de la côte en 2011 ont érodé 16.6×10^6 m^3 de sédiments ; 45% a été transporté dans l'océan. De plus, notre étude montre que les GRD ont un rôle majeur sur le budget du carbone dans les milieux côtiers : 17% des GRD identifiés en 2011 ont relâché 0.6% du carbone érodé annuellement du fait de l'érosion côtière. Nous avons aussi étudié la dégradation du pergélisol le long des pentes des vallées périglaciaires, dans l'objectif de comprendre leurs impacts sur les sols et sur les stocks de carbone et d'azote. Nos résultats montrent qu'il y a une grande variabilité dans la distribution du carbone et de l'azote dans les vallées. Ces disparités sont causées par de complexes processus thermiques au niveau des sols. Les processus de pente thermokarstiques ont un impact important sur la dégradation de la matière organique dans les sols et affectent le stockage du carbone et de l'azote dans les régions Arctiques de pergélisol.

List of Figures

List of Tables

Acronyms

AL Active Layer

BP Before Present

C Carbon

C:N Carbon-to-Nitrogen

CH_4 Methane

CO_2 Carbon Dioxide

DGPS Differential Global Positioning System

DOC Dissolved Organic Carbon

GHG Greenhouse Gases

N Nitrogen

NEE Net Ecosystem Exchange

OC Organic Carbon

PF Permafrost

POC Particulate Organic Carbon

RTS Retrogressive Thaw Slump

SOC Soil Organic Carbon

SOM Soil Organic Matter

TN Total Nitrogen

TOC Total Organic Carbon

TPI Topographic Position Index

Contents

1 Introduction

ᖁᑲᓇᖅᑕᖁᑎᒋᔭᐅᓂᖅ

Qanaqtaaqatigiiniq

"being resourceful and persistent to solve problems, recognizing that we must constantly explore many different opportunities in order to find the best ways to move forward"

Arctic air temperatures are rising faster than the global average. Autumn and winter air temperatures are expected to increase by a regional average of 4°C by 2050, twice the warming projected for the Northern Hemisphere [AMAP, 2017]. The increase in air surface temperature observed in the Arctic causes dramatic changes in two major components of the cryosphere: permafrost and sea ice. The coast is the interface between these components, and is among the most dynamic areas of the circumpolar landscape [Fritz et al., 2017]. Land, sea, and atmosphere form complex interactions in the coastal area and make it sensitive to changes. There, climate warming is expected to trigger landscape instability and increased hazard exposure [Forbes, 2011].

Permafrost, or permanently frozen ground, occurs on land and beneath offshore Arctic continental shelves. It underlies about 24% of the Earth's land surface in the Northern Hemisphere. Large quantities of Soil Organic Carbon (SOC) are stored in the permafrost. These stocks resulted from the slow decomposition of soil organic matter in permanently frozen soils, caused by low soil temperatures and impeded drainage. Increased air temperature in the Arctic modifies the ground thermal regime and leads to permafrost thaw and enhanced microbial activity in the soil. As a result, SOC is released to the atmosphere [Mackelprang et al., 2011, Schuur et al., 2008]. In turn, the release of carbon from the permafrost to the atmosphere creates a positive feedback in

the climate system (permafrost carbon feedback), elevating the effect of Greenhouse Gases (GHG) emissions on global-mean temperatures [Schuur et al., 2015]. Both expert assessments [Abbott et al., 2016] and model evaluations [McGuire et al., 2016] identified permafrost thaw as one of the most important sources of uncertainty in predicting the timing and magnitude of the permafrost carbon feedback.

Soil Organic Carbon (SOC) and nutrients are also released to streams, rivers, and to the Arctic Ocean by thermokarst, altering terrestrial and aquatic ecosystems [Abbott and Jones, 2015, Kokelj et al., 2013, Vonk et al., 2012, Lamoureux and Lafrenière, 2009]. Thermokarst is the process of thawing of ice-rich permafrost or melting of massive ice, leading to surface subsidence and formation of characteristic landforms [Van Everdingen, 2005]. Thermokarst landforms represent major sources of instability, affecting biomass and hydrologic fluxes in the Arctic [Abbott et al., 2016]. On hillslopes, thermokarst landforms erode and transport large quantities of sediments, SOC and nutrients from up- to downhill. However, there are no estimates of the impact of hillslope thermokarst on the permafrost Organic Carbon (OC) on a regional scale in the Arctic. In this thesis we bring the first such estimates and emphasize the necessity to take into account the complexity of hillslope thermokarst processes when estimating SOC storage in the Arctic. To achieve this, we addressed three research questions:

1. Where do hillslope thermokarst landforms develop along the Arctic coast?

2. How much material is eroded through hillslope thermokarst?

3. What is the impact of hillslope thermokarst on the storage of SOC?

1.1 Scientific background

1.1.1 The Arctic coast, permafrost and climate change

The Arctic Coast

The Arctic coast comprises the land-ocean interface, so called coastal interface, and includes portions of adjacent marine and terrestrial systems substantially influenced by processes occurring both on- and offshore [Forbes, 2011]. The Arctic coastal interface consists of coastal fringes, inland, and nearshore zones. Arctic nearshore zones are underwater areas adjacent to the coast, shallower than 20 m. They represent ca. 20% of the shelves and 7.5% of the Arctic Ocean [Fritz et al., 2017]. The Arctic coastal interface is a sensitive and important zone of interaction between land and sea, a long-lasting area of transport and a nutriment source for indigenous communities [Forbes, 2011].

Permafrost

The Arctic coast is characterized by the presence of permafrost, both on- and offshore. Permafrost is ground (soil, sediment, or rock) that remains at or below 0°C for at least two consecutive years [Van Everdingen, 2005]. The near surface layer of the permafrost, termed Active Layer (AL), thaws during summer and refreezes in winter. The transient layer is the ice-rich layer marking the long-term position of contact between the active layer and permafrost [Shur et al., 2005]. Permafrost underlays 30% to 34% of the world's coastlines (Fig. 1.1) [Lantuit et al., 2012a]. The Arctic coast has a mean backshore elevation of 8.4 m, ranging from sub-meter elevations to up to 120 m [Lantuit et al., 2012a]. About two-thirds of the permafrost coastlines are composed of unlithified frozen material prone to erosion, while the rest comprises frozen lithified cliffs, with lower erosion potential [Lantuit et al., 2012a]. Ice is an important component of the permafrost, and ground ice varies in type and content along the Artic coast. The volumetric ground ice content along the Arctic coast range between 0% and 30% with an average of 18.4% [Lantuit et al., 2012a]. Ground ice can be found as pore, segregated (including massive) or vein ice [French and Shur, 2010]. The coast is characterized by the presence of ground ice onshore and of sea ice offshore during most of the year. The presence of ice renders Arctic coastlines particularly sensitive to climatic changes [Barnhart et al., 2014].

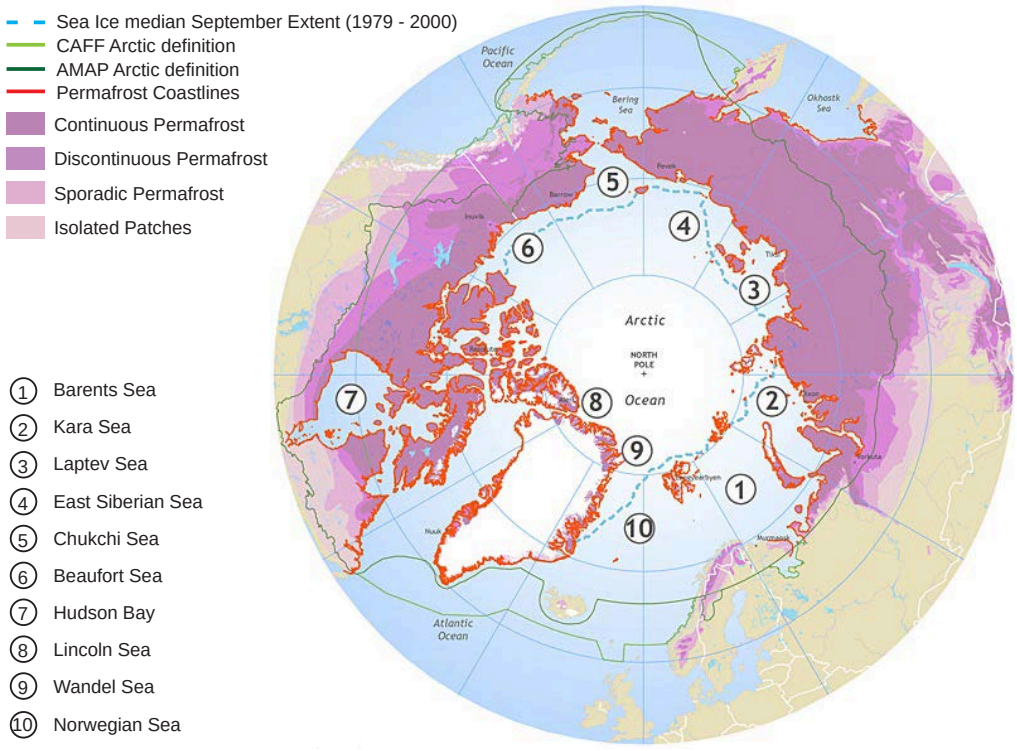

Figure 1.1 – Circum-Arctic map highlighting the extent of permafrost coastlines in red. The dotted blue line indicates the median sea ice extent for September 1979–2000 (modified after [Lantuit et al., 2012a, Brown et al., 1997])

Climate Change

Arctic air temperatures are rising faster than the global average (Fig. 1.2). Autumn and winter air temperatures are predicted to increase by a regional average of 4°C by 2050, twice the warming projected for the Northern Hemisphere [AMAP, 2017]. Climate warming is expected to trigger landscape instability and increased hazard exposure in the Arctic coastal interface [AMAP, 2017, Forbes, 2011].

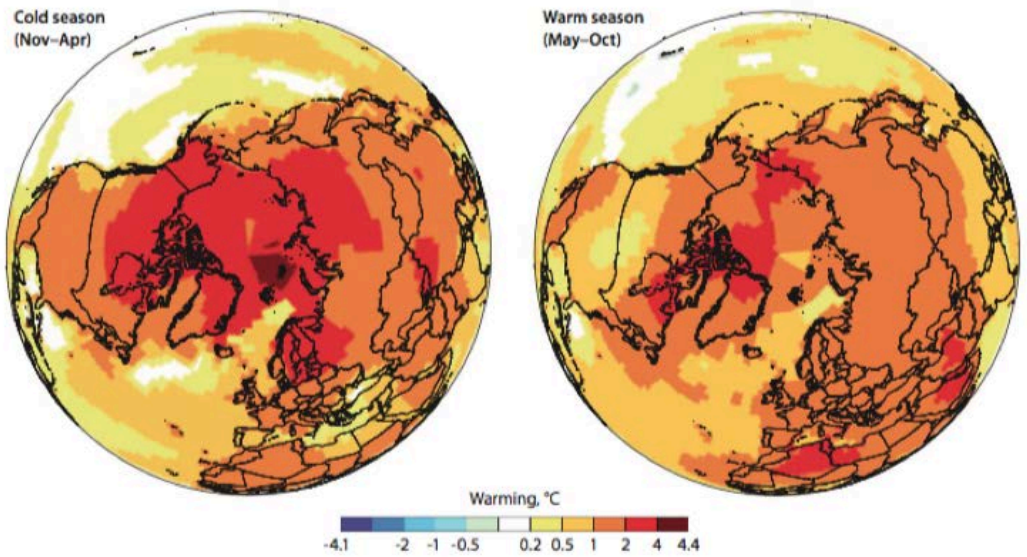

Figure 1.2 – Spatial pattern of Arctic warming for the period 1961 - 2014 in the cold season (Nov–Apr) and warm season (May–Oct) (NASA GISTEMP http://data.giss.nasa.gov/gistemp/maps/).

.

Increasing air temperatures in the Arctic affect both cryosphere and hydrosphere. Near-surface permafrost in the High Arctic has warmed by more than 0.5°C between 2007–2009 and 2017 [AMAP, 2017]. This leads to permafrost degradation, a term refering to the decrease in thickness and areal extent of permafrost. The permafrost area is projected to decline by a fifth by 2040, and could be reduced by two-thirds by 2080 [AMAP, 2017]. Coastal permafrost is degrading, as shown by the increase in the magnitude of oscillations of the permafrost bottom (deepest extent of permafrost), and greater variability in thickness [Romanovskii and Hubberten, 2001].
The length of the sea ice-free season and water temperature exert a great control over the long-term dynamics in coastal erosion. Many of the unlithified coastlines in the Arctic are in some areas still largely protected by sea ice during most of the year. However, the extent and thickness of sea ice follows a long-term downward trend [AMAP, 2017, Serreze et al., 2009], and the frequency of extreme storm events is increasing [Atkinson, 2005, Manson et al., 2005].

These changes make Arctic coasts more vulnerable to coastal erosion [Dallimore et al., 1996, Lantuit and Pollard, 2008]. The average rate of coastal retreat is 0.5 m yr^{-1}, with

high spatial variability between coastal segments [Lantuit et al., 2012a]. High erosion rates were reported for 3% of the coastlines in the Laptev Sea coast [Lantuit et al., 2011, Günther et al., 2013, Rachold et al., 2000], the East Siberian Sea coast, and the US and Canadian Beaufort Sea coast [Irrgang et al., 2018, Jones et al., 2009, Jones et al., 2008, Mars and Houseknecht, 2007]. The erosion rate in the remaining coastal segments ranges between 0 m and 2 m yr^{-1} [Lantuit et al., 2012a]. The volume of ground ice and geomorphology profoundly influence the nature of cliff response to coastal erosion [Dallimore et al., 1996]. Increased rate and uniformity of coastline erosion is also related to changes in the nearshore zone. Such changes include declining sea ice extent, rising sea level and increasing summertime sea surface temperature, storm power and wave action [Jones et al., 2009]. Coastal erosion plays an important role in displacing sediments and mobilizing OC in permafrost regions, releasing $14x10^9$ kg of Particulate Organic Carbon (POC) to the nearshore zone each year [Wegner et al., 2015]. This amount is comparable to the annual contribution of Arctic rivers [Koven et al., 2011]. Coastal erosion and river discharge increase the transport and concentrations of suspended sediments from upland regions to the nearshore zone [Dunton et al., 2006]. In some areas of the Arctic, up to 30-50% of the organic matter entering the nearshore zone is terrigenous [Naidu et al., 2000], delivered by river runoff and coastal erosion [Dunton et al., 2006].

1.1.2 Organic carbon in permafrost soils

Total Organic Carbon (TOC) or Organic Carbon (OC) refers to the carbon component of organic compounds in the Soil Organic Matter (SOM). OC comprises Soil Organic Carbon (SOC) and Dissolved Organic Carbon (DOC) and is a way to measure the SOM contained in soils. About 50% of the world's global SOC is stored in the permafrost. SOC stocks in the top three meters of soils, in deltas and the Yedoma regions across the northern circumpolar permafrost region are estimated to 1307 Pg; 76.4% (999 Pg) of them are stored in perennially frozen soils [Hugelius et al., 2014]. These stocks resulted from slow decomposition of soil organic matter SOM in permanently frozen soils, caused by low soil temperatures and impeded drainage. As the active layer thickens due to warmer air temperatures, increased microbial activity mobilizes more OC that is eventually released to the atmosphere [Mackelprang et al., 2011, Schuur et al., 2008].

The release of carbon from the permafrost to the atmosphere creates a positive feedback in the climate system, so-called permafrost carbon feedback, elevating the effect of GHG emissions on global mean temperatures [Schuur et al., 2015]. Permafrost carbon stocks were only recently included in global carbon models, highlighting the contribution of thawing permafrost to the overall climate and economic response to human greenhouse gas emissions [Kessler, 2017, Koven et al., 2015, MacDougall et al., 2012, Burke et al., 2012, von Deimling et al., 2012]. Schaefer et al. predicted 120 ± 85 Gt of carbon emissions from thawing permafrost by 2100, which represents 5.7 ± 4.0%

of the total anthropogenic emissions [Schaefer et al., 2014]. Nevertheless, these carbon models underestimate the potential impact of the permafrost feedback on the global climate for two reasons. First, they do not account for the spatial heterogeneity of permafrost terrains. Second, they omit the contribution of coastal erosion and abrupt thaw processes, such as thermokarst and thermo-erosion [Hugelius et al., 2014, MacDougall et al., 2012, Vonk et al., 2012]. Both expert assessments [Abbott et al., 2016] and model evaluations [McGuire et al., 2016] identified permafrost degradation as one of the most important sources of uncertainty in predicting both the timing and the magnitude of the permafrost carbon feedback.

1.1.3 Hillslope thermokarst processes

In ice-rich permafrost areas, changes in the thermal regime of the permafrost lead to permafrost degradation and disturbances. As a result of ground ice melt and active layer deepening, thermokarst landforms may develop.

Thermokarst widely defines the processes that lead to local collapse, subsidence, erosion, and instability of the ground surface as a result of permafrost thaw [Kokelj and Jorgenson, 2013, French, 2007]. It defines the process of thawing of ice-rich permafrost or melting of massive ice, leading to surface subsidence and formation of characteristic landforms [Van Everdingen, 2005]. Thermo-erosion is a process related to thermokarst activity [French, 2007] that leads to erosion of ice-rich permafrost by the combined mechanical and thermal action of moving water [Van Everdingen, 2005]. Thermo-erosion is common in terrains characterized by gentle slopes and is one of the most common processes of valley development in periglacial environments [French, 2007]. In this thesis, thermokarst processes include thermo-erosion processes.

Thermokarst landscapes (including landscapes formed by thermo-erosion) are estimated to cover ca. 20% of the northern permafrost region [Olefeldt et al., 2016]. They can be assigned to three types: wetland, lake and hillslope thermokarst landscapes. In this thesis we focus on hillslope thermokarst landscapes. While there is a large uncertainty in the areal coverage of hillslope thermokarst, Olefeldt et al. estimated that it covers ca. 5% of the northern permafrost region and is mostly found in relatively cold and dry regions (Fig. 1.3) [Olefeldt et al., 2016]. Hillslope thermokarst is more abundant in certain areas, such as the western Laptev Sea coastal lowlands, covering up to 29.1% of the area [Grosse et al., 2006].

Common hillslope thermokarst landforms include active layer detachment slides, retrogressive thaw slumps, thermo-erosional gullies, beaded streams and thermokarst water tracks [Olefeldt et al., 2016, Kokelj and Jorgenson, 2013]. These landforms develop on ice-rich and gently sloping permafrost terrains. They are climate sensitive: their initiation is often triggered by short periods of extreme weather, when unusually warm

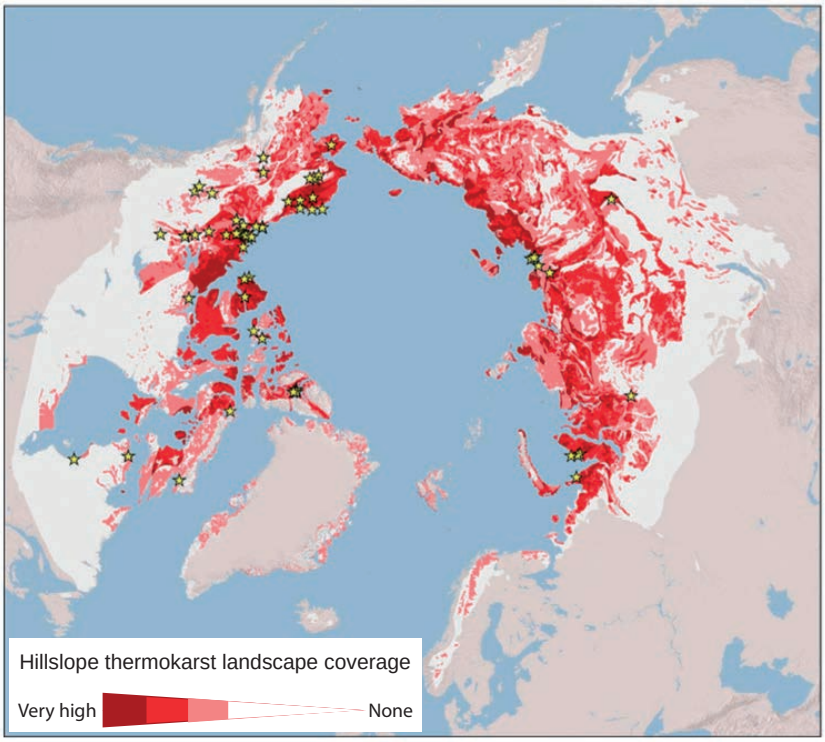

Figure 1.3 – Distribution and coverage of hillslope thermokarst landscapes in the northern circumpolar permafrost region. The yellow symbols represent the study sites mentioned in the literature (modified from [Olefeldt et al., 2016]).

temperatures and high precipitations coincide [Kokelj et al., 2015b, Balser et al., 2014]. Hillsopes are predominant in small Arctic valleys and along the coasts with high to medium elevation gradients. On these surfaces, thermal and geomorphic processes can rapidly degrade permafrost and modify slopes and valley morphologies [Kokelj et al., 2017]. Hillslope thermokarst disturbances can mobilize large quantities of OC, by displacing SOM along hillslopes and to streams and seas [Tanski et al., 2016, Abbott and Jones, 2015]. Hillslope thermokarst can therefore have consequent impacts on the landscape and soils of valleys and coasts. However, studies quantifying these impacts are missing.

Retrogressive Thaw Slumps

Retrogressive Thaw Slump (RTS)s are one of the most dramatic and dynamic hillslope thermokarst landforms. An RTS is a type of landslide caused by thermokarst (Fig. 1.4). RTSs are mainly found in ice-rich permafrost terrains. In Canada, RTSs develop in the marginal zone of the maximum extent of the last glacial maximum Ice Sheets [Kokelj et al., 2017]. RTSs have a distinctive horseshoe shape (Fig. 1.4), with three distinct features: a steep headwall, a large slump floor with gullies, and a lobe conveying melted

ice and sediments out of the RTS [Burn and Lewkowicz, 1990]. RTS activity involves three processes summarized by [Kokelj et al., 2015a]:

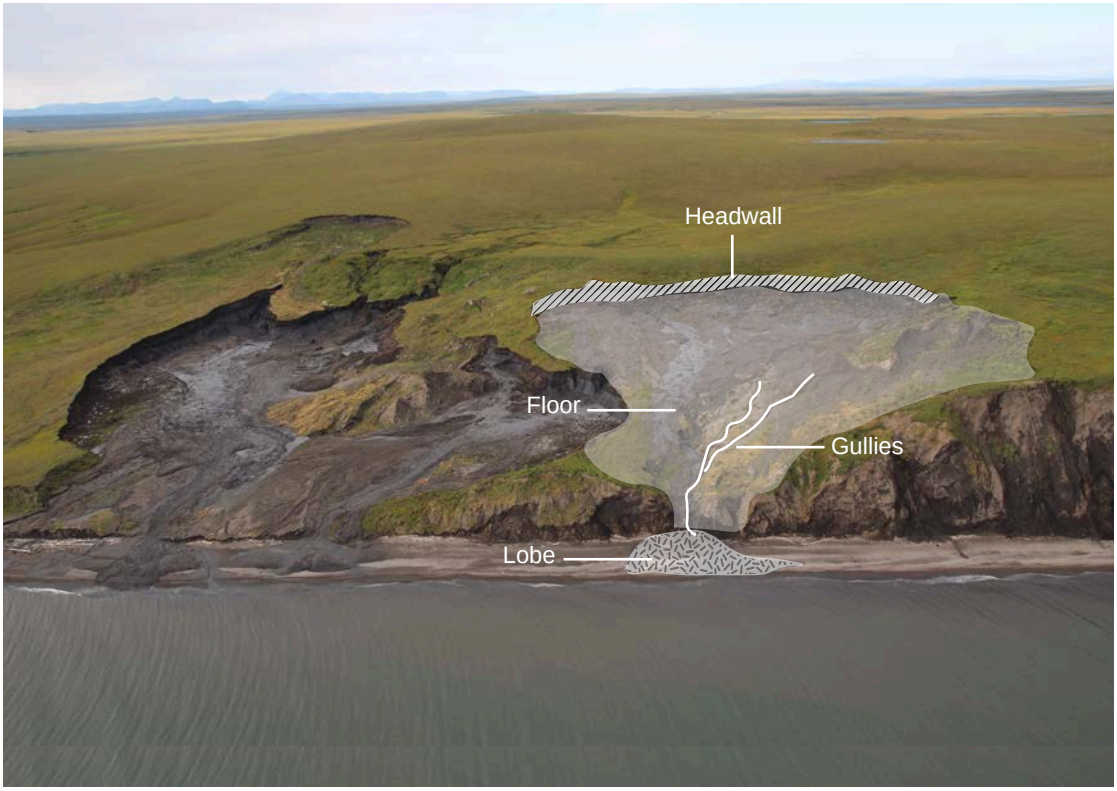

Figure 1.4 – Photograph of retrogressive thaw slumps, taken along the Yukon Coast. The sketch illustrates the different component of a retrogressive thaw slump: the headwall; the floor; the gullies and the lobe.

(1) exposure and ablation of large massive ice bodies, retreat of the headwall by retrogressive failure and supply of sediments and melt-water to the slump floor;

(2) evacuation of debris from the slump floor through fluvial transport, mass wasting processes, and mass flow;

(3) base-level erosion, or evacuation of outlet detritus.

RTSs follow different cycles of activity and are therefore polycyclic. Long lasting RTSs can grow to tens of hectares. Gullies can develop within RTSs to convey the debris flow out of the slump floor [Kokelj et al., 2015a]. RTSs can be active or stable, following a development cycle. Active RTSs are characterized by steep headwalls exposing ice-rich permafrost, slump floors with thawed sediments and incised gullies. Stable RTSs are characterized by gently sloping and vegetated headwalls, vegetated slump floors and no visible active gully systems [Lantuit and Pollard, 2008, Wolfe et al., 2001]. RTS activity has been accelerating since the 1950s, especially in ice-rich morainic landscapes of the western Canadian Arctic [Segal et al., 2016, Lacelle et al., 2010, Lantz and Kokelj, 2008, Lantuit and Pollard, 2008]. Segal et al. showed that the area covered by RTSs in

four areas of the western Canadian Arctic between the 1950s and the 2000s increased by ca. 139% and the density of RTSs by ca. 64% [Segal et al., 2016]. Along ice-rich coasts, RTSs are triggered by coastal erosion and then grow upslope, perpendicularly to the shoreline [Lewkowicz, 1987b]. The period of coastal RTS activity depends on the equilibrium between thermo-denudation and coastal erosion rates: an RTS remains active if its headwall erodes at a rate exceeding shoreline retreat [Lantuit et al., 2012b, Aré, 1999]. This equilibrium is strongly linked to the dynamics of environmental conditions that enhance coastal erosion, such as the occurrence of storm events and extension of the open water period [Overeem et al., 2011, Are et al., 2008, Solomon, 2005].

1.2 Aims

In the context of the permafrost carbon feedback, the impacts of hillslope thermokarst landforms on the valley and nearshore ecosystems are largely unknown. The objective in this thesis is to address this gap by quantifying the extent of hillslope thermokarst landforms and evaluating their impacts on the carbon budget in the coastal interface. The three main research questions that shaped this thesis are:

1. Are RTSs developing uniformly along the Arctic coast?

2. How much material do RTSs erode and transport offshore?

3. What are the impacts of thermokarst processes on soils and geochemical properties along hillslopes?

The aims of this thesis are to:

i) Document the terrains conducive to the development of coastal RTSs.

ii) Highlight the evolution of coastal RTSs between 1952 and 2011.

iii) Quantify the flux of sediments and OC mobilized through slumping.

iv) Understand the impact of hillslope processes on the distribution of OC and nitrogen in Arctic valleys.

1.3 Study region

The study region is located in the Canadian Arctic, along the westernmost coast of the Yukon Territory (Fig. 1.5). It comprises a 238-km portion of the Yukon Coastal Plain, including Herschel Island (Fig. 1.5). The area is in the continuous permafrost zone [Rampton, 1982] and tundra vegetation zone dominated by mosses, graminoids, and shrubs [CAVM, 2003]. The area is characterized by a subarctic climate with mean summer air

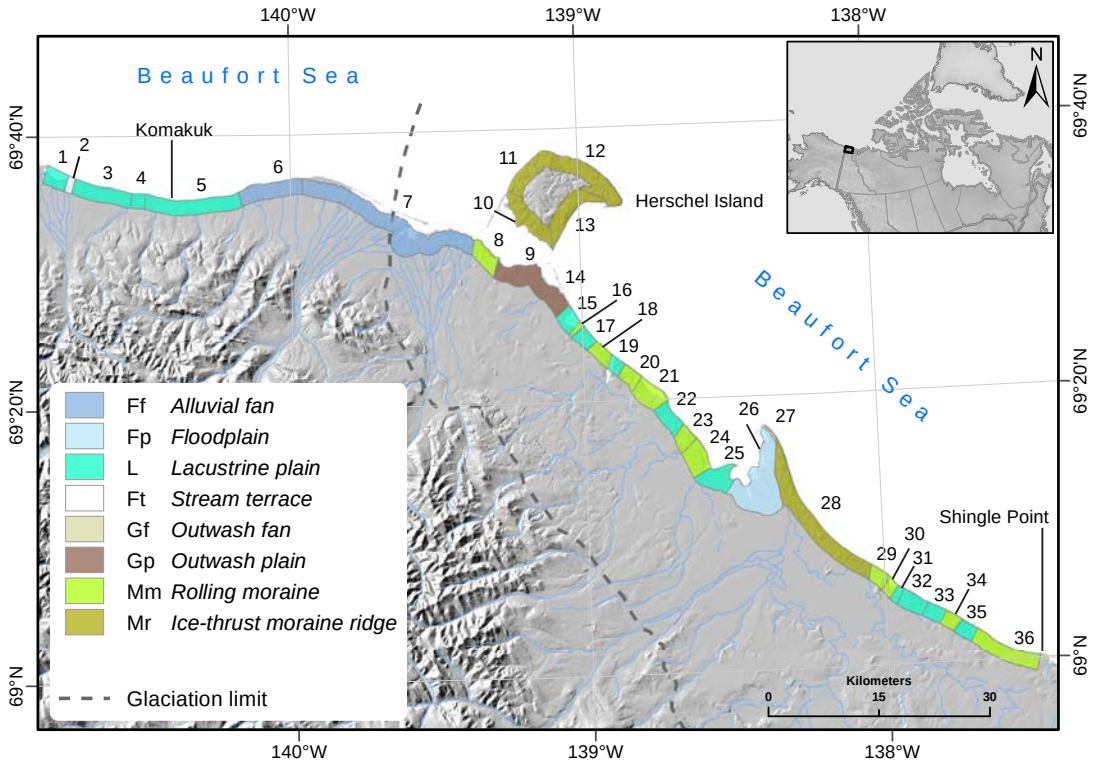

Figure 1.5 – Map of the study area. The numbers represent the coastal segments stretching along the coast from west to east. The limit of the glaciation was reproduced after [Fritz et al., 2012]. 1] Clarence Lagoon West; 2] Clarence Lagoon East; 3] Komakuk Beach West 2; 4] Komakuk Beach West 1; 5] Komakuk Beach; 6] Malcom River Fan; 7] Malcom River Fan with barrier Islands; 8] Workboat Passage West; 9] Workboat Passage East; 10] Herschel Island South; 11] Herschel Island West; 12] Herschel Island North; 13] Herschel Island East; 14] Whale Cove West; 15] Whale Cove; 16] Whale Cove East; 17] Rolland Bay northwest; 18] Rolland Bay West; 19] Rolland Bay East; 20] Stokes Point West; 21] Stokes Point; 22] Stokes Point Southeast; 23] Phillips Bay northwest; 24] Phillips Bay West; 25] Phillips Bay; 26] Babbage River Delta; 27] Kay Point Spit; 28] Kay Point South East; 29] King Point Northwest; 30] King Point Lagoon; 31] King Point; 32] King Point Southeast; 33] Sabine Point West; 34] Sabine Point; 35] Sabine Point East; 36] Shingle Point West.

temperature of 6°C on the eastern boundary of the study area and 8.7°C on the western boundary; the mean summer precipitations (June, July and August, 1971-2000) are 79.8 mm on the east end, and to 112.9 mm on the west end [1]. The Mackenzie River that enters the Beaufort Sea east of the study area influences seawater temperature and sea ice extent and is the main control on the local precipitation patterns [Burn and Zhang, 2009]. The western margin of the Laurentide ice sheet reached its maximum ice extent around Herschel Island (Fig. 1.5) at ca. 16 200 years BP [Fritz et al., 2012]. It shaped the topography of the Yukon Coastal Plain: long and high moraine ridges characterize most of the previously glaciated area. Stream valleys, fluvial deltas, alluvial fans, and thermokarst basins characterize the unglaciated area. Due to the widespread moraine deposits, 35% of the Yukon Coast is composed of ice-rich cliffs [Harper, 1990]. Volumetric ground ice contents (massive ice, pore ice and wedge ice) vary along the coast and range from 0% to

[1] Environment Canada,http://climate.weather.gc.ca/historical_data/search_historic_data_e.html,2017

74% [Couture and Pollard, 2017]. Previous studies divided the study area into 36 coastal segments (Fig. 1.5), based on ground ice contents, surficial geology and geomorphology [Lantuit et al., 2012a, Couture, 2010, Lantuit and Pollard, 2005]. Most segments fall into one of three surficial geologic units: ice-thrust moraines (30%); lacustrine plains (23%) and rolling moraines (16%). Alluvial fans, stream terraces, floodplains, and outwash plains underlay the remaining segments [Rampton, 1982]. The coast is rapidly eroding [Harper, 1990]: during the period 1952-2011, the average rate of shoreline change was –0.7 m yr^{-1} and was characterized by decreasing erosion rates from west to east [Irrgang et al., 2018]. RTSs are common along the coast and mostly develop on segments with massive ground ice thicker than 1.5 m, and coastal slope greater than 3.9° [Ramage et al., 2017].

The fieldwork took place along the eastern coast of Herschel Island (Fig. 1.5) (Qikiqtaruk Parc Territory), in three Arctic catchments. Herschel Island is a glacier ice-thrust remnant of ca. 111 km^2, located 2 km off the coast of Yukon Coast and characterized by rolling and hummocky moraines modified by thermokarst and periglacial processes [MacKay, 1959]. Ridges and hills reach up to 178 m a.s.l. inland; steep cliffs up to 60 m high characterize the coasts. The coast of Herschel Island is rapidly receding: between 1970 and 2000 the mean rate of shoreline change was -0.45 m yr^{-1} [Lantuit and Pollard, 2008], and 0.68 m yr^{-1} between 2000 and 2011 [Obu et al., 2017a]. Most of the soils are organic Cryosols [Group, 1998], with an organic upper horizon underlain by mineral silty-clay horizons. Ground ice is present throughout the island except on beaches and spits. Volumetric ground ice contents vary from 44% to 77% [Couture and Pollard, 2017] and mostly occur as pore and segregated ice lenses, ice wedges and massive ice beds [Pollard, 1990]. There are numerous active layer detachments and RTSs on the island [Lantuit and Pollard, 2008].

1.4 Methods

This section describes the methods used in the thesis for mapping, interpolation, fieldwork, laboratory work and statistical analyses.

1.4.1 Mapping

Remote sensing was a key method used in this thesis. The first step for this work was to identify permafrost degradation landforms in space and time along the Yukon Coast (Chapter 3 and 4). Permafrost degradation landforms were mapped using high-resolution multi-spectral satellite imagery (GeoEye-1 and World-View2) acquired in 2011. The images cover the entire Yukon Coast, including Herschel Island (1.8 m resolution in multi-spectral and 0.5 m in panchromatic view). The landforms were also identified in time using historical aerial photographs from 1951, 1952, 1972 and 1976 from the Cana-

dian National Air Photo Library (3 m resolution), geo-coded to the 2011 satellite images using PCI Geomatic's Geomatica Orthoengine© software.

RTSs and streams were manually mapped at a 1:2000 scale. The emphasis was made on coastal features, which were defined as features occurring within 500 m of the coast. All analyses were performed in ArcGIS 10.3. RTSs were classified as active or stable. RTSs were additionally classified according to their initiation date: RTSs initiated after 1972 were defined as RTSs occurring on surfaces that had not been affected by slumping processes before 1972. Differences in resolution between aerial photographs and satellite imagery were ca. 1.2 m and were deemed satisfactory for interpretation and mapping purposes. For the purpose of this thesis, streams were only mapped for Herschel Island using the high-resolution imagery from 2011. Streams were mapped from the source to the outlet. The watersheds were delineated using a Digital Elevation Model from TandeM-X created in 2012 (12 m resolution). The streams were classified as: large valley streams with permanent flow; valley streams with temporary flow; gullies; thermo-erosional gullies; and ravines.

1.4.2 Spline interpolation and volumes estimations

Spline interpolation was used to model pre-slump topographies, later used to calculate the volume of material eroded through slumping (Chapter 4). The spline method allows to estimate elevation points outside the range of input sample points and to minimize the total curvature of a surface. It creates accurate surfaces based on few sample points. However, it is sensitive to outliers, and there is no indication of errors [Wu and Hung, 2016]. Elevation points were taken outside the area of the RTSs and interpolated over the surface of the RTSs (Fig. 1.6).

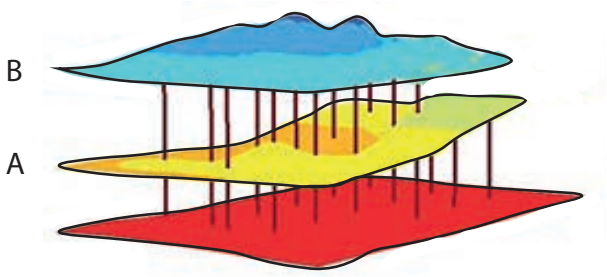

Figure 1.6 – Schematic of the spline interpolation method used to model pre-slump topographies. Surface A is the RTS surface in 2011 and surface B represents the surface before initiation of the RTS (Modified after [Wu and Hung, 2016]).

1.4.3 Fieldwork

Fieldwork was conducted in three valleys located on the eastern coast of Herschel Island between July 27^{th} and August 8^{th}, 2015 (Chapter 5). The aim was to assess the spatial variability of SOC and Total Nitrogen (TN) within the catchments.

Longitudinal profiles of the valleys were surveyed using a Differential Global Positioning System (DGPS). Following a sampling scheme, each valley was dissected perpendicularly in three transects in the upper, middle and lower parts of the valleys. Along each transect three to five sampling sites were established, chosen to be representative of each geomorphological unit. We systematically described qualitatively the vegetation and the slope. Active layer depth was determined for each profile as the depth to the top of the permafrost on the sampling day. At each site, soil pits were excavated down to the permafrost table, if reached before 1 m depth (Fig. 1.7). The soil horizons in the active layer were described and sampled using fixed volume cylinders. A steel pipe was hammered from the top of the permafrost down to 1 m depth at 10 cm increments to collect permafrost samples (Fig. 1.7). The samples were kept cool and were transported after fieldwork to the laboratory in Potsdam for geochemical analyses.

Figure 1.7 – Hammering a steel pipe in the permafrost to collect soil samples. Photograph taken in July 2016.

1.4.4 Geochemical analyses

Standard geochemical methods were used to measure the content of OC and Total Nitrogen (TN) in the soil samples. The samples were freeze-dried for 72 hours at -20°C. We

weighted the samples before and after freeze-drying to assess for volumetric water content. The dry bulk density was calculated using the dry-weight (dWi) and the volume of each sample (Vi), according to the following formula:

(1) ρ_b = dWi / Vi

The samples were separately analysed for %C and %N in a carbon-nitrogen analyser (Vario EL III elemental analyser). The Total Organic Carbon (TOC) was measured using a Vario Max C analyser (Elementar). SOC was then calculated using Eq. (2), where %TOC is the total organic carbon content (wt%), ρ_b the bulk density, and L the length of a sample (cm).

(2) SOC = %TOC * ρ_b * L * 10

The Carbon-to-Nitrogen (C:N) was calculated using the ratio between %TOC and %N. Stable carbon isotopes (δ^{13}C) values were analysed with a DELTAplusXL Finnigan mass spectrometer (Thermo Fisher Scientific, Germany) coupled to a Carlo-Erba NC2500 elemental analyser. Isotope signatures are reported in per mille (‰) against Vienna Pee Dee Belemnite (VPDB).

1.4.5 Statistical analyses

Statistical analyses were performed using R Studio (The R Foundation, version 3.3.1). Machine learning methods, especially univariate regression tree models were used to characterize the terrain controls on RTS distribution (Chapter 3). This statistical method explores the relationship between a single response variable and multiple explanatory variables [Zuur et al., 2007]. In the scope of this thesis, the regression trees were used to highlight the environmental parameters that explained most variation in RTS abundance along the Yukon Coast as well as the main thresholds in the datasets. Through recursive partitioning, the regression trees repeatedly split the dataset into binary groups. Each split is defined by a simple rule, which minimizes the sums of squares within the two groups formed by the split [Breiman et al., 1984]. The optimal tree size was determined by the complexity parameter, used when pruning the tree to minimize the mean relative square error. This method is robust and can incorporate dependent variables as well as discrete data [De'ath and Fabricius, 2000].

Statistical correlations were performed in Chapter 5 to test the spatial distribution of geochemical parameters in Arctic valleys. We tested the dependency of SOC, TN, and C:N ratio against spatial and soil variables. The relationship between spatial and geochemical variables was assessed using the Kruskal-Wallis non-parametric test and Dunn's posthoc test. Linear correlations between soil and geochemical variables were assessed using student t-tests.

1.5 Thesis outline

This thesis is composed of six chapters, including an introduction to the topic (Chapter 1), a synthesis (Chapter 2), and three main chapters (Chapters 3,4,5). The three main chapters consist of research articles.

Chapter 3 describes the distribution of coastal RTSs and highlights the spatial links between RTS development along the Yukon coast and surficial deposits, massive ice and topography. Chapter 4 furthers the first study and analyses the evolution of RTSs between 1952 and 2011 along the Yukon Coast. This chapter also presents volumes of sediment and OC mobilized by the RTSs and estimates the contribution of RTSs to the transfer of OC from the terrestrial to the marine ecosystem. Chapter 5 investigates the spatial variability of SOC in three valleys located on Herschel Island. Chapters 3 and 4 focus on RTSs and were published in the peer-reviewed journals indicated below and are reprinted under permission of the respective publishers. Chapter 5 focuses on the impacts of hillslope thermokarst on soils and is an unpublished manuscript.

> **Chapter 3**: Ramage, J.L., Irrgang A.M., Herzschuh U., Morgenstern A., Couture N., Lantuit H., 2017: Terrain Controls on the Occurrence of Coastal Retrogressive Thaw Slumps along the Yukon Coast, Canada. Journal of Geophysical Research: Earth Surface. http://onlinelibrary.wiley.com/doi/10.1002/2017JF004231/epdf
>
> **Chapter 4**: Ramage, J.L., Irrgang A.M., Morgenstern A., Lantuit H., 2018: Increasing coastal slump activity impacts the release of sediment and organic carbon into the Arctic Ocean, Biogeosciences, 15, 1483-1495, https://www.biogeosciences.net/15/1483/2018/
>
> **Chapter 5**: Ramage, J.L., Fortier D., Hugelius G., Lantuit H., Morgenstern A.: Dissecting valleys: Snapshot of carbon and nitrogen distribution in Arctic valleys. Manuscript submitted to Catena, 13.04.2018.

Two datasets were published in a scientific data repository:

> **DS01**: Ramage, J.L., Konopczak, A.M., Herzschuh, U., Morgenstern A., Lantuit H., 2016: Coastal retrogressive thaw slumps along the Yukon Coast (Canada).Alfred Wegener Institute, Helmholtz Center for Polar and Marine Research, Bremerhaven, PANGAEA. https://doi.org/10.1594/PANGAEA.869573
>
> **DS02**: Ramage, J.L., 2017: Valleys of Herschel Island, Yukon, Canada. Alfred Wegener Institute, Helmholtz Center for Polar and Marine Research, Bremerhaven, PANGAEA. https://doi.org/10.1594/PANGAEA.883524

1.6 Authors' contributions

Co-authors are abbreviated as follows: Justine Lucille Ramage (JLR); Anna Maria Irrgang (AMI); Nicole Couture (NC); Ulrike Herzschuh (UH); Anne Morgenstern (AM); Daniel Fortier (DF); Gustaf Hugelius (GH); Hugues Lantuit (HL).

Paper I: JLR and HL designed the study. JLR was the main contributor in terms of analyses, wrote the initial version of the paper and created the figures. HL and AM provided feedback on the study design and interpretation of the results. AMI geocoded the historical aerial photographs for the Yukon Coast and provided the rates of coastal change. NC provided a part of the dataset used in the statistical analyses. UH directed the statistical analyses. All authors contributed with interpretation of the results and editing of the manuscript. HL and AM provided guidance and help throughout the study.

Paper II: JLR and HL designed the study. JLR was the main contributor in terms of analyses (mapping, spline interpolation, eroded volumes of material from retrogressive thaw slumps), wrote the initial version of the paper and made the figures. AMI geocoded the historical photographs used for mapping the retrogressive thaw slumps. AM helped with adjusting the dataset. All authors contributed with interpretation of the results and editing of the manuscript. HL and AM provided guidance and help throughout the study.

Paper III: JLR, HL, and AM designed the study. JLR was the main contributor in terms of analyses, wrote the initial version of the paper and made the figures. DF provided scientific inputs and feedback to the study design. GH took part in the fieldwork and sampling procedure, provided scientific inputs, and contributed to the interpretation of the data. HL led the fieldwork campaign, acquired financial support and provided scientific inputs. AM provided scientific inputs to the study design. All authors contributed with interpretation of the results and editing of the manuscript. HL and AM provided guidance and support throughout the study.

2 Synthesis

Hillslope thermokarst landscapes cover up to 5% of the northern circumpolar permafrost region [Olefeldt et al., 2016]. The incidence of hillslope thermokarst landforms (e.g. active layer detachment, thaw slumps and thermo-erosional gullies) is increasing all over the Arctic [Kokelj et al., 2017, Segal et al., 2016, Rudy et al., 2013, Lantuit and Pollard, 2008, Godin and Fortier, 2012, Fortier et al., 2007]. In this thesis, we aimed at quantifying the occurrence of hillslope thermokarst and estimating its environmental impacts in the Arctic coastal fringe. The main objectives were to: 1) assess the distribution of Retrogressive Thaw Slump (RTS), and reveal the terrain factors controlling their development; 2) estimate the release of material and Organic Carbon (OC) through these landforms to the nearshore zone; 3) understand the impact of hillslope processes on soil geochemical properties. The study area comprises the western part of the Yukon Coast (Yukon Territory, Canada), a total of 238 km from Shingle Point West to Komakuk Beach (east to west), including Herschel Island.

2.1 RTSs are widely spread in ice-rich permafrost areas

Earlier studies pointed out the intense activity of single hillslope thermokarst landforms on Herschel Island and in specific areas of the Yukon Coast [Lantuit and Pollard, 2008, Wolfe et al., 2001]. In Chapter 3 of this thesis, we showed that while hillslope thermokarst is widespread along the Yukon Coast, its distribution is heterogeneous. We described and explained the spatial distribution of RTSs on a large scale, along the entire Yukon Coast and on Herschel Island. There were 287 RTSs along the coast in 2011: 203 active and 84 stable. The study area as a whole was characterized by active slumping, 71% of the RTSs were active. Active RTSs were 7 times smaller (med = 0.15 ha) than stable RTSs (med = 1.09 ha), their floors had slightly steeper slopes, and they had narrower slump lobes.

Along the entire Yukon Coast, RTSs occurred with an average density of 1.2 RTSs per km

of coast. On ice-thrust moraines, where 60% of the RTSs occurred, the average density was 2.4 RTSs per km of the coast. Thickness of massive ice bodies within a coastal segment was the main factor explaining high density of RTSs, whereas the volume of massive ice in the soil was the most influential factor for large coverage of RTSs (Chapter 3). Coastal RTSs are highly dynamic and evolve with the coast: shoreline changes impact the coastal geomorphology which in turn can create optimal conditions for RTSs to develop (Chapter 3). During the period 1952-2011, the average rate of shoreline change was –0.7 m yr^{-1} [Irrgang et al., 2018]. Throughout the same period of time, the number of RTSs increased by 73%; active RTSs were more abundant and increased faster in number than stable RTSs (Chapter 4). We showed in Chapter 3 that the slope and coastal height are the primary factors controlling the activity of RTSs: active RTSs are found in coastal segments with a slope angle greater than 3.9° and cliff heights more than 11.0 m.

We measured the most rapid development of RTSs on geomorphic units with highest ground ice contents: the number of RTSs doubled on rolling moraines and increased by 69% on ice-thrust moraines (Chapter 4). Similar observations were made previously on distinct landforms [Balser et al., 2014, Lantuit et al., 2012a, Burn, 2000, Burn and Lewkowicz, 1990, Lewkowicz, 1987b]. A study that investigated RTS occurrences in northern Canada highlighted the strong correlation between RTS development and ice-rich moraine deposits found on the eastern margin of the late Wisconsinan glaciation [Kokelj et al., 2017]. However, Chapter 3 of this thesis is the first study to statistically show the relationship between RTS activity, ground ice, and coastal geomorphology.

Many RTSs that were stable or stabilized between 1952 and 1972 re-activated between 1972 and 2011. Our study confirms the pattern of RTS reactivation, referred to as polycyclicity. Polycyclicity was previously observed on Herschel Island [Lantuit and Pollard, 2008] and between Kay Point and Shingle Point [Wolfe et al., 2001]. Reactivation of RTSs is associated with incomplete melting of massive ice bodies during the first period of RTS activity [Burn, 2000] and depends on the capacity of the slump headwall to remain exposed until the ice is exhausted [Lantuit and Pollard, 2008, Lewkowicz, 1987a]. These results are consistent with the observations made in other parts of the Canadian Arctic, where RTS activity is accelerating since the 1950s [Segal et al., 2016, Lacelle et al., 2010, Lantz and Kokelj, 2008, Lantuit and Pollard, 2008]. Lantuit and Pollard showed that the number of RTSs on Herschel Island increased by 61% between 1952 and 2000 [Lantuit and Pollard, 2008]. RTSs develop following changes that affect geomorphic settings (Chapter 3) [Kokelj et al., 2017] and are induced by climatic conditions such as increased air temperature [Lacelle et al., 2010], precipitation events [Kokelj et al., 2015a, Lacelle et al., 2010], and storm events [Lantuit et al., 2012b, Lantuit and Pollard, 2008, Dallimore et al., 1996].

2.2 Retrogressive thaw slumps contribute significantly to the nearshore organic carbon

The average rate of erosion for the Arctic coast is 0.5 m yr^{-1} [Lantuit et al., 2012a]. Coastal retreat rates are highly variable both spatially and temporally, due to variations in the lithology, cryology, and geomorphology of coastal cliffs [Lantuit and Pollard, 2008, Solomon, 2005]. Along the Yukon Coast, the mean erosion rate was -0.7 m yr^{-1} between the 1950s and 2011 [Irrgang et al., 2018]. As a result of erosion, 5.5×10^{6} kg SOC yr^{-1} [Couture et al., 2018] and $54.9\text{x}10^{3}$ kg DOC yr^{-1} is released to the nearshore zone of the Beaufort Sea [Tanski et al., 2016]. Rivers also contribute to the release of sediments and OC to the Arctic Ocean. Arctic rivers deliver ca. $34\text{-}38\text{x}10^{9}$ kg DOC yr^{-1} to the Arctic Ocean and surrounding basins [Holmes et al., 2012]. The Mackenzie River delivers 820 kg km^{2} yr^{-1} of DOC to the Beaufort Sea [Holmes et al., 2012]. As a result of the massive sediment and organic carbon inputs, terrestrial influences are particularly strong in the nearshore zone of the Arctic Ocean.

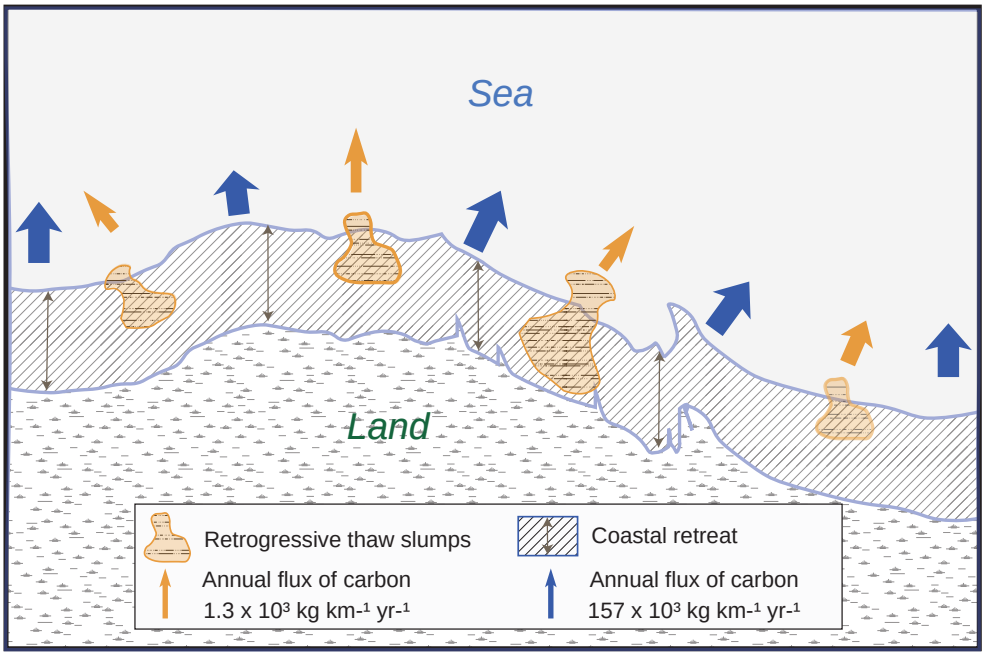

Figure 2.1 – Flux of organic carbon to the Beaufort Sea from RTSs and coastal retreat. The numbers are provided for the length of the Yukon Coast (238 km) and for 17% of the RTSs identified in 2011 along the coast.

Part of the eroded OC is directly or indirectly delivered to the nearshore zones through press disturbances such as hillsplope thermokarst [Vonk et al., 2015], which strongly impacts the aquatic environments [Chin et al., 2016, Houben et al., 2016, Chipman et al., 2016, Kokelj et al., 2013]. Sustained increase of suspended sediments observed in the streams several years following the initiation of hillslope thermokarst suggests that dis-

turbances have a long-term effect on stream ecosystems [Lamoureux and Lafrenière, 2009, Lewkowicz, 2007]. The impact of these disturbances on aquatic ecosystems is reflected in the high proportion of old carbon measured in rivers within watersheds affected by hillslope thermokarst [Lamoureux and Lafrenière, 2009]. The displacement of OC from the land to the aquatic ecosystem favors anaerobic decomposition, accelerating mineralization and decreasing CH_4 release [Abbott and Jones, 2015, Abbott et al., 2014, Aufdenkampe et al., 2011].

The observed increase in the number of RTSs modifies the quantity of OC released to the nearshore zone, which have strong consequences on the environment [Vonk et al., 2015].
In Chapter 4, we show that hillslope thermokarst developing along the coast released a non-negligible amount of OC to the nearshore zone of the Beaufort Sea (Fig. 2.1). We estimated the volumes of sediment, ice, and OC eroded by the RTSs identified along the Yukon Coast. We found that these RTSs released an average of 0.6 x 10^3 kg m^3 yr^{-1} of material to the nearshore zone. The annual OC flux released by 17% of the RTSs identified along the coast in 2011 was 0.6% of the annual OC flux from coastal retreat calculated in [Couture, 2010]. A large part of these fluxes (89%) originated from ice thrust moraines, where the number of RTS initiated after 1972 was highest. However, the landforms we investigated were on average smaller than other coastal RTSs [Segal et al., 2016], therefore the release of material from RTSs that we calculated are underestimating the real impact of RTSs on the nearshore zone.

Terrestrial OC plays a major role in Arctic estuarine food webs. It can contribute as much as 30–50% of the dietary requirements of fish species [Dunton et al., 2006]. Important quantities of the material and OC mobilized through coastal RTSs are transported to the nearshore zone through streams [Vonk et al., 2015]. However, part of the material and OC eroded by thermokarst is deposited along hillslopes. About 5% of the sediments eroded from RTS headwalls accumulates in the slump floors [Obu et al., 2017a]. There, SOM is subject to rapid degradation due to mineralization by microorganisms, as indicated by significant decreases in C:N ratios in the RTSs floor [Tanski et al., 2017]. Hence, OC is mobilized in RTSs prior to its release to the ocean [Cassidy et al., 2016, Pizano et al., 2014], which modifies the amount of OC exported to the coastal ecosystem [Tanski et al., 2017].

2.3 Thermokarst impacts the distribution of soil organic carbon along hillslopes

Hillslope thermokarst landforms erode surfaces, scar the landscape, and displace sediments from up- to downhill [Berhe et al., 2007]. Active hillslope thermokarst landforms and minor disruptions on the land in headwater locations deliver large quantities of material to streams and to the sea [Bowden et al., 2008, French, 2007]. The resulting

sediment transfer from terrestrial to aquatic ecosystems causes increased stream turbidity and concentration of total suspended sediments [Kokelj et al., 2013]. It impacts the aquatic ecosystem by modifying the geochemistry of the streams [Malone et al., 2013] and by decreasing freshwater invertebrate communities [Chin et al., 2016].

As shown in Chapter 4, individual active disturbances have the potential to transport up to 10^6 m^3 of sediments from up- to downhill, modifying slope morphology and drainage networks [Kokelj et al., 2015a, Lacelle et al., 2015]. As a result of downslope soil transport – through soil creep, slump and fluvial processes, as well as accumulation of locally produced organic material - hillslopes commonly accumulate thick soil deposits at hilltoe position (Fig. 2.2 a) [Shelef et al., 2017, Berhe et al., 2007, Yoo et al., 2005]. Hillslope

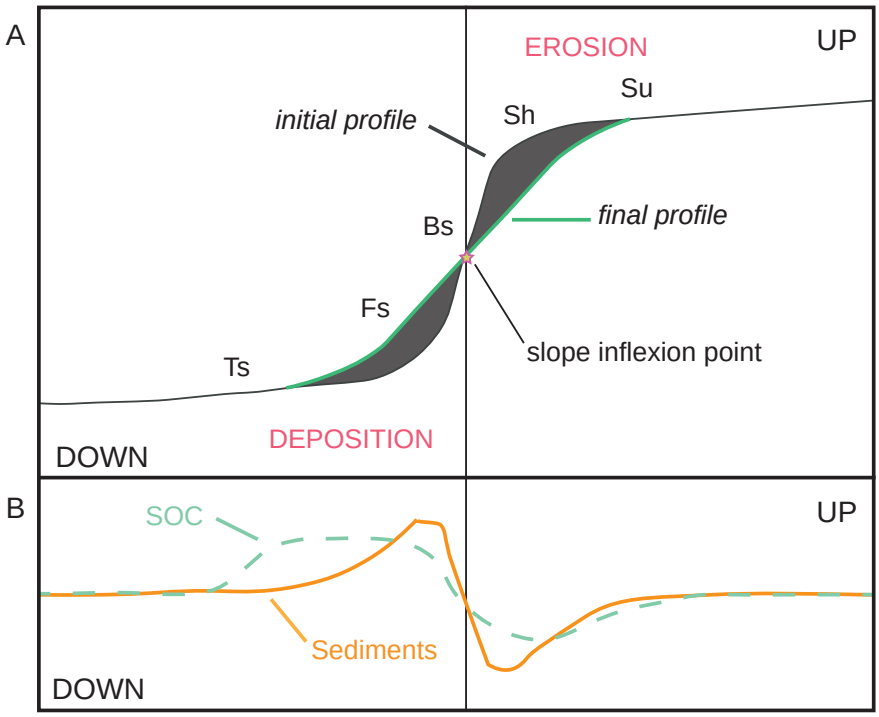

Figure 2.2 – Profile of a slope affected by erosion. A) Initial and final profiles of the slope. Slope units are described as: Su, Summit; Sh, Shoulder; Bs, Backslope; Fs, Footslope; Ts, Toeslope. B) Typical pattern of sediment and SOC redistribution following slope erosion. Adapted from [Rosenbloom et al., 2001]

thermokarst can displace between 6% and 51% of the initial organic-layer SOC and lead to a SOC and DOC decrease of 77% and 55%, respectively [Tanski et al., 2017, Abbott and Jones, 2015]. As a result, the Soil Organic Matter (SOM) significantly decreases in the impacted areas (Fig. 2.2 b). SOM redistribution leads to a decrease in ecosystem respiration in environments impacted by hillslope thermokarst [Abbott and Jones, 2015]. A large amount of these sediments are transported downhill, where they accumulate. There, soils are composed of a thin organic layer and a thick uniform mineral horizon, that lacks structure. On hilltoes, SOM decomposition is slowed down due to wetter and less oxygenated environments. As a result, SOM in depositional areas is preserved bet-

ter than in eroding landform positions and hilltoes accumulate large amount of SOC [Berhe et al., 2012].
However, as explained in Chapter 5, this pattern of soil redistribution and SOC accumulation is more complex. At the scale of hillslopes, SOC can be redistributed both horizontally and vertically in soils and this process represents a nonsteady state transfer of carbon from short to long residence time SOM pools [Rosenbloom et al., 2006]. There is a high variability in SOC storage along hillslopes and field observations taken along slope transects may overlook significant intraslope variations in SOC accumulation [Shelef et al., 2017, Rosenbloom et al., 2006].

In Chapter 5, we shed light on the impacts of hillslope thermokarst on the spatial distribution of SOC and TN storage. The study site is located in three V-shaped valleys on Herschel Island, where hillslopes predominate. We defined three transects, cutting each valley perpendicularly: in the upper, middle and lower parts of the valleys. Along each transect we established three to five sampling sites, chosen to be representative of each geomorphic unit (upland, midslope, hilltoe, floor). On each of the sites we sampled the active layer and the permafrost to a depth of 1 m and analyzed the soil geochemistry. Within geomorphic units, we found strong heterogeneity in the soils physical and chemical properties, distance to the shore and slope orientation. Soil profiles reflected different geomorphic processes that acted on the sites. The average SOC and TN 0-100 cm stocks in the valleys on Herschel Island were 26.4 ± 8.9 kg C m^2 and 2.1 ± 0.6 kg N m^2. These values are lower than previous estimates of mean SOC and TN 0-100 cm stocks for Herschel Island [Obu et al., 2017b, Siewert, 2016], and correspond to the stocks found in strongly disturbed terrain [Obu et al., 2017b]. SOC stocks were higher on the uplands compared to the slopes, but with a strong heterogeneity between sites. We showed that differences in soil properties explained the variability in SOC and TN stocks. Differences in the levels of cryoturbation and volumetric water content were most influential on the SOC and TN stocks. Cryoturbation was previously identified as a major component in explaining the strong contrast in SOC density at meter to decameter scale on Herschel Island [Siewert, 2016].
The C:N ratios were significantly higher in the uplands and lower on the hillslopes, suggesting that SOM was more degraded downhill. Similar results were found in temperate environments indicating that soil erosion has important implications on the storage and stability of SOM in dynamic landscapes [Berhe et al., 2012, Rosenbloom et al., 2006].

Alteration of soil properties on hillslopes is amplified by changes in hydrology, vegetation and snow cover in the areas impacted by hillslope thermokarst [Kokelj and Lewkowicz, 1998, Lamoureux and Lafrenière, 2009, Cray and Pollard, 2015]. For example, in the active and recently stable stages of RTS activity, there is a change in species composition characterized by an increase in low-diversity, grass-dominated vegetation communities [Cray and Pollard, 2015]. The effect of RTSs on vegetation composition persists over centuries [Cray and Pollard, 2015] and has a significant effect on the carbon balance of tundra systems. Through these changes, RTSs affect the Net Ecosystem Exchange

(NEE) of CO_2 in high Arctic tundra and modify the role of the high Arctic tundra system from a sink to a source of CO_2 during the majority of the growing season [Cassidy et al., 2016]. Hillslope thermokarst can also affect snow accumulation and impact the hydrology on the slopes. For example, active layer detachments scars trap greater amounts of snow, leading to increased surface runoff coefficients during snowmelt [Kokelj and Lewkowicz, 1998].

2.4 Outlook

Permafrost thaw in lowland Arctic regions is enhanced by increased air temperatures. Upon thawing, soil microorganisms are triggered and may release large quantities of GHG to the atmosphere that in turn contributes to the increase in air temperatures. This positive permafrost feedback is now well known [Schaefer et al., 2014, Schuur et al., 2008, Schuur et al., 2015]. However, the intensity of the feedback partly depends on the storage and availability of OC in permafrost soils. On gently sloping surfaces, thawing of permafrost through thermokarst processes leads to the redistribution of large quantities of sediments, nutrients and OC from up- to downslope. However, this redistribution is not well constrained. Commun pattern of soil erosion shows that OC storage decreases in eroded zones and increases in accumulation zones (Fig. 2.2) [Shelef et al., 2017, Rosenbloom et al., 2001]. However, this is challenged by the differences in soil properties, vegetation recovery rates, and soil burial processes that impact SOC turnover [Rosenbloom et al., 2006].

In this thesis, we highlight the major impact of hillslope thermokarst on the coastal fringe (Chapter 3) and nearshore carbon budget (Chapter 4), as well as the uncertainties in the redistribution of this carbon across the landscape (Chapter 5).
We attributed part of these latter uncertainties to differences in soil properties, ground ice contents and type of thermokarst landform occuring along hillslopes. Thermokarst landforms vary in shape and size, depending on the environment on which they are triggered and they develop in response to complex environmental changes.
We show in Chapter 5 that the distribution of SOC along hillslope is complex. There is a need to better relate the physical mechanisms that control SOC turnover (inputs and decomposition) to hillslope thermokarst in permafrost terrains. Identifying specific geomorphological processes that act along hillslopes will allow us to better constrain their impact on soil redistribution and SOC turnover, both horizontally and vertically.

3 Terrain Controls on the Occurrence of Coastal Retrogressive Thaw Slumps along the Yukon Coast, Canada

3.1 Abstract

Retrogressive Thaw Slump (RTS)s are among the most active landforms in the Arctic; their number has increased significantly over the past decades. While processes initiating discrete RTSs are well defined, the major terrain controls on the development of coastal RTSs at a regional scale are not well constrained. Our research reveals the main geomorphic factors that determine the development of RTSs along a 238 km coastal segment of the Yukon Coast, Canada. We 1) show the current extent of RTSs, 2) ascertain the factors controlling their activity and initiation, and 3) explain the differences in the density and areal coverage of RTSs. We mapped and classified 287 RTSs using high-resolution satellite images acquired in 2011. We highlighted the main terrain controls over their development using univariate regression trees. Both activity and initiation of RTSs were influenced by coastal geomorphology: active RTSs and RTSs initiated after 1972 occurred primarily on terrains with slope angles greater than 3.9° and 5.9°, respectively. The density and coverage of RTSs were constrained by the volume and thickness of massive ice bodies. Differences in coastal erosion rates along the coast did not affect the model. We infer that coastal erosion rates averaged over a 39-year period are unable to reflect the complex relationship between RTSs and coastline dynamics. We emphasize the need for large-scale studies of RTSs – to evaluate their impact on the ecosystem and to measure their contribution to the global carbon budget.

3.2 Introduction

Permafrost degradation processes are highly dynamic and profoundly reshape Arctic landscapes. Disturbances caused by ground subsidence and collapse (thermokarst and thermal erosion) induced by these processes can greatly affect the tundra ecosystem [Kokelj et al., 2013, Malone et al., 2013, Lantz et al., 2009]. Dynamic degrading permafrost landforms represent major sources of instability, affecting biomass and hydrologic fluxes in the Arctic [Abbott et al., 2016]. Thermokarst landforms develop when ice-rich permafrost thaws. Retrogressive thaw slumps (RTSs) are a type of slope failure, which are amongst the most dynamic thermokarst landforms in the Arctic. These slope failures can be initiated following active layer detachment, lateral and thermal erosion along the coast [Kokelj and Jorgenson, 2013, Kokelj et al., 2009a, Lantuit et al., 2012a, Burn and Lewkowicz, 1990], expansion of thermoerosional gullies [Bowden et al., 2008], or wildfire [Lacelle et al., 2010]. RTS morphology comprises a vertical headwall, an inclined headscarp, a floor filled with flow deposits and a lobe that conveys thawed sediments downslope [Burn and Lewkowicz, 1990].

The number of RTSs has increased considerably across the Arctic in the last decades [Brooker et al., 2014, Lantuit et al., 2012b, Lacelle et al., 2010, Kokelj et al., 2009a, Lantuit and Pollard, 2008, Lantz and Kokelj, 2008], mostly in ice-rich permafrost terrains located on the ice marginal glaciated landscapes [Kokelj et al., 2017]. Studies describing the dynamics of inland RTSs, occurring on plateaus [Segal et al., 2016, Lacelle et al., 2015, Brooker et al., 2014, Lacelle et al., 2010], in deltas, and along lakeshores [Kokelj et al., 2009a, Lantz and Kokelj, 2008] have shown that RTSs have increased in both size and number. Moreover, their headwalls have retreated extensively over the past decades [Lantuit and Pollard, 2005, Lewkowicz, 1987a]. These disturbances have a considerable impact on the surrounding ecosystems, strongly affecting terrestrial [Tanski et al., 2016, Cray and Pollard, 2015, Cannone et al., 2010, Lantz et al., 2009, Lantz and Kokelj, 2008] and aquatic ecosystems [Chin et al., 2016, Houben et al., 2016, Chipman et al., 2016, Kokelj et al., 2013] by reworking sediments and mobilizing carbon, nitrogen and nutrients.

RTSs can go through several cycles of activation and stabilization. Many RTSs are polycyclic; they superimpose on surfaces previously affected by RTS activity. Polycyclicity is associated with the destabilization of formerly stabilized surfaces, when incompletely melted massive ground ice is being re-exposed by erosional processes [Lantuit and Pollard, 2008, Burn, 2000]. In coastal settings, polycyclicity occurs when coastal and surficial erosion or changes in the physical properties of the sediments expose massive ice bodies to solar radiation and sensible heat [Lantuit et al., 2012b, Lantuit and Pollard, 2008].

While climatic factors influence the development of RTSs [Kokelj et al., 2015b, Balser et al., 2014, Lantz and Kokelj, 2008], their impact only becomes decisive in a certain

geomorphic context [Kokelj et al., 2017, Kokelj et al., 2009b]. For example, the effect of incoming solar radiation on the permafrost greatly varies depending on slope aspect and ground ice content [Lacelle et al., 2010, Lewkowicz, 1988]. Precipitation influences the activity of RTSs through its impact on the surficial flow on gently sloping scar zones: increased surficial flow allows maintaining RTSs activity and therefore contribute to the occurrence of larger RTSs [Kokelj et al., 2015b]. In coastal environments, RTSs are undergoing a period of enhanced activity since the 1950s [Segal et al., 2016, Kizyakov et al., 2013, Lantuit et al., 2012b, Lantuit and Pollard, 2005, Wolfe et al., 2001]. Sixty five percent of Arctic coasts are unlithified and characterized by high ice contents [Lantuit et al., 2012b], which are subject to erosion and slumping. Along the Canadian Beaufort Sea, 60% of the coast which is comprised of unconsolidated sediments is eroding [Harper, 1990]. Wave energy, through its impact on coastal erosion likely plays a major role in RTSs initiation [Lantuit et al., 2012a, Jones et al., 2008, Mars and Houseknecht, 2007]. As it is the case for inland RTSs, coastal RTSs are rather triggered by shoreline erosional processes rather than by changes in air temperature [Lacelle et al., 2010]. Therefore, the reported accelerating rates of coastal erosion in the Arctic [Barnhart et al., 2014, Overduin et al., 2014, Jones et al., 2009] likely influence coastal RTS dynamics. In turn, the variability of short-term shoreline dynamics in the Arctic is partially influenced by mass-wasting processes acting along permafrost coasts since coastal RTSs greatly contribute to the release of sediments from land to the nearshore zone in the Arctic [Tanski et al., 2017, Obu et al., 2017a, Lantuit and Pollard, 2005].

The impact of coastal erosional processes on coastal RTSs has been reported in previous studies [Obu et al., 2017a, Lantuit et al., 2012a]. We hypothesize that coastal erosion rates will emerge as the most decisive factor in the development of coastal RTSs. However, one must understand the impacts of coastal erosion processes on a regional scale in order to reach a conclusive insight. Using statistical analyses, our research provides new understanding of the distribution and dynamics of coastal RTSs. It highlights the main geomorphic factors influencing the development of RTSs along a 238 km coastal segment of the Yukon Coastal Plain, Canada. We 1) describe the current extent of RTSs, 2) ascertain the factors controlling their activity and initiation, and 3) explain differences in the density and areal coverage of RTSs. Our findings will help predict the future evolution of RTSs and their potential impacts on the coastal ecosystem.

3.3 Study area

The study area comprises a 238 km-long coastal segment of the Yukon Coastal Plain including Herschel Island, Canada (Fig. 3.1). The Yukon Coastal Plain is an erosional surface underlain by unconsolidated glacial and glacial-marine deposits, which accumulated during the Pleistocene and Holocene [Rampton, 1982]. The study area is located at the interface between the easternmost part of Beringia (Fig. 3.1) – unglaciated during the Late Wisconsin (MIS 2) – and the westernmost margin of the Laurentide

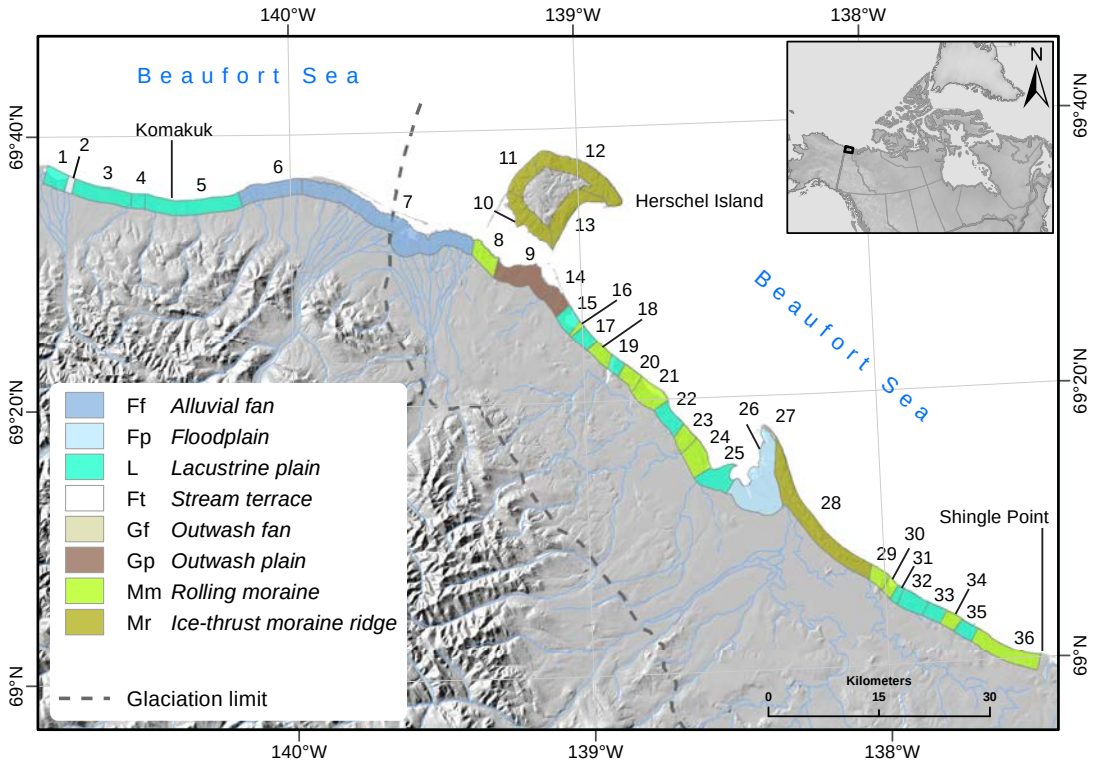

Figure 3.1 – Location of the study area. The numbers represent the coastal segments stretching along the coast from west to east. The limit of the glaciation was reproduced after [Dyke and Prest, 1987] and the surficial sediments after [Rampton, 1982].

ice sheet, which reached a maximum ice extent at ca. 16 200 years BP [Fritz et al., 2012]. The overall landscape reflects this history. The formerly non-glaciated part of the Yukon Coastal Plain is gently sloping and only incised by stream valleys, fluvial deltas, alluvial fans and thermokarst basins. The formerly glaciated part is underlain by ice-rich permafrost and has a heterogeneous topography, comprising areas of ice-rich permafrost of glacial origin and moraine deposits highly reworked by periglacial processes. Ice-rich cliffs constitute 35% of the coast [Harper, 1990]. Herschel Island is a moraine thrust deposited at the margin of the glaciated area, located 2 km off the Yukon mainland coast. It is one of the largest moraine deposits in the area, consisting of unconsolidated and fine-grained marine and glacigenic sediments [MacKay, 1959, Pollard, 1990]. On average, 30% to 60% of Herschel Island is composed of ground ice, mostly expressed as massive ice [Lantuit et al., 2012a, Pollard, 1990, Rampton, 1982].

Available air temperature records (from west to east: Komakuk Beach, Herschel Island and Shingle Point) are similar across the study area throughout the year [Burn and Zhang, 2009]. The meteorological stations located at the extremities of the study area – Komakuk Beach in the west and Shingle Point in the east – recorded highly correlated air temperatures ($r^2 > 0.90$ for most months) between 1995 and 2007 [Burn and Zhang,

2009]. The mean summer air temperature (June, July and August, 1971-2000) is 6.0°C at Komakuk and 8.7°C at Shingle Point [1]. Precipitation is the main climatic difference between the two stations. Komakuk Beach receives an average summer precipitation of 79.8 mm, while 112.9 mm of precipitation falls at Shingle Point (June, July, August, 1971-2000)[1]. The influence of the Mackenzie River on seawater temperature and sea ice extent is the main forcing on the local precipitation patterns [Burn and Zhang, 2009]. The western Yukon Coast is undergoing widespread coastal retreat [Harper, 1990]. The mean annual erosion rate between Komakuk Beach and Shingle Point was -1.2 m per year between 1951 and 2009. There is a general spatial pattern of decreasing erosion rates from west to east along the Yukon Coast [Konopczak et al., 2014].

The study area is divided into 36 coastal segments (Fig. 3.1), derived from the Arctic Coastal Dynamics Database [Lantuit et al., 2012a, Lantuit and Pollard, 2005] and refined by Couture to account for ground ice, surficial geology and geomorphology [Couture, 2010]. Coastal heights range from 0.5 m to 27.6 m (Appendix A.1, ds03) and average slopes are between 0° and 22°. Ten of the segments are protected from direct wave influence by spits and barrier islands. Estimates of the volume of ground ice in the different coastal segments along the coast come from the model developed by Couture and Pollard [Couture and Pollard, 2017]. The model takes into account 14 input variables including soil characteristics, measured volumetric ice contents and geomorphic information. Ground ice varies between coastal segments; occurring as massive ice, pore ice and wedge ice, and ranges from 0% to 74% [Couture and Pollard, 2017]. The heterogeneity of coastal segments, including the surficial geology, is inherited from the glacial history of the area. Most of the segments fall into one of three surficial geology units: ice-thrust moraines (30%); lacustrine plains (23%) and rolling moraines (16%). The remaining segments (30%) are underlain by alluvial fans, stream terraces, floodplains and outwash plains [Rampton, 1982].

3.4 Methods

3.4.1 Mapping of retrogressive thaw slumps and landform classification

We manually digitized each RTS at a 1:2000 scale using ArcMap (ESRI, version 10.3) from high-resolution satellite images acquired in July (13^{th} and 18^{th}), August (31^{st}) and September (13^{th}) 2011 (multispectral GeoEye-1 and WorldView-2 – 1.8 m resolution in multi-spectral and 0.5 m in panchromatic view). We exclusively mapped coastal RTSs, which we defined as features occurring within 500 m of the coast.
We classified RTSs according to their activity (Fig. 3.2). Active RTSs are characterized by steep headwalls exposing ice-rich permafrost, slump floors with thawed sediments and incised gullies. Stable RTSs comprise gently sloping and vegetated headwalls, vegetated

[1] Environment Canada,http://climate.weather.gc.ca/historical_data/search_historic_data_e.html,2017

slump floors and no visible active gully systems [Lantuit and Pollard, 2008, Wolfe et al., 2001]. Stable polycyclic RTSs include the areas of active RTSs located within their boundaries. We additionally classified RTSs according to their initiation date, defining RTSs

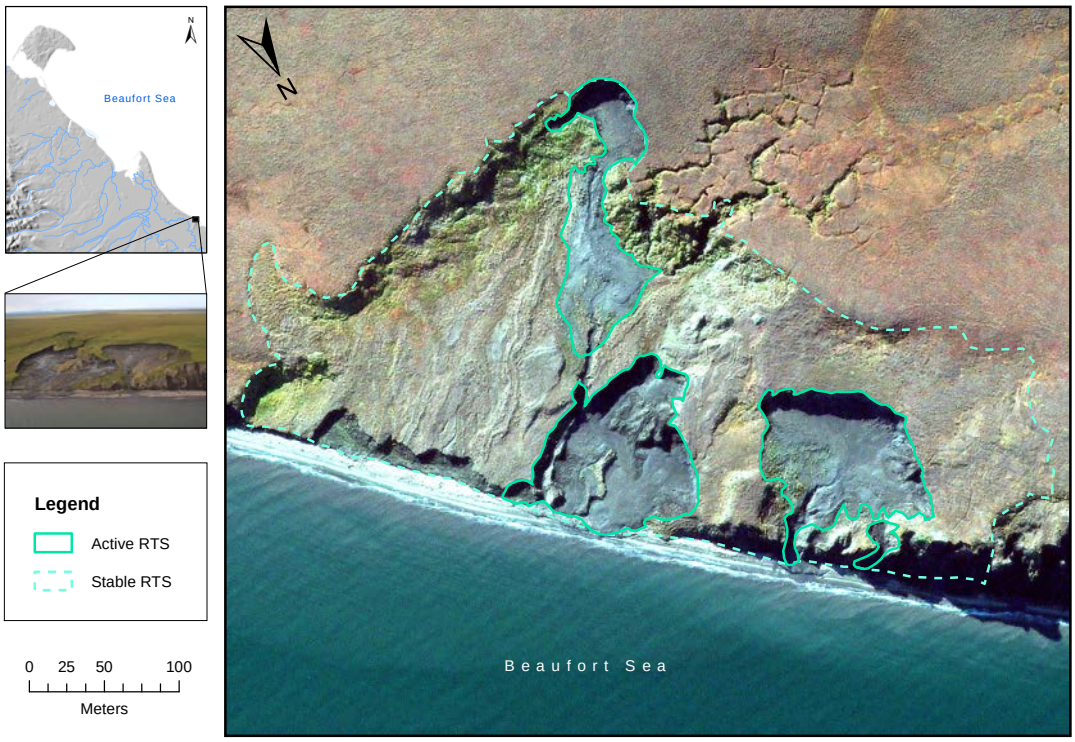

Figure 3.2 – GeoEye image from July 18^{th} 2011 illustrating the differences between active and stable Retrogressive Thaw Slump (RTS)s. The depicted RTS is located in the eastern part of the study area, at King Point (segment 32). The oblique photograph was taken from a helicopter during fieldwork in July 2015.

initiated after 1972 as occurring on surfaces that had never been affected by slumping processes before the 1970s. For this purpose, we used a series of 21 aerial photographs from 1972 and one photograph from 1976 (Appendix A.1, ds05), which jointly cover the entire study area (National Air Photo Library, Canada) and geo-coded all images to the 2011 satellite images using PCI Geomatic's Geomatica Orthoengine© software. Again, RTSs were digitized in ArcGIS 10.3 at a 1:2000 scale. The aerial photographs have a resolution of 3 m (Appendix A.1, ds05). We distinguished between two kinds of RTSs. The first class comprised RTSs initiated after 1972, identified in 2011 on surfaces that were not affected by slumping on the historical aerial photographs. All the other RTSs (i.e. RTSs already detectable in 1972) were put into the second class. Even if we were not able to define the specific date of RTS initiation, the distinction between RTSs that initiated after 1972 and other RTSs allowed us to better understand RTS dynamics related to polycyclic activity. The use of different imagery for mapping RTSs might have affected the size of the RTSs that were detectable and introduced some limitations related to accuracy. However, differences in resolution between aerial photographs and satellite

imagery were ca. 1.2 m and were deemed satisfactory for interpretation and mapping purposes.

3.4.2 Environmental variables

Environmental data that we used include local geomorphic parameters and coastal erosion rates. We did not take into account climatic factors. Geomorphic parameters and erosion rates are derived from various sources with different temporal and spatial resolution. For consistency, we refined the boundaries of the coastal segments defined by [Couture, 2010] based on the satellite imagery from 2011.

RTS characteristics

Using ArcMap 10.3, we derived RTS morphologies (Table 3.1, RTS characteristics) and extracted morphological and spatial information for each coastal segment (Table 3.1, spatial information) from an airborne LiDAR dataset acquired in July 2013 [Kohnert et al., 2014]. The LiDAR dataset has a final georeferenced point cloud data vertical accuracy of 0.15 ± 0.1 m and covers most of the study area, with a scan width of 500 m. While visible on the satellite images, a total of 39 RTSs occurred in areas outside of the area covered by the LiDAR so we discarded those features from further analyses. RTS characteristics (Table 3.1) summarize the morphologic information for the area within each RTS shapefile. The mean elevation above sea level (Z_MEAN) provides information about the relative elevation of the slump floor of a RTS (Fig. 3.3). We used the mean slope of the slump floors (S_MEAN) as an indicator of the potential for removal of material from the slumps (Fig. 3.3).

Spatial information

Information concerning the coastal segments on which the RTSs developed is summarized in the spatial information (Table 3.1). This information was calculated using the high-resolution satellite imagery, except for the mean cliff heights and coastal slopes, which we derived from the LiDAR dataset. The mean cliff height represents the mean values of elevation points 25 m inland from the shoreline, measured along transects placed every 100 m within a coastal segment. Elevation points that fell within a RTS were discarded. Coastal change rates from 1972 to 2011 were measured using the Esri ArcGIS extension Digital Shoreline Analysis System (DSAS) version 4.3 [Thieler et al., 2009] applied on the satellite imagery from 2011 [Irrgang et al., 2018].

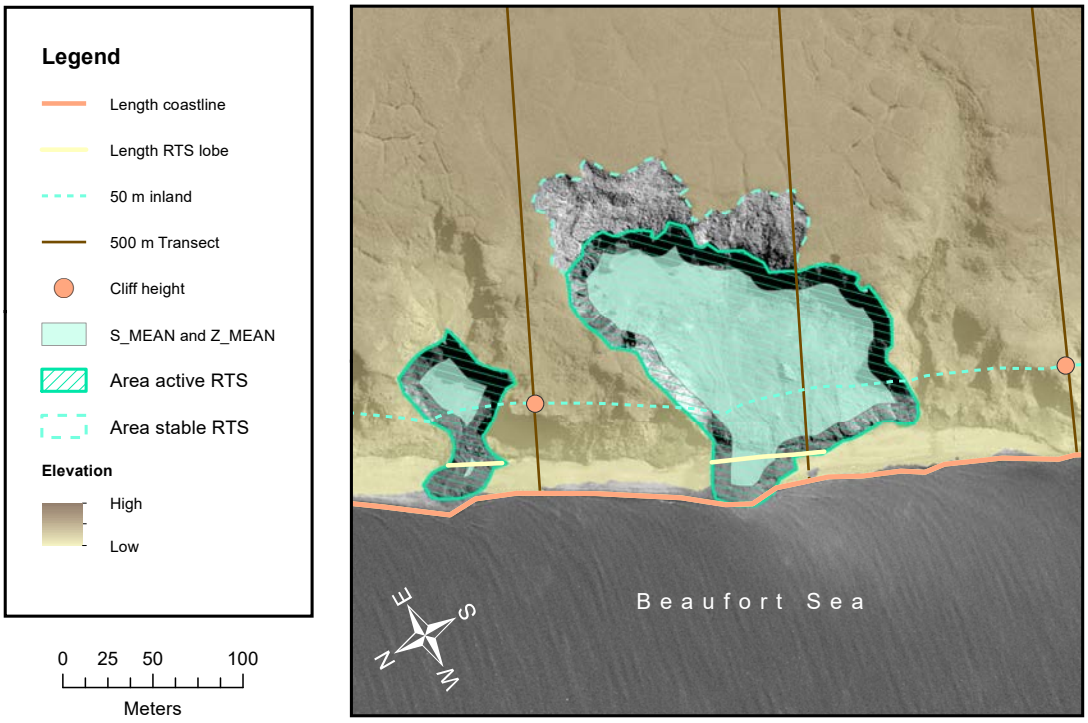

Figure 3.3 – Scheme of Retrogressive Thaw Slump (RTS)s with their characteristics. All elevation data were derived from the LiDAR dataset. The length of the coastline (CoastL) was manually digitized for the entire study area. RTS lobe width was defined as the part of the RTS that intersect the shoreline. RTS elevation (Z_MEAN) and slope (S_MEAN) were calculated for the RTS floor while the area of the RTS included the whole surface including the headwall. The cliff heights (CH) were defined for each segment as points located on transect every 100 m along the coast, 25 m inland. The segment slopes (S500) were an average of the slopes calculated for a whole segment, starting from 25 m inland to 500 m.

Terrain characteristics

In addition to the spatial information, we used terrain characteristics from a study from Couture (see Data S1 in Appendix A.1)[Couture, 2010]. Terrain characteristics for each segment were either derived from direct measurements from bluff exposures and shallow cores or were estimated from published datasets. Couture and Pollard quantified ground ice at a landscape level and provided ice contents (volumes of each type of ice - pore ice, wedge ice and massive ice, volumetric ice content and volume of excess ice), for each coastal segment [Couture and Pollard, 2017]. The variable "Thickness of massive ice" (DMI) was estimated by subtracting the depth to the top of massive ice bodies (Dm) in a coastal segment from the depth to the bottom (Dbm) (Table 3.1). When the bottom of the massive ice was buried under reworked sediments, it was assumed to extend to the base of the bluff [Couture, 2010].

Table 3.1 – Summary of spatial information and terrain parameters extracted for each coastal segment. The data was calculated for this study based on satellite imagery from 2011, aerial photographs from 1972 and LiDAR dataset from 2013 or derived after (a) Rampton [1982] and (b) Couture [2010]. Environmental variables used as response variables in the model are indicated in bold. See Appendix A.1, ds02 and ds03.

Variable Name	Description	Unit	Source
RTS CHARACTERISTICS			
Area_ha	Areal extent of a RTS	ha	Satellite imagery
Activity	Activity of the RTS in 2011: active or stable		Satellite imagery
Initiation	RTSs initiated after 1972 and their activity (active–stable)		Aerial photographs
Azimuth	**Orientation of the RTS**	°	Satellite imagery
Z_MEAN	Mean height within the slump floor of a RTS	m (asl)	Lidar
S_MEAN	Mean Slope within the slump floor of a RTS	°	Lidar
Coastal_le	Width of the RTS lobe	m	Satellite imagery
NEAR_DIST	Distance from the RTS to the shore	m	Satellite imagery
SPATIAL INFORMATION			
Segment_name	Name of the coastal segments		[b]
Glaciated	Glacial history—Yes: glaciated; No: nonglaciated		[b]
Geolunit	Surficial geology		[a]
Area	Areal extent of the coastal Segments	ha	Satellite imagery
CL	Coastal length	km	Satellite imagery
CH	**Cliff height: median of elevation points (25 m inland)**	m	Lidar
S500	**Slope 500 m: average slope calculated over 500 m inland**	°	Lidar
Spit	**Presence (1) or absence (0) of spit along the coast**		Satellite imagery
E50-11	**Erosion rate between 1952 and 2011**	m $yr^{-}1$	Satellite imagery
E70-11	**Erosion rate between 1972 and 2011**	m $yr^{-}1$	Satellite imagery
TERRAIN CHARACTERISTICS			
PEI	**Percentage of excess ice**	%	[b]
PIV	**Percentage of ice volume**	%	[b]
AL	**Active layer depth**	cm	[b]
e	**Soil porosity**	g cm^3	[b]
Dm	Depth to the top of massive ice	m (asl)	[b]
Dbm	Depth to the bottom of massive ice	m (asl)	[b]
DMI	**Thickness of the massive ice (Dbm-Dm)**	m (asl)	[b]
Wt	**Mean ice wedge width**	m (asl)	[b]
Ws	**Mean ice wedge spacing**	m (asl)	[b]
PI	**Pore ice**	%	[b]
WI	**Wedge ice**	%	[b]
MI	**Massive ice**	%	[b]

3.4.3 Univariate regression trees

Univariate regression tree models were fitted using R (The R Foundation, version 3.3.1) in order to characterize terrain controls on RTS distribution. We applied univariate regression trees (rpart package version 4.1-10, [Breiman et al., 1984]) to highlight the environmental parameters (explanatory variables) that explained most variation in RTS abundance (univariate response variables) and the main thresholds in the datasets. Response variables used in the models (Table 3.2) are univariate and were tested against 16 environmental parameters (Table 3.1). Through recursive partitioning, the regression trees repeatedly split the dataset into binary groups (Appendix A.1, ds01). Each split is defined by a simple rule, which minimizes the sums of squares within the two groups

formed by the split [Breiman et al., 1984]. The optimal tree size was determined by the complexity parameter, which is used when pruning the tree to minimize the mean relative square error. This method is robust and can incorporate dependent variables as well as discrete data [De'ath and Fabricius, 2000]. The scripts are available in the Appendix A.1.

Table 3.2 – List of the response variables used in the univariate regression tree algorithms. The response variables are given for each coastal segment.

Response Variables	Explanation
Density	Number of RTSs / coastal length
Coverage	(Sum of surface areas of RTSs / total surface area) * 100
Activity	Percentage of active RTSs
Initiation	Percentage of RTSs that initiated after 1972

3.5 Results

3.5.1 Characteristics of retrogressive thaw slumps

Distribution

Based on the 2011 satellite imagery, we detected 287 coastal RTSs along the Yukon Coast. All RTSs were located in the formerly glaciated part of the study area; more than half (53%) faced north-northeast, reflecting the general orientation of the coast. In total, 12% (28.1 km) of the entire coastline was incised by RTS lobes, which had a median width of 31 m. The size of RTSs varied both over the entire area and within the coastal segments (Fig. 3.4). The median size was 0.24 ha (mean = 1.52 ha) (Table 3.3). The largest RTS was observed on Herschel Island East (segment 13, 20.81 ha), the smallest at Stokes Point West (segment 20, 0.01 ha). On average, the largest RTSs were found on ice-thrust moraines (med = 0.27 ha, range = 20.80 ha) and lacustrine plains (med = 0.20 ha, range = 13.60 ha), while the smallest RTSs occurred on rolling moraines (med = 0.17 ha, range = 14.65 ha).

Table 3.3 – main characteristics of Retrogressive Thaw Slump (RTS)s derived from the Lidar dataset. RTSs are subdivided between active and stable and further information is given for the RTSs that initiated after 1972

Type	N	Size (ha, med, range)	Slope (°, mean)	Aspect (°, med)	Lobe Width (m, med, range)
Active	203	0.15, 20.8	15.3 ± 6.7	NE, 45.8	29.3, 1109
Stable	84	1.09, 19.9	13.3 ± 4.2	NE, 48.2	40.5, 963
All	287	0.24, 20.8	14.7 ± 6.1	NE, 46.7	31.1, 1109
Initiated after 1972	119	0.16, 16.7	11.3 ± 9.4	NE, 49.7	26.1, 1024

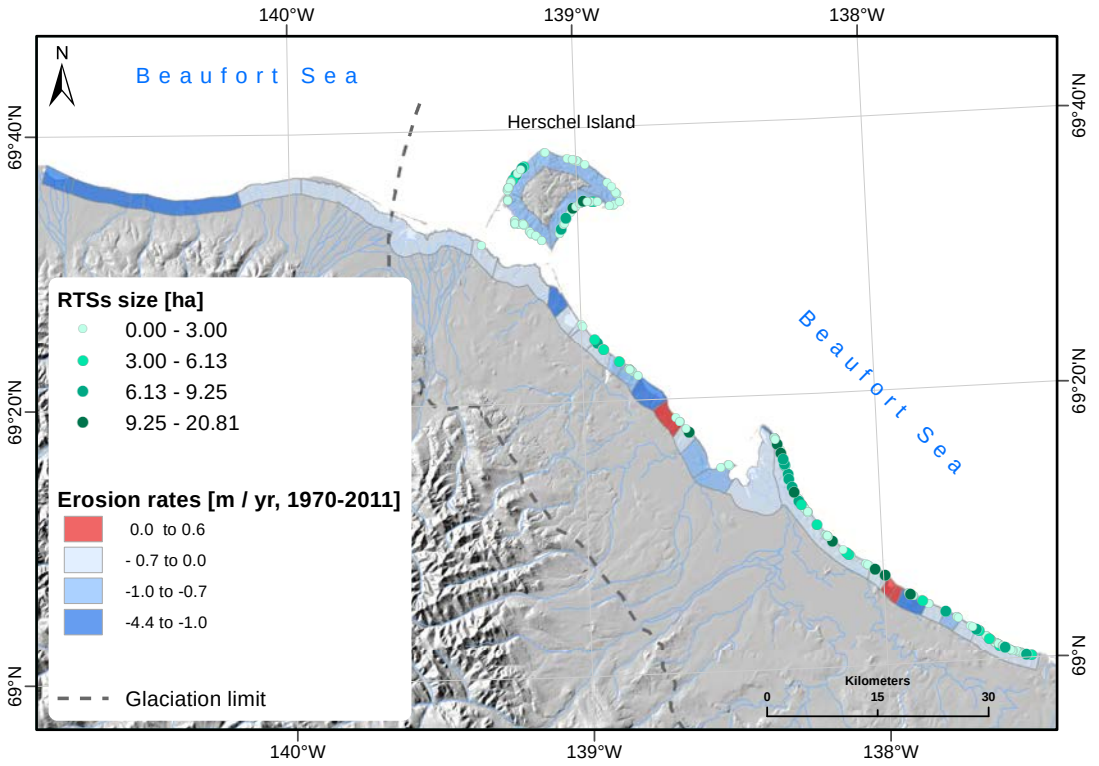

Figure 3.4 – Distribution of Retrogressive Thaw Slump (RTS)s according to their size and coastal erosion rates between the 1970s and 2011 along the study area. All RTSs were found in the eastern part of the study area, which was glaciated during the last glacial maximum. The largest RTSs were found on ice-thrust moraines. Rates of coastal change are described in Irrgang et al. [Irrgang et al., 2018].

Among the 287 RTSs, 203 (71%) were active and had clear morphological differences compared to the stable RTSs (Table 3.3): active RTSs were 7 times smaller (med = 0.15 ha) than stable RTSs (med = 1.09 ha), their floors had slightly steeper slopes, and they had narrower slump lobes (Table 3.3). In total, 119 of the 287 RTSs (41%) were initiated after 1972. Compared to the overall RTSs, RTSs initiated after 1972 were smaller (med = 0.18 ha), with gentler slopes and narrower slump lobes (Table 3.3). RTSs initiated after 1972 were found on 14 coastal segments. At Sabine Point West (segment 33) and Workboat Passage West (segment 8), the three observed RTSs initiated after 1972, and on Herschel Island North 77% of the RTSs initiated after 1972. In total, 51% of the RTSs occurring on ice-thrust moraines had developed since the 1970s, 35% of the RTSs initiated after 1972 on lacustrine plains and 24% of the RTSs initiated after 1972 on rolling moraines. Of the RTSs that initiated after 1972, 72 were active and 47 were stable in 2011 (Appendix A.1, ds02). Active RTSs that initiated after 1972 had most likely remained active until 2011. On the other hand, stable RTSs that initiated after 1972 went through a period of activity and stabilized within this period. Forty percent of the RTSs that initiated after 1972 were stable, which is higher than the percentage of stable RTSs (22%). RTSs were more active, or reactivated, where slumping processes had previously affected the coast. Active RTSs

that initiated after 1972 were smaller than stable RTSs that initiated after 1972 (0.10 ha vs. 0.68 ha), had steeper slopes (16.4° vs. 12.6°) and narrower slump lobes (20.7 m vs. 46.0 m).

Terrain factors controlling the activity and initiation of retrogressive thaw slumps

Both the activity and the initiation of the RTSs were related to the geomorphology of the coastal segments (Fig. 3.5). The slope (S500) and coastal height (CH) were the primary factors controlling the activity of RTSs (Fig. 3.5, a). The model did not show other factors because their contribution was not significant. Most of the active RTSs (n = 200, 98%) were found in coastal segments (n = 21) with a slope angle greater than 3.9°. Of these 200 active RTSs, 149 (74%) were found within coastal segments (n = 9) with cliff heights higher than 11.0 m. The median cliff height in the latter segments was 15.5 m.

RTSs initiated after 1972 (Fig. 3.5, b) occurred mainly on segments with a slope equal to or greater than 5.0°. We observed only two RTSs initiated after 1972 on a segment with a smaller slope angle (1.8°): Philips Bay (segment 25). However the mean slope did not represent the area on which RTSs occurred, because this coastal segment is characterized by the presence of different coastal types: the western and eastern parts of the segment are bay areas, protected by spits. RTSs were observed along the central part of the segment, a north-facing coast open to the sea. The average slope angle on which RTSs occurred was 9.2°, while RTSs initiated after 1972 occurred on steeper slopes, with an average angle of 10.6°.

3.5.2 Density and areal coverage of retrogressive thaw slumps

Differences among coastal segments

Along the entire Yukon Coast, RTSs occurred with a density of 1.2 RTSs per km of coast. However there was great heterogeneity, with RTSs present in only 19 of 36 segments. They all occurred within the formerly glaciated area (Fig. 3.6), where the mean density was 2.3 RTSs per km of coast. RTSs were most abundant at Shingle Point West and Stokes Point West (segments 36 and 20, 4.2 RTSs per km of coast). At Shingle Point West, 87% of RTSs were active while at Stokes Point West, active RTSs represented 42% of the total RTSs. The study area as a whole was characterized by active slumping; active RTSs (71%) were more abundant than stable RTSs in most of the coastal segments. Differences in the occurrence of RTSs were observed between geological units (Table 3.4). In total, 60% of the RTSs occurred on ice-thrust moraines with a density of 2.4 RTSs per km of the coast. In contrast, 29% of the RTSs occurred on rolling moraines with a density of 2.0 RTSs per km of coast, and 11% on lacustrine plains with a density of 0.6 RTSs per km of coast.

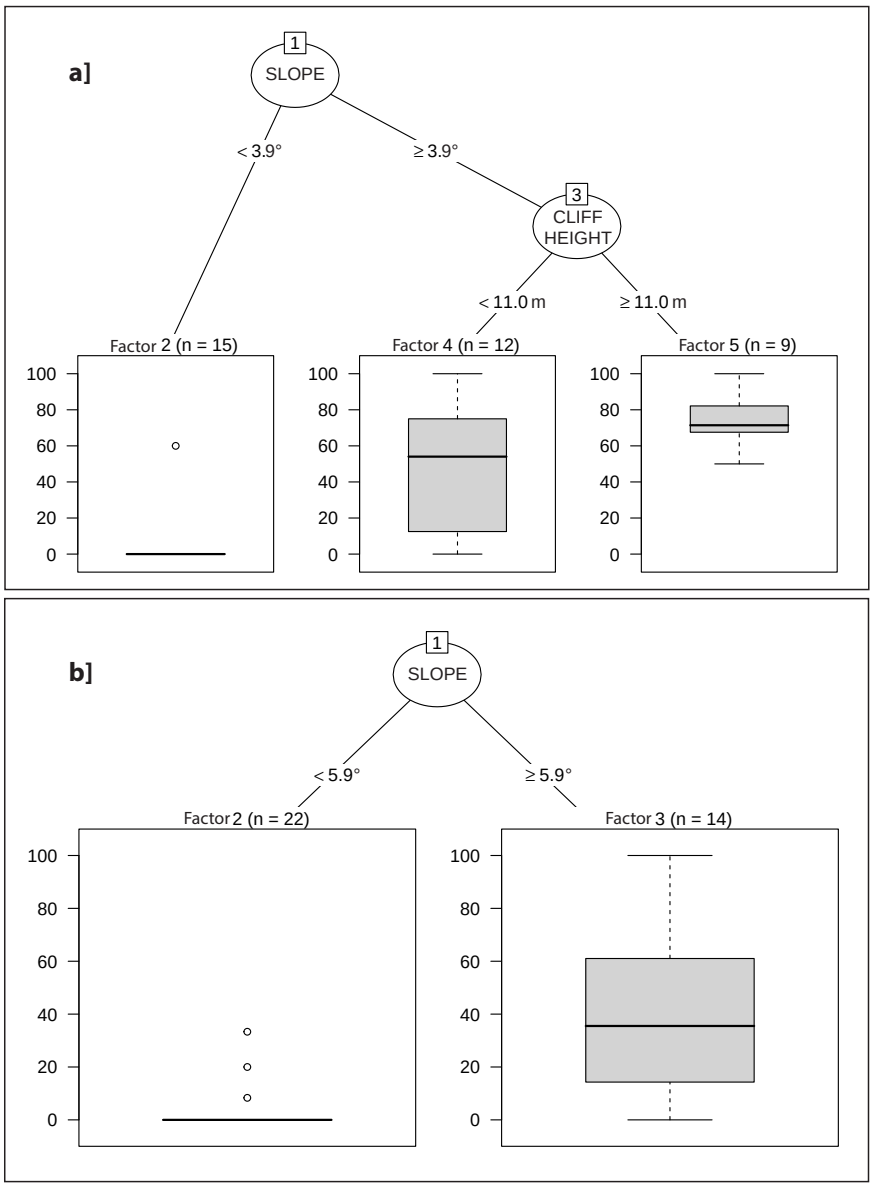

Figure 3.5 – Univariate regression tree relating (a) the activity and (b) the initiation of Retrogressive Thaw Slump (RTS)s to the 16 environmental variables used in the model; n indicates the number of segments included in each node. The slope and cliff height of the coastal segments were most influential in controlling both activity and initiation of RTSs. The box and whisker plots display variation in the activity and initiation of RTSs (%) for the segments (n) that fall in each node.

RTSs covered a total area of 401.8 ha, which represents 3% of the 500 m-wide and 238-km long study area strip and 7% when considering only the coastal segments where RTSs occurred. In all segments except Herschel Island East (segment 13), West (segment 11), North (segment 12) and on Sabine Point East (segment 35) the area covered by stable RTSs was two thirds larger than the area covered by active RTSs. The coverage of RTSs

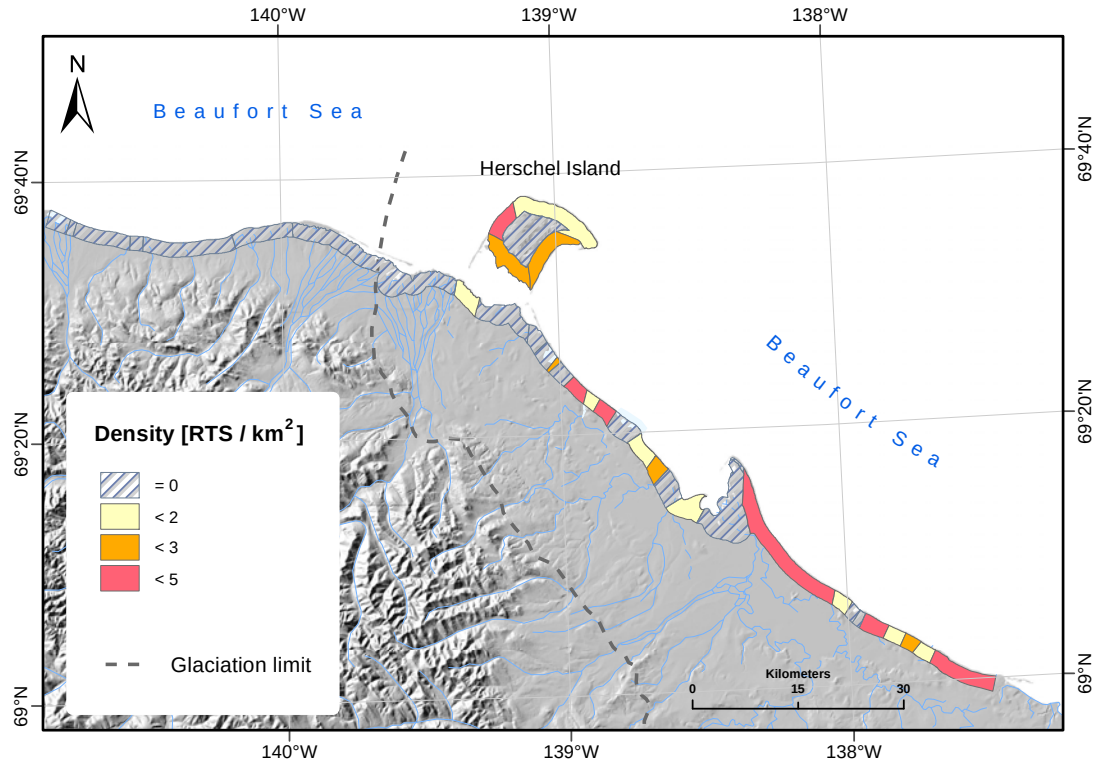

Figure 3.6 – Density map of Retrogressive Thaw Slump (RTS)s along the Yukon Coast. No RTSs were found in the unglaciated area. The density varied greatly among the segments in the glaciated area.

was heterogeneous: the area covered by RTSs was less than 1% in 4 segments and more than 10% in 8 segments. King Point North West (segment 29) had the largest coverage of RTSs: 6 RTSs (4 active and 2 stable) covered 16% of the segment area. Herschel South (segment 10) had the smallest area covered by RTSs relative to the number of RTSs occurring on this segment (1% coverage, 31 RTSs).

The total area occupied by RTSs that initiated after 1972 was proportionally smaller than the total area occupied by RTSs. Active RTSs represented 71% of the total number of RTSs and occupied 38% of the total area covered by RTSs while active RTSs that initiated after 1972 represented 25% of the total amount of RTSs and covered 4% of the total area covered by RTSs. Similarly, stable RTSs represented 29% of the total number of RTSs and occupied 62% of the total area covered by RTSs while stable RTSs that initiated after 1972 represented 16% of the total amount of RTSs and covered 20% of the total area covered by RTSs. Those results emphasize the difference in size between RTSs that initiated after 1972 and the others.

Table 3.4 – Number, density and coverage of Retrogressive Thaw Slump (RTS)s for each coastal segment. Abbreviations for the surficial geology are given in Table 3.1

Segment Number	Surficial Geology	Coastal Length (km)	Number of RTS (RTS/km of Coast)	Density of RTS (%)	Coverage of RTS
1	Ff	3.2	0	0.0	0.0
2	Ft	1.1	0	0.0	0.0
3	L	8.1	0	0.0	0.0
4	L	1.8	0	0.0	0.0
5	L	13.5	0	0.0	0.0
6	Ff	8.9	0	0.0	0.0
7	Ff	28.4	0	0.0	0.0
8	Mm	5.0	1	0.2	0.1
9	Gp	10.3	0	0.0	0.0
10	Mr	12.5	31	2.5	1.4
11	Mr	5.5	18	3.3	12.9
12	Mr	17.3	22	1.3	1.4
13	Mr	11.3	28	2.5	12.9
14	Gp	3.8	0	0.0	0.0
15	Mm	2.7	0	0.0	0.0
16	Mm	0.8	2	2.4	13.6
17	L	2.8	0	0.0	0.0
18	Mm	2.9	10	3.5	10.6
19	L	2.2	4	1.8	4.1
20	Mm	2.9	12	4.2	1.7
21	Mm	5.0	0	0.0	0.0
22	L	3.9	4	1.0	0.6
23	Mm	2.6	7	2.7	12.8
24	Mm	5.2	0	0.0	0.0
25	L	9.7	5	0.5	0.6
26	Fp	13.5	0	0.0	0.0
27	Gf	1.4	0	0.0	0.0
28	Mr	24.2	74	3.1	12.7
29	Mm	3.3	6	1.8	16.3
30	L	2.5	0	0.0	0.0
31	L	1.1	0	0.0	0.0
32	L	3.8	12	3.2	9.4
33	L	2.7	2	0.7	0.1
34	Mm	2.4	7	2.9	6.9
35	L	2.5	4	1.6	3.0
36	Mm	9.0	76	4.2	5.5

Terrain factors controlling the density and areal coverage of retrogressive thaw slumps

The main terrain factors controlling the density and coverage of RTSs are presented in Figure 3.7. The thickness of massive ice bodies within a coastal segment (DMI) was the main factor explaining the high density of RTSs (Fig. 3.7, a), whereas the percentage of massive ice by volume (MI) was the most influential factor for large coverage of RTSs (Fig. 3.7, b).

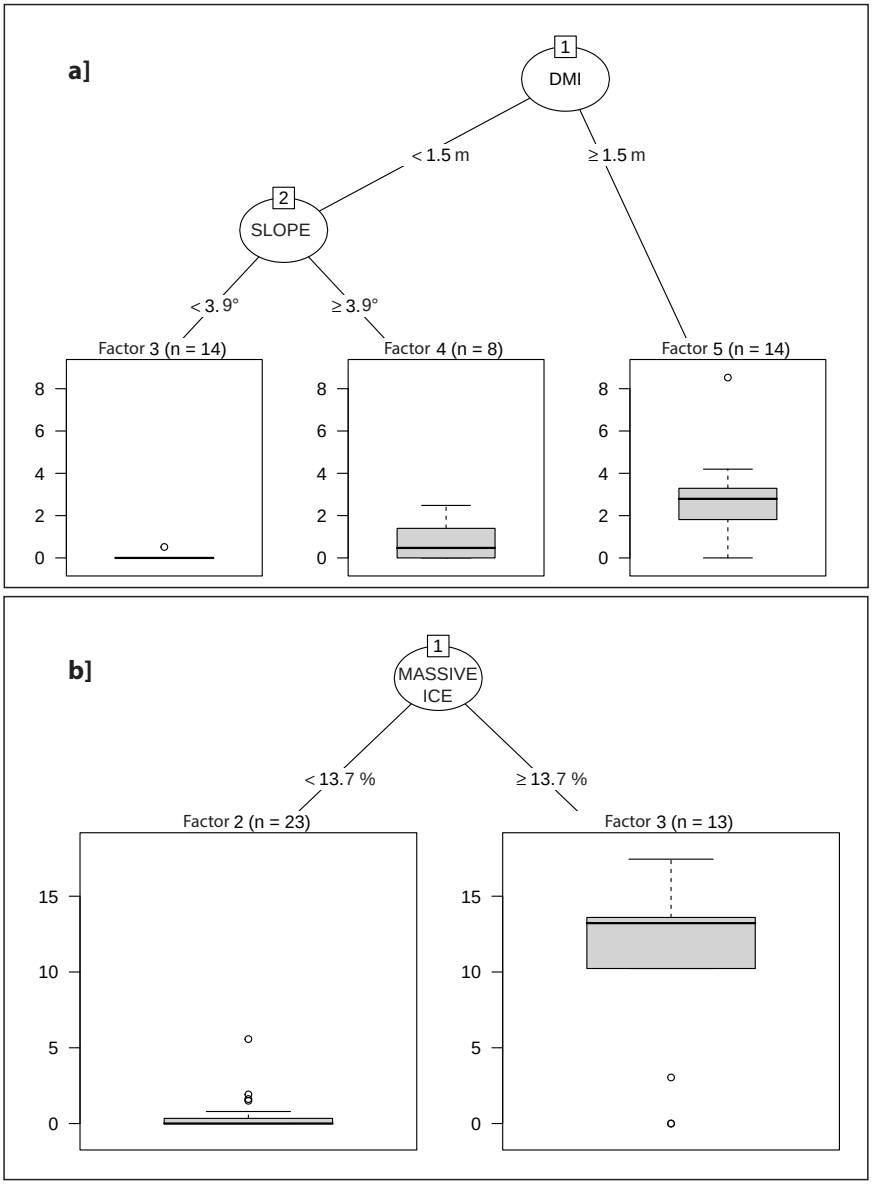

Figure 3.7 – Univariate regression tree relating (a) the density and (b) the areal coverage of Retrogressive Thaw Slump (RTS)s to the 16 environmental variables used in the model, n indicates the number of segments included in each node. (a) Ground ice characteristics (DMI, the thickness of the massive ice bodies, and the percentage of massive ground ice) were the most influential factors for explaining the density and coverage of RTSs. (b) Geomorphology (slope angle) was the factor, which explained the differences in coverage (ha) of RTSs. The box and whisker plots display the variation in coverage for the segments (n) that fall in each node. Secondary factors were not named because they were not considered having a relative importance by the model.

The model showed that high densities of RTSs were found in coastal segments that contained massive ice with an average thickness of more than 1.5 m (DMI > 1.5). This was

the case in 14 coastal segments and explained the occurrence of 240 RTSs (84%). In 22 coastal segments where massive ice was absent or less than 1.5 m thick – 47 RTSs (16%) – the slope angle was the main factor controlling the density of RTSs. Among those RTSs, 42 were located on segments which had a slope angle greater than 3.9°, with a median slope of 6.2. In one of the coastal segments (Philips Bay, segment 25, 5 RTSs), the occurrence of RTSs was not explained by either the thickness of the massive ice bodies or the degree of slope. However, as mentioned earlier, this coastal segment is characterized by the presence of different coastal types and average values might not reflect adequately the environment on which RTSs were occurring.
The main terrain control over the coverage of RTSs was the percentage of massive ice. RTSs affected a larger surface area of coastal segments that contained massive ice equal to or greater than 14%. For 13 coastal segments, mostly underlain by moraine deposits the massive ice was greater than 14%. Of those segments, 2 had no RTSs while 11% of the surface area of the remaining 11 segments was affected by RTSs.

3.6 Discussion

3.6.1 Characteristics and distribution of retrogressive thaw slumps

With a density of 1.2 RTSs per km of coast, the Yukon Coast is one of the Arctic areas most affected by retrogressive thaw slumping [Segal et al., 2016, Kokelj et al., 2015b, Lacelle et al., 2010].
The Yukon Coast is undergoing a period of active slumping: 71% of all mapped RTSs were active in 2011 and 60% of the total number of RTSs initiated after 1972. Our results confirm the observations made by Lantuit et al. and Wolfe et al. who show that RTSs increased greatly between 1970 and 2000 in some areas of the Yukon Coast: the number of RTSs increased by 22% on Herschel Island and by 25% along the eastern part of the Yukon Coast [Lantuit et al., 2012b, Wolfe et al., 2001].
With a median size of 0.16 ha, RTSs initiated after 1972 were smaller than RTSs, which initiated prior to 1972 (0.24 ha). Stable RTSs were 7 times larger than active RTSs, however they often conjoin several former active RTSs. For polycyclic RTSs, we could only identify stable RTSs whose extent exceeded the area of the active RTSs located within them and therefore only accounted for large stable RTSs. RTSs along the Yukon Coast had a median size of 0.24 ha, relatively small compared to the size of other RTSs occurring in the Arctic: Segal et al. found that in other previously glaciated areas of the Canadian Arctic, RTSs size varied on average between 0.98 ha and 5.35 ha, with the majority of the disturbances larger than 0.05 ha [Segal et al., 2016]. Coastal RTSs were the smallest (0.98 ha on average in the Jesse Moraine area, Banks Island), but still larger than along the Yukon Coast. One reason for this peculiarity may be that compared to Segal et al., the high-resolution dataset from 2011 used in our study allowed identification of RTSs as small as 0.01 ha [Segal et al., 2016]. However, when removing RTSs

smaller than 0.05 ha, the median size of the RTSs still remained low with 0.28 ha. Overall, 30% of the active RTSs identified in 2011 developed on surfaces occupied by stable RTSs in the 1970s. The reactivation of formerly stabilized surfaces, combined with the small size of the RTSs in the region, reflects the polycyclic behavior of the RTSs along the coast. In coastal environments, stable RTSs can reactivate when erosion exposes buried massive ice bodies, often as a result of storm events [Lantuit et al., 2012b, Kokelj et al., 2009a, Lewkowicz, 1987a].

3.6.2 Terrain factors explaining retrogressive thaw slump occurrence

Ground ice characteristics favored RTS occurrence and extent along the coast. As observed by [Harper, 1990], ground ice plays a crucial role in influencing coastal morphology and stability along the Yukon Coast and is of crucial importance for RTS development.

While focusing on coastal RTS dynamics, our results confirm the general patterns identified in previous studies on RTS occurrences in northern Canada. Kokelj et al. mapped RTSs in northern Canada and highlighted the strong correlation between RTS development and ice-rich moraine deposits found on the eastern margin of the late Wisconsinan glaciation [Kokelj et al., 2017]. Our results support these observations; the density and coverage of RTSs along the Yukon Coast were higher on moraine deposits. Moraine deposits usually combine all factors favorable for RTS development: they form crested ridges made up of a mixture of sediments and ice - including massive ground ice - that had been deposited during the melt of the ice sheet, and remained as permafrost under cold conditions. The thickness of the massive ice body was the most important factor explaining high densities of RTSs along the Yukon Coast. Lantuit et al. showed that during polycyclic RTS activity, the first phase of RTS development depends on the pace of the headwall retreat and the angle of repose of the slump floor, while the second stage of RTS development depends on the depth of the remaining massive ice body and the coastal retreat rate [Lantuit et al., 2012b]. Our results – through the relationship between the density of RTSs and the thickness of the massive ice body – suggest that not only the depth but also the thickness of the massive ice bodies plays a role in the polycyclicity of RTSs.

The volume (thickness and area) of massive ice was the main factor explaining the expansion of RTSs within a segment. In the case of reactivated RTSs, the size of the RTSs depends on the volume of the buried massive ice remaining underneath the stabilized RTS surface on which they reactivate. RTSs grow until ground ice is exhausted. This is supported by Burn following observations of RTSs along the Stewart River in Mayo, Canada [Burn, 2000]. However, RTSs can stop growing if the remaining massive ice bodies become buried under thawed sediments. The condition for a RTS to grow therefore depends on the capacity of the slump headwall to remain exposed [Lantuit et al., 2012b], which is constrained by the geometry of the RTS [Lewkowicz, 1987a].

3.6.3 Coastal Processes

Our statistical analyses highlight the direct relation between coastal geomorphology and RTS activity and initiation (Fig. 3.8). Active RTSs occurred in areas where the slope angle was greater than 3.9° and where cliff heights were higher than 11.0 m. RTSs that were initiated after 1972 were found on terrain with slope angles greater than 5.9°. Slope angle was one of the main factors sustaining RTSs in ice-rich permafrost terrain. In general, RTSs occurred only on terrain with slopes angles steeper than 3.9° and more specifically on terrain with mean slope angles of 6.2°.

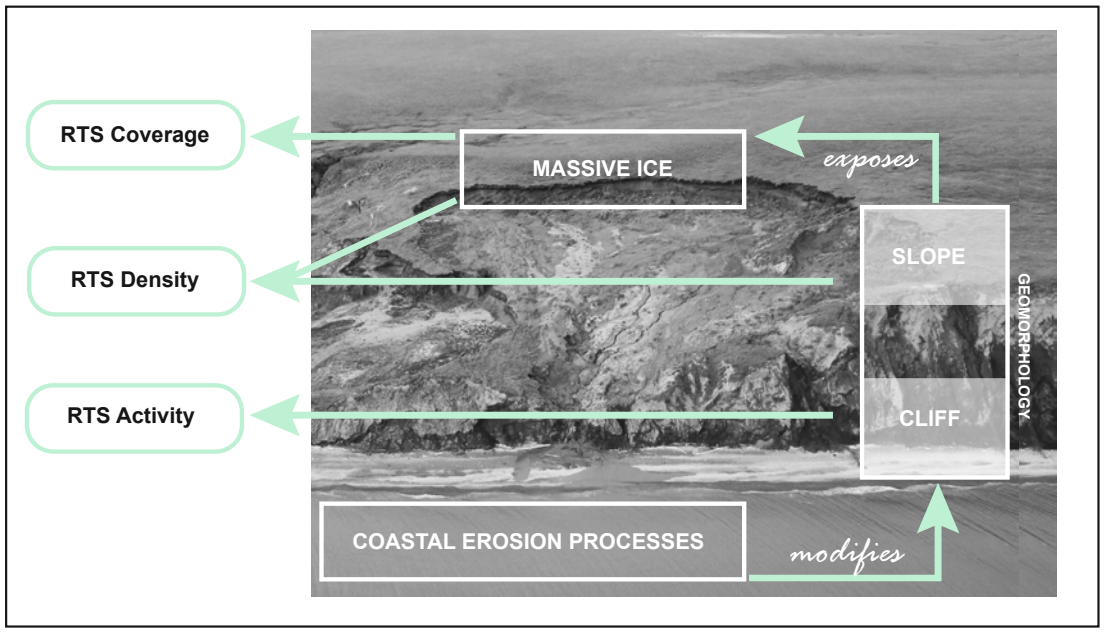

Figure 3.8 – Scheme illustrating the processes contributing in the development of coastal Retrogressive Thaw Slump (RTS)s, highlighted by the model. In the model, the response variables (RTS coverage, density and activity) were explained by a complex interaction between the environmental variables (coastal erosion processes, geomorphology and massive ice content). Thickness of the massive ice bodies and slope angle explained high density of coastal RTSs. Likewise, areal coverage of coastal RTSs was related to the amount of massive ice within a segment. Coastal erosion processes indirectly create the preconditions for the development of coastal RTSs by destabilizing coastal geomorphology and maintaining massive ground ice exposed.

These results are in the same range as the observations from Lantuit et al. for coastal RTSs (Herschel Island; mean slope angles of 6.2° and 5.8° for stable and active RTSs, respectively) and Balser et al. for inland RTSs (Noatak Basin; mean slope angles of 9.4°)[Lantuit et al., 2012b, Balser et al., 2014]. The slope angle has an effect on the activity of RTSs because it influences the evacuation of thawed material, which is a precondition to expose massive ice and to perpetuate headwall retreat [Lantuit et al., 2012b, Lacelle et al., 2010]. The condition for a slope to remain at an angle that allows the headwall to be exposed depends on the intensity of coastal erosion processes on the coast.

Wave erosion at the base of the slope can lead to slope destabilization, thus triggering or reactivating RTSs through removal of the insulating soil layer fronting the massive ice [Lantuit et al., 2012b, Lantuit and Pollard, 2008, Burn and Lewkowicz, 1990, Aré, 1988]. The intensity and direction of the waves lead to different dynamics along the coast [Harper, 1990] and are major factors controlling coastal erosion and potential RTS initiation. Contrary to our initial hypothesis, coastal erosion rates did not have a direct influence on the response variables in our model. The erosion rates used in the model did not emerge as significant predictors. This could be due to discrepancies related to the temporal scale of our dataset, or it could suggest an indirect influence of coastal erosion on the dynamics of coastal RTSs. We used mean erosion rates that were calculated for each segment over long time spans, 1972-2011 [Irrgang et al., 2018]. Those long-term erosion rates average out the effects of discrete storm events which crucially influence the magnitude of coastal erosion along the Yukon Coast [Lantuit et al., 2012b]. In turn, RTSs can also affect the rates of shoreline movement along the Yukon Coast [Obu et al., 2017a] by offsetting coastal retreat by sediments release to the shore and nearshore. For example, the shoreline may advance during a period of a RTS activity due to the accumulation of sediment on the shore, which forms the slump lobe. This fluctuating supply of material from the eroding RTS, combined with inter-seasonal variability in wave energy, can weaken the effect of waves in eroding the coast. The complexity of this interaction makes it challenging to estimate the impact of coastal erosion on RTS dynamics using long term averaged coastal erosion rates.
However, we suggest that coastal erosion processes – through their destabilization of the coast – contribute to maintaining RTSs activity and setting the pace of polycyclicity. Erosion impacts the dynamics of RTSs along the Yukon Coast through its indirect action on coastal geomorphology. Coastal erosion processes maintain preconditions for RTSs [Lantuit et al., 2012b]; they expose buried massive ice bodies and sustain the slope angle of the RTS floors, allowing further retreat of the headwall [Lewkowicz, 1987a].

3.7 Conclusion

From the 2011 imagery, we identified 287 RTSs along a 238 km coastal segment of the Yukon Coast. All RTSs occurred within the boundary of the last glacial maximum. The majority of the RTSs along the coast were polycyclic and active.

Our study defined the main terrain factors controlling the development of RTSs along a 238 km coastal segment of the Yukon Coastal Plain. Geomorphology – slope angle and cliff height – explained the occurrence of both active coastal RTSs and coastal RTSs that initiated after 1972. Thickness of the massive ice bodies and slope angle explained high density of coastal RTSs. Likewise, areal coverage of coastal RTSs was related to the amount of massive ice within a segment. RTSs grow until all ice is thawed or is buried under thawed sediments [Burn, 2000]. Coastal erosion processes were not fully reflected by coastal erosion rates. However, by their action on coastal geomorphology,

coastal erosion processes maintain the preconditions for reactivation of RTSs and thus have an indirect effect on the development of RTSs.

This is the first study showing terrain controls on coastal RTSs using statistical analyses at a regional scale. It confirms earlier observations on terrain control over RTSs in the Arctic [Segal et al., 2016, Kokelj et al., 2015b, Lantuit et al., 2012b, Lewkowicz, 1987a]. We emphasize the need for large-scale studies of RTSs to evaluate their impact on the ecosystem and to measure their contribution to the global carbon budget.

4 Increasing coastal slump activity impacts the release of sediment and organic carbon into the Arctic Ocean

4.1 Abstract

Retrogressive Thaw Slump (RTS)s are among the most active thermokarst landforms in the Arctic and deliver a large amount of material to the Arctic Ocean. However, their contribution to the organic carbon budget is unknown. We provide the first estimate of the contribution of RTSs to the nearshore organic carbon budget of the Yukon Coast, Canada, and describe the evolution of coastal RTSs between 1952 and 2011 in this area. We (1) describe the evolution of RTSs between 1952 and 2011; (2) calculate the volume of eroded material and stocks of Organic Carbon mobilized through slumping, including Soil Organic Carbon and Dissolved Organic Carbon; and (3) estimate the organic carbon fluxes mobilized through slumping between 1972 and 2011. We identified RTSs using high-resolution satellite imagery from 2011 and geocoded aerial photographs from 1952 and 1972. To estimate the volume of eroded material, we applied spline interpolation on an airborne lidar dataset acquired in July 2013. We inferred the stocks of mobilized Soil Organic Carbon and Dissolved Organic Carbon from existing related literature. Our results show a 73% increase in the number of RTSs and 14% areal expansion between 1952 and 2011. In the study area, RTSs displaced at least 16.6×10^6 m^3 of material, 53% of which was ice, and mobilized 145.9×10^6 kg of organic carbon. Between 1972 and 2011, 49 RTSs displaced 8.6×10^3 m^3 yr^{-1} of material, adding 0.6% to the organic carbon flux released by coastal retreat along the Yukon Coast. Our results show that the contribution of RTSs to the nearshore organic carbon budget is non-negligible and should be included when estimating the quantity of organic carbon released from the Arctic coast to the ocean.

4.2 Introduction

Soil Organic Carbon (SOC) stocks in the top 3 m of soils, in deltas and the Yedoma regions across the northern circumpolar permafrost region are estimated to 1307Pg; 76.4% (999Pg) of them are stored in perennially frozen soils [Hugelius et al., 2014].
These stocks resulted from the slow decomposition of soil organic matter in permanently frozen soils, caused by low soil temperatures and impeded drainage.

Surface air temperature in the Arctic increased by 0.755°C per decade during 1998–2012 [Huang et al., 2017]. As the active layer, the upper part of the permafrost that thaws during summer and refreezes in winter, thickens due to warmer air, increased microbial activity in the soil mobilizes more Organic Carbon (OC) that is eventually released to the atmosphere [Mackelprang et al., 2011, Schuur et al., 2008]. OC and nutrients are also released to streams, rivers, and to the Arctic Ocean by thermokarst and thermo-erosional processes [Schuur et al., 2015, Abbott and Jones, 2015, Kokelj et al., 2013, Vonk et al., 2012, Ping et al., 2011, Lamoureux and Lafrenière, 2009].
Permafrost carbon stocks were only recently included in calibrating global carbon models, highlighting a relevant contribution of thawing permafrost to the overall climate and economic response to human greenhouse gas emissions [Kessler, 2017, Koven et al., 2015, MacDougall et al., 2012, Burke et al., 2012, von Deimling et al., 2012]. Schaefer et al. predicted 120 ± 85 Gt carbon emissions from thawing permafrost by 2100, which represents 5.7 ± 4.0% of the total anthropogenic emissions[Schaefer et al., 2014]. Nevertheless, these carbon models underestimate the potential impact of the permafrost feedback on the global climate because they do not account for the spatial heterogeneity of permafrost terrains and omit the contribution of coastal erosion and abrupt thaw processes, such as thermokarst and thermo-erosion [Hugelius et al., 2014, MacDougall et al., 2012, Vonk et al., 2012]. Both expert assessments [Abbott et al., 2016] and model evaluations [McGuire et al., 2016] identified permafrost degradation as one of the most important sources of uncertainty in predicting the timing and magnitude of the permafrost carbon feedback.

Thermokarst and thermo-erosional processes occur by the thawing of ice-rich permafrost and the melting of massive ice. Thermokarst landscapes cover up to 20% of the northern circumpolar permafrost region and store half of the SOC from this region [Olefeldt et al., 2016]. Retrogressive thaw slumps (RTSs), a type of slope failure caused by permafrost thaw, are among the most active landforms in the Arctic and have increased both in number and size over the past decades [Ramage et al., 2017, Segal et al., 2016, Brooker et al., 2014, Lacelle et al., 2010].
RTSs rework sediments and mobilize carbon, nitrogen, and nutrients; as a result, RTSs affect terrestrial [Cassidy et al., 2016, Tanski et al., 2016, Cray and Pollard, 2015, Cannone et al., 2010] and aquatic ecosystems [Malone et al., 2013, Kokelj et al., 2009a, Kokelj et al., 2013]. Along the coasts of the Arctic, RTSs directly contribute to the transport of terrestrial OC to the nearshore zone [Obu et al., 2017a], which has the potential to affect

the nearshore marine ecosystem [Fritz et al., 2017]. However, there are currently no estimates on the volume of sediments and thus on the OC displaced by RTSs from the land to the nearshore zone in the Arctic.

To provide better estimates of the contribution of abrupt thaw processes on the OC budget along Arctic coasts, our study quantifies the impact of RTSs on the OC budget in a coastal permafrost environment along the Yukon Coast, Canada. We (1) describe the evolution of RTSs in the area between 1952 and 2011; (2) calculate the volume of material eroded and stocks of organic carbon (OC) mobilized through slumping – including SOC and Dissolved Organic Carbon (DOC) – and (3) estimate the OC fluxes mobilized through slumping between 1972 and 2011.

4.3 Study Area

The study area is located in the Canadian Arctic, along the westernmost coast of the Yukon Territory (Fig 4.1). The study area comprises a 238 km portion of the Yukon Coastal Plain, including Herschel Island (Fig. 4.1). The area is in the continuous permafrost zone [Rampton, 1982] and tundra vegetation zone dominated by mosses, graminoids, and shrubs [CAVM, 2003]. The area is characterized by a sub-arctic climate with a mean summer air temperature of 6°C on the eastern boundary of the study area and 8.7°C on the western boundary; the mean summer precipitation (June, July, and August, 1971–2000) is 79.8 mm at the east end and 112.9 mm at the west end [1].
The Mackenzie River, which enters the Beaufort Sea east of the study area, influences seawater temperature and sea ice extent and is the main control on the local precipitation patterns [Burn and Zhang, 2009].

The western margin of the Laurentide ice sheet, which reached its maximum ice extent around Herschel Island at ca. 16 200 years BP [Fritz et al., 2012], shaped the topography of the Yukon Coastal Plain. Long and high moraine ridges characterize most of the previously glaciated area. Herschel Island is a moraine thrust at the margin of the formerly glaciated area and is one of the largest moraine deposits in the region [MacKay, 1959]. Stream valleys, fluvial deltas, alluvial fans, and thermokarst basins characterize the unglaciated area. Due to widespread moraine deposits, 35% of the Yukon Coast is composed of ice-rich cliffs [Harper, 1990]. Volumetric ground ice contents (massive ice, pore ice, and wedge ice) vary along the coast and range from 0% to 74% [Couture and Pollard, 2017].
Previous studies divided the study area into 36 coastal segments (Fig. 4.1), based on ground ice contents, surficial geology, and geomorphology [Lantuit et al., 2012a, Couture, 2010, Lantuit and Pollard, 2005]. Most segments fall into one of three surficial geologic units: ice-thrust moraines (30%), lacustrine plains (23%), and rolling moraines (16%). Alluvial fans, stream terraces, floodplains, and outwash plains underlay the re-

[1] Environment Canada,http://climate.weather.gc.ca/historical_data/search_historic_data_e.html,2017

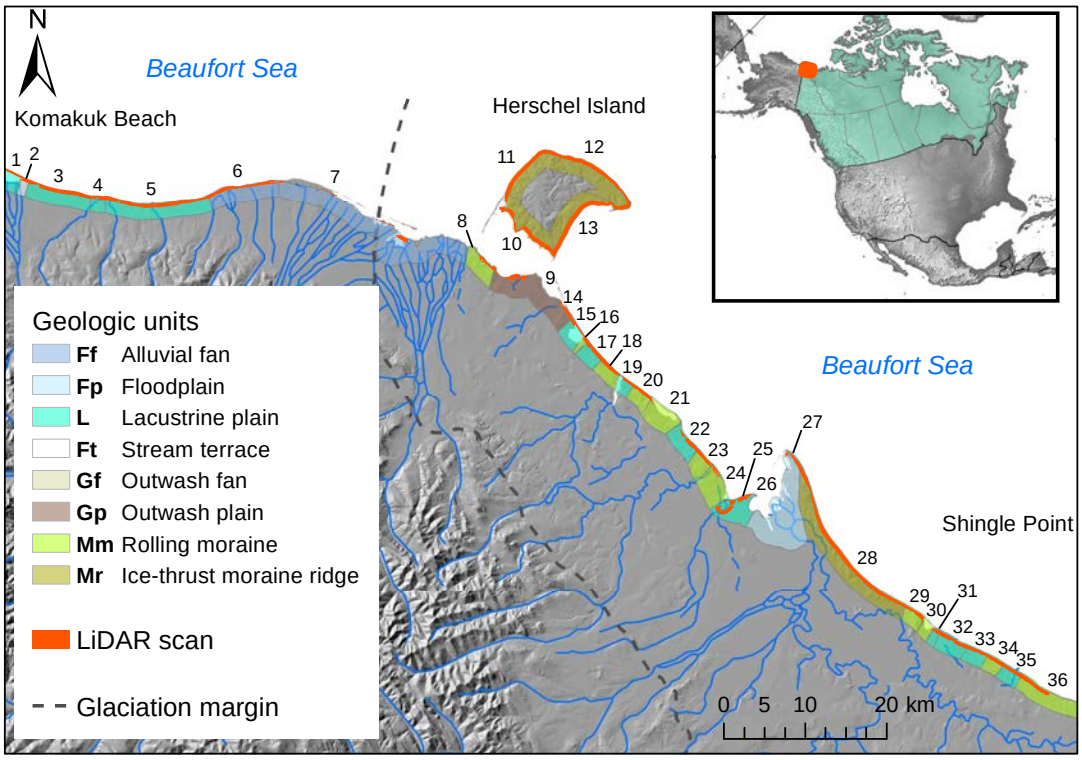

Figure 4.1 – Study area. The coastal subset defined as the lidar scan is represented in red. The limit of the glaciation was reproduced after Dyke and Prest and the surficial sediments after Rampton [Dyke and Prest, 1987, Rampton, 1982]. The numbers stand for the coastal segments stretching along the coast from west to east (the names of the coastal segments are available in Appendix A.2).

maining segments [Rampton, 1982]. The coast is rapidly eroding [Harper, 1990]: during the period 1952-2011, the average rate of shoreline change was -0.7 m yr^{-1} and was characterized by decreasing erosion rates from west to east [Irrgang et al., 2018]. RTSs are common along the coast and mostly develop on segments with massive ground ice thicker than 1.5 m and coastal slope greater than 3.9° [Ramage et al., 2017].

4.4 Methods

4.4.1 Evolution of retrogressive thaw slumps

We used two data inputs to measure the evolution of RTSs between 1952 and 2011: a dataset with RTSs present in 1972 and 2011 (dataset A) and a dataset with RTSs present in 1952 (dataset B). All RTSs were mapped using ArcMap 10.3 (ESRI) on a scale of 1 : 2000 and classified as active or stable. Active RTSs are characterized by steep headwalls exposing ice-rich permafrost, slump floors with thawed sediments, and incised gullies. Stable RTSs comprise gently sloping and vegetated headwalls, vegetated slump floors, and no visible active gully systems [Ramage et al., 2017, Lantuit and Pollard, 2008, Wolfe

et al., 2001]. Ramage et al. provided dataset A [Ramage, 2017]. RTSs present in 2011 were mapped based on multispectral GeoEye-1 and WorldView-2 satellite images acquired in July, August, and September 2011. RTSs present in 1972 were mapped using a series of geocoded aerial photographs from the 1970s obtained from the National Air Photo Library in Canada [Irrgang et al., 2018]. The mapping methodology is explained in detail in [Ramage et al., 2017]. Dataset B comprises RTSs present in 1952 that we mapped using a series of geocoded aerial photographs from the 1950s, obtained from the National Air Photo Library in Canada [Irrgang et al., 2018].

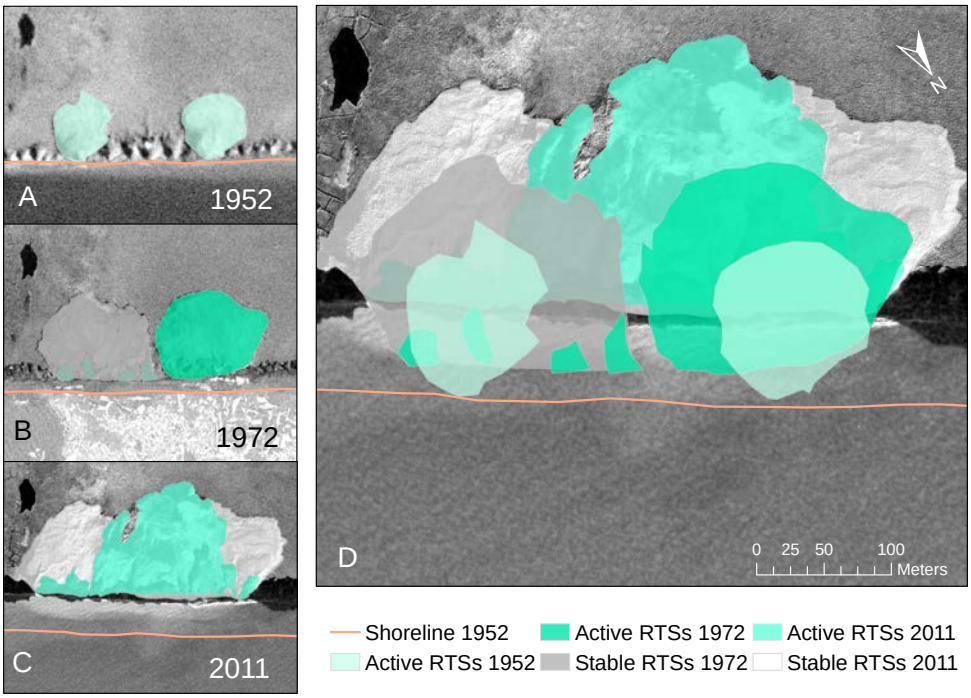

Figure 4.2 – Geomorphological map of Retrogressive Thaw Slump (RTS) illustrating the complexity of RTS evolution along the Yukon Coast. (D) RTSs identified in 1952 (A) and in 1972 (B) overlap the 2011 RTSs (C). The underlying imagery is a GeoEye-1 satellite image from 2011 (18 July). RTS areas from 1952 and 1972 closer to the shore have eroded due to coastal retreat. The remaining parts have either extended and merged with other RTSs or stabilized in 2011. (A) Two active RTSs in 1952 (aerial photo from 1952, National Air Photo Library, Canada). (B) RTSs in 1972 (aerial photo from 1972, National Air Photo Library, Canada). RTSs expanded and one had stabilized. New active RTSs developed within the stabilized RTS. (C) RTSs in 2011 (GeoEye-1, 18 July 2011). Former RTSs had partly stabilized and newer RTSs developed within the boundaries of the stabilized RTSs.

We compared the number and size of RTSs present in 1952, in 1972, and in 2011. RTSs are polycyclic and can occur on surfaces previously affected by RTSs. As a result, several active RTSs can be located within the boundary of a stable RTS (Fig. 4.2). In this case, stable polycyclic RTSs include the areal surfaces of active RTSs located within their boundaries.

4.4.2 Volume Estimations

Lidar Dataset

For each RTS identified in 2011 we extracted morphological information – size and mean surface elevation – from an airborne lidar dataset acquired in July 2013 [Kohnert et al., 2014]. The lidar dataset has a scan width of 500 m; the lidar point data was interpolated with inverse distance weighting to obtain digital elevation models with a horizontal resolution of 1 m [Obu et al., 2017a]. The lidar dataset has a final georeferenced point cloud data vertical accuracy of 0.15 ± 0.1 m and covers 80% of the coastline in our study area. We selected a subset of the 2011 RTS dataset comprising RTSs that occurred within the boundary of the lidar dataset to measure the volume of eroded material from RTSs (Fig. 4.1). We discarded the 125 RTSs outside of the lidar scan from the volume and flux analyses. In addition to the RTSs present in 2011 within the lidar area, we defined a subgroup with RTSs present in 2011 on surfaces not affected by slumping before 1972; we defined this subgroup as RTSs initiated after 1972.

Interpolation Method

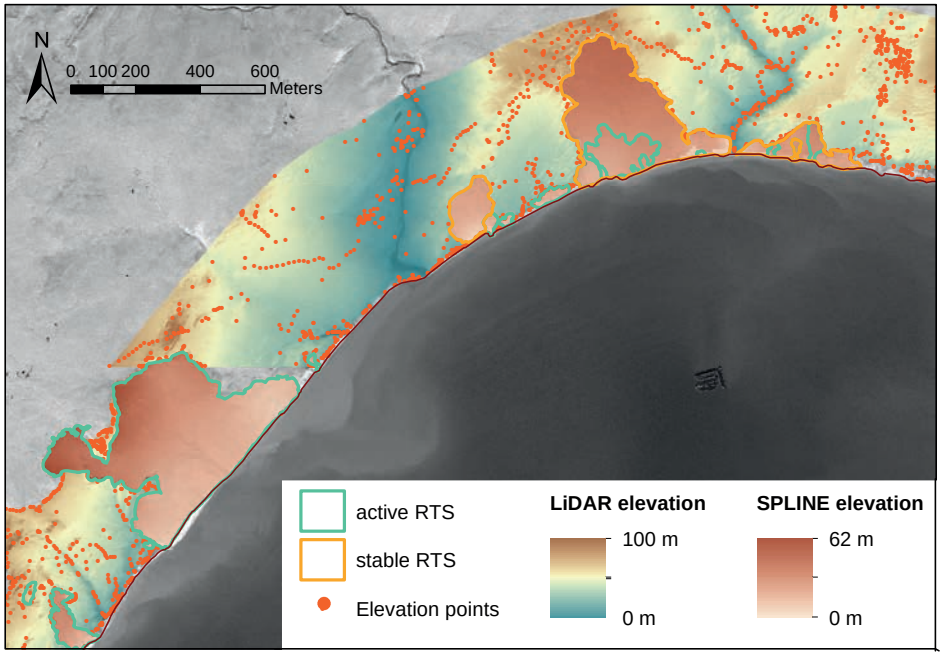

Figure 4.3 – Map illustrating the different datasets used to model pre-slump topographies. Retrogressive thaw slumps (RTSs) are outlined in green for the active RTSs and orange for the stable RTSs. The background satellite imagery is a GeoEye-1 image taken on July 18 2011. The background elevation and the random elevation points outside the RTS areas are derived from the lidar dataset. Elevation surface within the RTS borders represents the elevation before RTS occurred and is interpolated using a spline interpolation.

We applied a regularized spline interpolation technique to model pre-slump topographies used for calculating the volume of material eroded through slumping. The spline method allows us to estimate elevation points outside the range of input sample points and to minimize the total curvature of the surface. We therefore selected spline among other interpolation methods. We based our interpolation on the extensive point elevation data available for the study area from the lidar dataset (Fig. 4.3).

Volume of Eroded Material

To calculate the volume of eroded material from the retrograding headwall of the RTSs identified in 2011, we subtracted the mean surface elevation values obtained from the lidar dataset from the mean interpolated surface elevation values (Fig. 4.3). However, these volumes do not account for the material eroded from the RTS headwalls that settles within the RTS floors and for the material eroded and transported alongshore by coastal processes (Fig. 4.4). Due to ground ice melting, ca. 5.5% of the reworked sediments subside and remain compacted in the RTS floor, i.e. do not get transported out of the RTS [Obu et al., 2017a]. We therefore adjusted the material volumes to take into account the 5.5% of the material that subside in the RTS floors (Fig. 4.4 c).

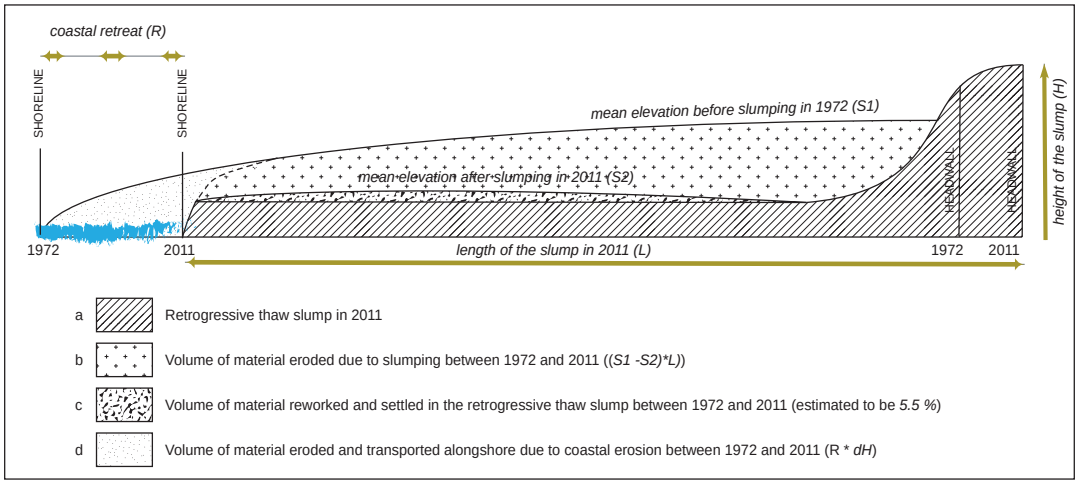

Figure 4.4 – Cross section of a retrogressive thaw slump (RTS) (a) illustrating the calculated volumes of sediments eroded through slumping between 1972 and 2011. The calculation estimates the amount of material released to the nearshore zone through slumping (b) and takes into account the material eroded from the RTS headwalls that remains within the RTS floors where it settles (c) and (d) the material eroded and transported alongshore by coastal erosion. The volume of material that remains within the RTS floors was estimated from Obu et al. [Obu et al., 2017a].

In addition, we calculated the volumes of material eroded and transported by coastal erosion using the rate of shoreline change between 1952 and 2011 from Irrgang et al. [Irrgang et al., 2018]. Using this rate, we calculated the volumes of eroded material between 1952 and 2011 for each RTS. For the RTSs that initiated after 1972, we calculated the volumes of eroded material between 1972 and 2011 (Fig. 4.4 d). To differentiate

between the volumes of ice and sediments eroded, we used the volumetric ice content provided for each coastal segment in Couture and Pollard [Couture and Pollard, 2017]. The model interpolates the data collected on 19 coastal segments to the whole Yukon Coast based on similarities between surficial geology and permafrost conditions. Ice contents were determined from shallow cores collected from upper soil layers and from bluff exposures.

4.4.3 Estimates of soil and dissolved organic carbon values

We inferred mobilized SOC and DOC stocks and fluxes from RTSs from the mass of SOC and DOC per meter column in each coastal segment provided in Couture and Tanski et al. in relation to the estimated volume of material displaced by each RTS [Couture, 2010, Tanski et al., 2016]. The OC values were derived from in situ measurements collected at 31 locations and were interpolated to each coastal segment following the same approach as for the determination of ground ice [Couture, 2010]. The SOC was measured for different soil unit layers along the bluffs and averaged for the upper first meter and lower meter of the soil columns [Couture, 2010]. It therefore takes into account the heterogeneity of SOC contents at depth. DOC values account for the differences in DOC concentrations between wedge ice, massive ice, and non-massive ice [Tanski et al., 2016], based on the ice volumes summarized in Couture and Pollard [Couture and Pollard, 2017]. The OC values are therefore coarse but consistent for the whole Yukon Coast. The dataset is provided in Appendix (Appendix A.2).

SOC and DOC stocks

We used Eq. (1) to calculate the stocks of SOC eroded from RTSs:

(1)
$$RTS_{\mathrm{SSOC}} = \sum_{\mathrm{i=1,j=1}}^{\mathrm{n,m}} (M_{\mathrm{CTj}} * A_{\mathrm{i}}) + (M_{\mathrm{CBj}} * (VS_{\mathrm{i}} - A_{\mathrm{i}})),$$

where RTS_{SSOC} is the stock of SOC eroded from RTSs (expressed in kg), M_{CTj} is the mass of SOC in the upper 1 m (expressed in kg) per coastal segment j out of m total, A_i is the total surface area of an RTS i out of n total (expressed in m^2), M_{CBj} is the mass of SOC in the lower soil column (expressed in kg) per coastal segment j, and VS_i is the volume of sediment eroded by per RTS (expressed in m^3). M_{CTj} and M_{CBj} take into account differences in dry bulk density per coastal segment j [Couture, 2010]. We used Eq. (2) to calculate the stocks of DOC eroded from RTSs:

(2)
$$RTS_{\mathrm{SDOC}} = \sum_{\mathrm{i=1,j=1}}^{\mathrm{n,m}} D_{\mathrm{j}} * VI_{\mathrm{i}},$$

where RTS_{SDOC} is the total stock of DOC eroded from RTSs (expressed in kg), D_j is the stock of DOC per coastal segment j (expressed in kg m^3), and VI_i is the volume of ice eroded from a RTS (expressed in m^3). D_j is given per coastal segment j [Tanski et al., 2016].

SOC and DOC fluxes

We calculated the flux of material – including ice and sediments – as well as SOC and DOC fluxes for the RTSs initiated after 1972. To calculate the SOC flux we used Eq. (3):

(3) $RTS_{FSOC} = RTS_{SSOC} \div 39$,

where RTS_{FSOC} is the annual flux of SOC mobilized from RTSs (expressed in kg yr^{-1}), RTS_{SSOC} is the quantity of SOC eroded from an RTS (expressed in kg) (Eq. 1), and 39 is the number of years during the time period 1972-2011.

Similarly, we used Eq. (4) to calculate the DOC flux:

(4) $RTS_{FDOC} = RTS_{SDOC} \div 39$,

where RTS_{FDOC} is the annual flux of DOC eroded from RTSs (expressed in kg yr^{-1}), TS_{SDOC} is the quantity of DOC eroded from an RTS (expressed in kg) (Eq. 2), and 39 is the number of years during the time period 1972-2011.

4.5 Results

4.5.1 Evolution of retrogressive thaw slumps between 1952 and 2011

The number of RTSs increased by 73% between 1952 and 2011. The increase was more pronounced throughout the time period 1952-1972 (Fig. 4.5). Between 1952 and 2011, active RTSs were more abundant and their number increased faster than stable RTSs.

While the number of active RTSs progressed steadily throughout the period, the number of stable RTSs decreased between 1972 and 2011: stable RTSs had either been reactivated or been washed away due to coastal retreat. Between 1952 and 2011, the number of RTSs increased by 40% on lacustrine plains and by 100% on rolling moraines (Fig. 4.5). On ice-thrust moraines, the number of RTSs increased by 69% between 1952 and 2011 (1.2 RTS yr^{-1}). On both moraine units, the rise was greater between 1952 and 1972. The total areal coverage (sum of the total RTS sizes) expanded by 14% between 1952 and 2011 and was observed in all geologic units (Fig. 4.5). This expansion was driven by an increase in the areal coverage of stable RTSs (25%); the areal coverage of active RTSs decreased by 2% (Fig. 4.1). The expansion in areal coverage was caused by an increase in the number of RTSs rather than by a growth in the size of single RTSs alone: RTSs became smaller;

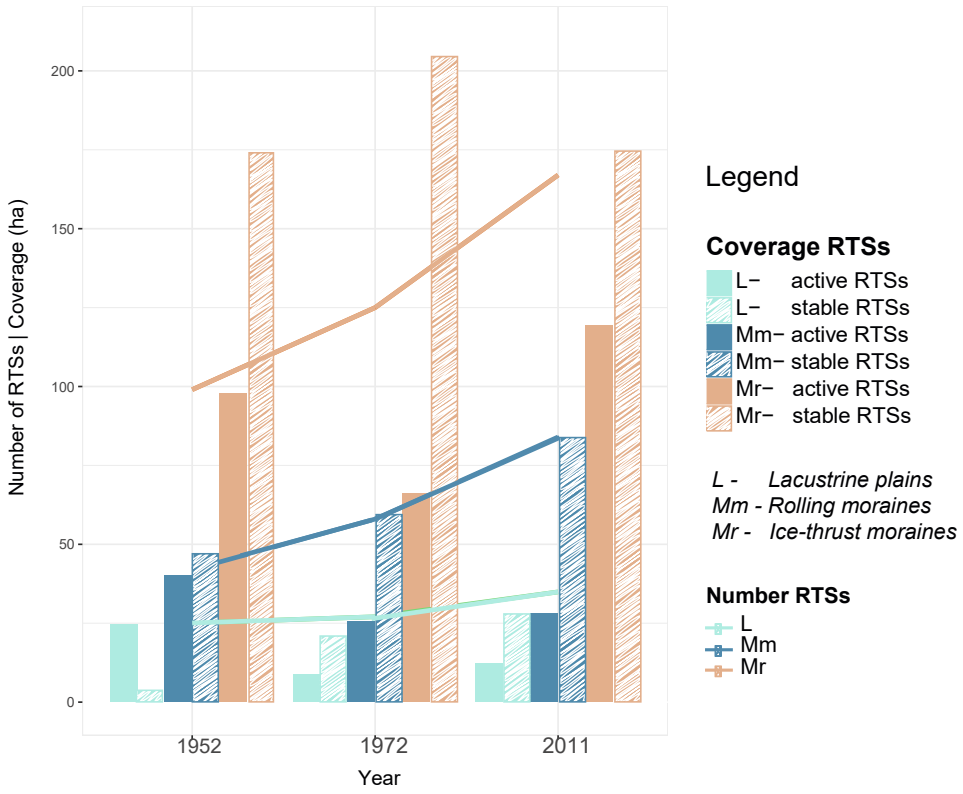

Figure 4.5 – Graph showing the evolution in the number and areal coverage of retrogressive thaw slumps (RTSs) between 1952 and 2011 for each geologic units (L, lacustrine plains; Mm, rolling moraines; Mr, ice-thrust moraines). The y axis shows both variations in the number of RTSs and variations in the areal coverage of RTSs (ha), which differentiate between active and stable RTSs.

their median size decreased by 67% throughout the period. Among RTSs present in 2011, 119 initiated after 1972 on previously undisturbed surfaces: in 2011, 72 were still active and 47 had stabilized (Appendix A.2). RTSs initiated after 1972 were on average smaller than other RTSs and occupied 98.6 ha of the whole study area or 22% of the total area affected by RTSs in 2011. Most of the RTSs initiated after 1972 (74%) developed on ice-thrust moraines.

4.5.2 Eroded material and estimated amount of mobilized SOC and DOC

In the following sections, volumes are given for the RTSs that occurred within the lidar area. This comprises 56% of the total number of RTSs present in the investigated coastal area (n = 162) and 41% of the number of RTSs initiated after 1972 (n = 49).

Eroded material and OC stocks mobilized from RTSs

The total volume of material displaced by the 162 RTSs was 16.6×10^6 m^3, 54% of which was ice (Appendix A.2). It corresponds to a volume of material of 0.1×10^6 m^3 km^{-1} along the Yukon Coast. On average each RTS eroded 102.2×10^3 m^3 of material. The volume of eroded material was positively correlated to the size of the RTSs ($r^2 = 0.5$, $p<0.05$).

Table 4.1 – Volume of material, including ice and sediments, eroded by Retrogressive Thaw Slump (RTS)s along the Yukon Coast per geologic unit. The values are normalized to the shoreline length of the geologic units (km).

	Sediments (10^3 m^3 km^{-1})	Ice (10^3 m^3 km^{-1})	Total material (10^3 m^3 km^{-1})
Lacustrine plains (L)	16.1	46.2	75.8
Rolling moraines (Mm)	40.1	44.7	76.9
Ice-thrust moraines (Mr)	56.2	90.9	152.7

On average, 52% of the material was displaced due to the retreat of the RTS headwalls and 45% was transported alongshore due to coastal processes. The remaining 3% of material settled in the RTS floors. Overall, 65% of the material eroded by RTSs originated from ice-thrust moraines, 19% from lacustrine plains and 16% from rolling moraines (Table 4.1). However, RTSs located on lacustrine plains eroded more material per RTS (135.5×10^3 m^3 RTS^{-1}) than RTSs located on ice-thrust moraines (103.9×10^3 m^3 RTS^{-1}) and on rolling moraines (75.1×10^3 m^3 RTS^{-1}). The largest volumes of eroded material came from RTSs occurring at the glaciation limit (Fig. 4.6).

The 24 RTSs located on Herschel Island East (segment 13) eroded 22% of the total volume of material displaced by the 162 RTSs. The RTSs located on Herschel Island West (segment 11) had the highest volume of material eroded per RTS, on average 4% of the total volume of material displaced by RTSs (Fig. 4.6). Ice-thrust moraine deposits underlie both coastal segments 11 and 13.
Between 1952 and 2011, a total of 162 RTSs displaced 7.6×10^6 m^3 of sediments (Appendix A.2), comprising a mass of mineral sediment of 6.8×10^9 kg. On ice-thrust moraines RTSs eroded 72% of the mass of mineral sediments and 19% on rolling moraines. The total stock of SOC mobilized by RTSs was 145.7×10^6 kg, with the upper 1 m of soil contributing 49%. RTSs on ice-thrust moraines contributed to 72% of the total SOC stock. Out of this, RTSs on Herschel Island West and East (segments 11 and 13) mobilized 47% of the total SOC stock. The total stock of DOC mobilized by RTSs was 164.5×10^3 kg. RTSs on ice-thrust moraines mobilized 63% of the total DOC, which corresponds to 103.8×10^3 kg (Appendix A.2).

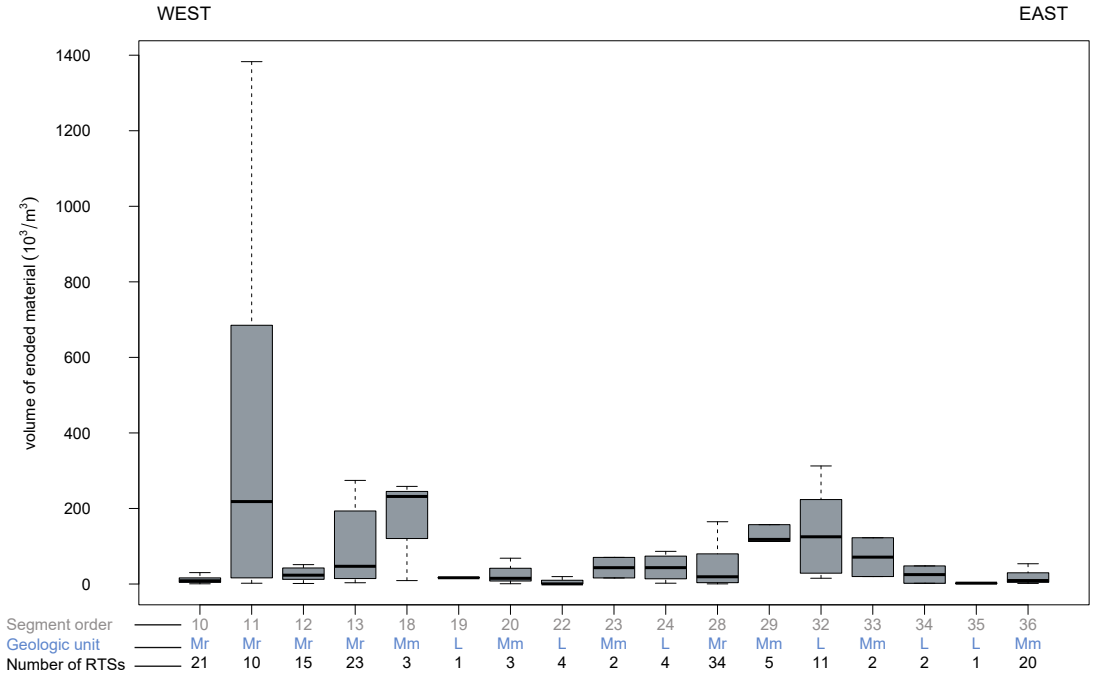

Figure 4.6 – Box plot of volumes of eroded material (sediments and ice) per retrogressive thaw slump (RTS) for the coastal segments where RTSs occurred in 2011. Each bar corresponds to a coastal segment, following a geographic order from west on the left to east on the right. The number of the respective coastal segment is indicated in the first line on the x axis. The geologic units are indicated below the bars and referred to as L (lacustrine plains), Mm (rolling moraines), and Mr (ice-thrust moraines). The values on the lowest line of the x axis indicate the total number of RTSs per coastal segment.

Eroded material and OC fluxes from RTSs initiated after 1972

The 49 RTSs initiated after 1972 eroded a volume of material of 1.1×10^6 m^3, 50% of which was ice (Appendix A.2). It corresponds to 27.2×10^3 m^3 yr^{-1} (0.6×10^3 m^3 RTS^{-1} yr^{-1}) between 1972 and 2011.

Table 4.2 – Volume of material, including ice and sediments, eroded by RTSs initiated after 1972 along the Yukon Coast per geologic unit. The values are normalized to the shoreline length of the geologic units (km).

	Sediments (10^3 m^3 km^{-1})	Ice (10^3 m^3 km^{-1})	Total material (10^3 m^3 km^{-1})
Lacustrine plains (L)	0.24	0.52	0.75
Rolling moraines (Mm)	0.46	0.46	0.92
Ice-thrust moraines (Mr)	6.84	7.18	14.02

This represents 6% of the total volume of material eroded by the 162 RTSs. Most of the material was eroded and transported alongshore due to coastal erosion (67%). Retreat of the RTS headwalls contributed to 31% of the reworked material from RTSs, and 2%

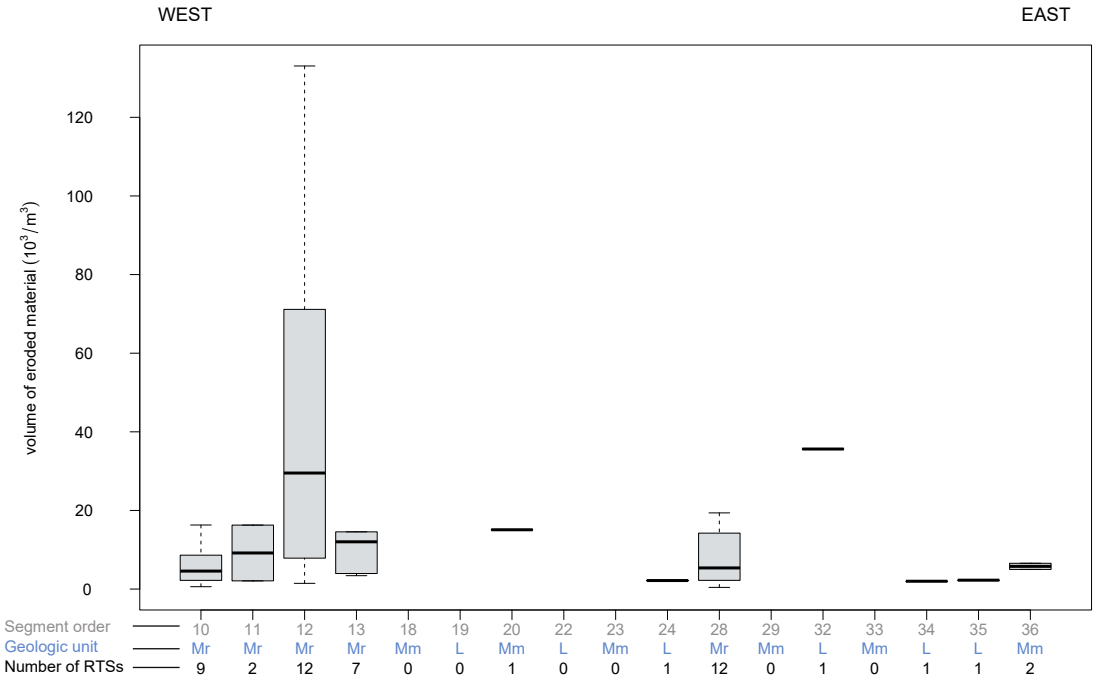

Figure 4.7 – Box plot of volumes of eroded material (sediments and ice) per Retrogressive Thaw Slump (RTS) for the coastal segments where RTSs initiated after 1972 occurred in 2011. Each bar corresponds to a coastal segment, following a geographic order from west on the left to east on the right. The number of the respective coastal segment is indicated in the first line on the x axis. The geologic units are indicated below the bars and referred to as L (lacustrine plains), Mm (rolling moraines), and Mr (ice-thrust moraines). The values on the lowest line of the x axis indicate the number of RTSs on the coastal segments.

of material remained in the RTS floors where it settled. In total, 94% of the reworked material from RTSs initiated after 1972 came from those located on ice-thrust moraines (Table 4.2), where the largest volumes of material per RTS initiated after 1972 was 23.6 $\times$ 10^3 m^3 RTS^{-1}. The RTSs initiated after 1972 on Herschel Island North (segment 12) reworked the largest volume of material: 42.4 $\times$ 10^3 m^3 RTS^{-1} (Fig. 4.7).

The 49 RTSs initiated after 1972 eroded a mass of mineral sediments of 454.1 $\times$ 10^6 kg, which represents a flux of 11.6 $\times$ 10^6 kg yr^{-1}. Since 1972, these RTSs mobilized an SOC flux of 250.1 $\times$ 10^3 kg yr^{-1} (Table 4.3), representing an average of 0.5 kg m^3 yr^{-1}. Most of the SOC fluxes originated from the RTSs initiated after 1972 on Herschel Island North (segment 12, 123.4 $\times$ 10^3 kg yr^{-1}) and on Kay Point Southeast (segment 28, 36.8 $\times$ 10^3 kg yr^{-1}) (Appendix A.2). On ice-thrust moraines, RTSs initiated after 1972 mobilized 94% of the total SOC flux (Table 4.3). The total DOC flux from RTSs initiated after 1972 was 5.1 kg yr^{-1}, with high variability between the geologic units: 0.1 kg yr^{-1} were mobilized from rolling moraines and from lacustrine plains and 4.9 kg yr^{-1} from ice-thrust moraines (Appendix A.2). The highest DOC fluxes came from ice-thrust moraines from Herschel Island North (segment 12), where 12 RTSs initiated after 1972 mobilized a total flux of 3.1 kg yr^{-1} of DOC (Table 4.3).

Table 4.3 – Total SOC and DOC flux mobilized between 1972 and 2011 by retrogressive thaw slumps initiated after 1972, per year and kilometer for each geologic unit.

	SOC flux ($kg\ km^{-1}\ yr^{-1}$)	DOC flux ($g\ km^{-1}\ yr^{1}$)
Lacustrine plains (L)	115.5	4.3
Rolling moraines (Mm)	308.5	4.6
Ice-thrust moraines (Mr)	3316.6	68.6

4.6 Discussion

4.6.1 Increase in slump activity

With a total of 287 RTSs in 2011, the Yukon Coast is one of the Arctic areas most affected by retrogressive thaw slumping [Ramage et al., 2017]. The number of RTSs along the Yukon Coast increased by 73% between 1952 and 2011, with on average two RTSs initiated per year (Fig. 4.5). The rise was more pronounced between 1952 and 1972 but the number of RTSs continued to increase steadily between 1972 and 2011.

The evolution of RTSs along the Yukon Coast is consistent with the observations made in other parts of the Canadian Arctic, where RTS activity has been accelerating since the 1950s [Segal et al., 2016, Lacelle et al., 2010, Lantz and Kokelj, 2008, Lantuit and Pollard, 2008]. Lantuit and Pollard showed that the number of RTSs on Herschel Island increased by 61% between 1952 and 2000 [Lantuit and Pollard, 2008]. RTSs develop following changes that affect geomorphic settings [Ramage et al., 2017, Kokelj et al., 2017] and are induced by climatic conditions – such as increased air temperature [Lacelle et al., 2010], precipitation events [Kokelj et al., 2015a, Lacelle et al., 2010], and storm events [Lantuit et al., 2012b, Lantuit and Pollard, 2008, Dallimore et al., 1996]. Many RTSs that were stable or stabilized between 1952 and 1972 were reactivated between 1972 and 2011. Our results confirm the pattern of RTS reactivation previously observed on Herschel Island (Lantuit and Pollard, 2008) and between Kay Point and Shingle Point [Wolfe et al., 2001], referred to as polycyclicity. Reactivation of RTSs is associated with the incomplete melting of massive ice bodies during the first period of RTS activity [Burn, 2000] and depends on the capacity of the slump headwall to remain exposed until ice is exhausted. In coastal settings, storm events can reactivate RTSs [Lantuit et al., 2012b]. The period of RTS activity partly depends on the equilibrium between thermodenudation and coastal erosion rates: the RTS remains active if the RTS headwall erodes at a rate exceeding shoreline retreat [Lantuit et al., 2012b, Aré, 1999]. This equilibrium is strongly linked to the dynamics of environmental conditions that enhance coastal erosion, such as the occurrence of storm events and the elongation of the open-water period [Overeem et al., 2011, Are et al., 2008, Solomon, 2005].

Climate data recorded at Komakuk Beach (segment 2) and Shingle Point (segment 36)

show that the average summer air temperature decreased between the periods 1957–1971 (Komakuk, 7.4°C; Shingle Point, 10.8°C) and 1971–2000 (Komakuk, 4.9°C; Shingle Point, 7.4°C). However, the annual average precipitation increased at both stations by 30% and 41%, respectively, during the same periods [2]. Similar patterns were observed for the summer months (July to September).
As suggested by Kokelj et al. in other Arctic areas, higher rainfall might intensify RTS activity [Kokelj et al., 2015b]. However, a series of environmental factors seems to be jointly responsible for the intensification of RTS activity along the Yukon Coast [Ramage et al., 2017]. Along the Yukon Coast, RTSs developed mainly on ice-thrust moraines, where their number increased by 1.1 RTS yr^{-1} throughout the whole period 1952–2011. Differences in ice content and coastal geomorphology explain the disparities in the evolution of RTSs observed among geologic units [Ramage et al., 2017, Lewkowicz, 1987a]. Our results confirm the results of Kokelj et al., who showed evidence of a spatial link between RTS occurrence in North America and the maximum extent of the Laurentide Ice Sheet [Kokelj et al., 2017]. Similar to our observations along the Yukon Coast, most of the RTSs in North America are found along the marginal moraines of the Laurentide Ice Sheet. Along with the increase in the number of RTSs, the total areal coverage of RTSs along the Yukon Coast increased by 14% between 1952 and 2011 (Fig. 4.5). However, RTSs along the Yukon Coast were on average smaller in 2011 compared to 1952 and 1972. This differs from RTSs observed in other parts of the Canadian Arctic [Segal et al., 2016, Kokelj et al., 2017]. Our results support those reported by Ramage et al.; coastal RTSs are on average smaller compared to inland RTSs, and coastal RTSs along the Yukon Coast are smaller than the ones found in other coastal areas of the Arctic [Ramage et al., 2017]. The large number of RTSs initiated after 1972 along the Yukon Coast partly explains this: RTSs initiated after 1972 represented 17% of the total number of RTSs in 2011; these RTSs were still developing in 2011 and thus had not reached their maximal expansion size.

4.6.2 Eroded material from retrogressive thaw slumps and organic carbon fluxes

The expansion of RTSs along the coast causes the displacement of large volumes of material from the land to the sea. We show that the 56% of the RTSs identified in 2011 for which we could calculate volumes (162 RTSs out of 287 that occur in the coastal area investigated) have reworked at least 16.6×10^6 m^3 of material along the Yukon Coast, which is 102.5×10^3 m^3 RTS^{-1} of material eroded per RTS (Fig. 4.6). Among these RTSs, 49 RTSs initiated after 1972 reworked 27.2×10^3 m^3 yr^{-1} of material, which is 0.6×10^3 m^3 RTS^{-1} yr^{-1} (Fig. 4.7).

These estimates are low compared to material removal from other RTSs in the Arctic. Lantuit and Pollard calculated a sediment volume loss of 105×10^3 m^3 between 1970 and

[2] Environment Canada,http://climate.weather.gc.ca/historical_data/search_historic_data_e.html,2017

2004 for a single RTS located on Herschel Island [Lantuit and Pollard, 2005]; Kokelj et al. and Jensen et al. measured material displacements up to 10^6 m^3 per RTS located in NW Canada and Alaska [Kokelj et al., 2015a, Jensen et al., 2014]; the Batagay mega-slump located in Siberia eroded more than 24×10^6 m^3 of ice-rich permafrost in 2014 [Günther et al., 2015].
The size of the observed RTSs is one reason behind such differences: most of the RTSs examined in the abovementioned studies are classified as mega-slumps (> 0.5 ha). The RTS studied in Lantuit and Pollard was the largest (24 ha) RTS identified along the entire Yukon Coast in 2011 [Lantuit and Pollard, 2005]. However, most of the RTSs along the Yukon Coast are small, with an average size of 0.2 ha [Ramage et al., 2017]. This has implications for studies that attempt to model the impact of RTSs on the eroded material budgets in the Arctic.

Couture estimated the annual flux of mineral sediment eroded by shoreline retreat along the Yukon Coast to 7.3×10^6 kg km^{-1} yr^{-1} [Couture, 2010]. We show that along a 190 km portion of the Yukon Coast, 17% of the RTSs identified along the coast in 2011 (49 RTSs) contributed to 1% of the annual flux of material eroded along the Yukon Coast (61×10^3 kg km^{-1} yr^{-1}).These RTSs initiated after 1972 incised 1% (2 km) of the shoreline in 2011 and were on average smaller than the average RTSs. Increasing the number and areal coverage of coastal RTSs therefore has significant consequences on the flux of eroded material along the Arctic coasts. We estimated the annual OC fluxes (SOC and DOC) from these 49 RTSs to be 1.3×10^3 kg km^{-1} yr^{-1}, including 0.02 kg km^{-1} yr^{-1} DOC. The average OC flux from coastal retreat along the entire Yukon Coast is 157×10^3 kg km^{-1} yr^{-1} [Couture, 2010] with an average DOC flux of 0.2×10^3 kg km^{-1} yr^{-1} [Tanski et al., 2016].
We show that the annual OC flux released by the 49 RTSs initiated after 1972 was 0.6% of the annual OC flux from coastal retreat. Most of these fluxes originated from ice-thrust moraines, where the number of RTSs initiated after 1972 was highest. RTSs develop mainly on ice-thrust moraines because of the presence of large volumes of massive ground ice [Ramage et al., 2017]. As a result, only half of the material eroding from the RTS headwall is sediment and most of the OC is released as DOC. The volumes and stocks of material and OC mobilized by RTSs along the Yukon Coast account for 56% of the RTSs identified on the 2011 imagery. We did not calculate the volumes for all RTSs present along the Yukon Coast due to the restricted area covered by the lidar dataset.
Therefore, the fluxes of sediment and OC mobilized by 49 RTSs initiated after 1972 underestimate the annual contribution from RTSs to the nearshore sediment and OC budgets along the Yukon Coast. These fluxes account for 41% of the flux from RTSs initiated after 1972 and 17% of the total number of RTSs identified in 2011 along the Yukon Coast.

4.6.3 Impact of retrogressive thaw slumps on the coastal ecosystem

RTSs erode surfaces and scar the landscape, impacting the coastal fringe ecosystems. RTSs alter the vegetation composition: after they stabilize, their effects on the vegetation persist over centuries [Cray and Pollard, 2015, Lantz et al., 2009]. Inland, RTSs modify stream sediment transport by raising the stream turbidity and the concentration of total suspended sediments [Kokelj et al., 2013].

Moreover, RTSs alter coastal retreat [Obu et al., 2017a, Lantuit and Pollard, 2008, Leibman et al., 2008] and strongly influence sediment transport along the coast. Segments with intense slumping show the highest volume of eroded and accumulated material [Obu et al., 2017a].
Most of the material and OC mobilized through slumping are transported to the nearshore zone [Vonk et al., 2012]. However, a fraction of this material and OC remains in the slump floor for several years [Tanski et al., 2017, Obu et al., 2017a] where it degrades and is mineralized by microorganisms. Hence, OC is mobilized in RTSs prior to its release to the ocean, which modifies the amount of OC available to the coastal ecosystem [Tanski et al., 2017, Cassidy et al., 2016, Pizano et al., 2014]. Tanski et al. show that SOC and DOC decrease by 77% and 55%, respectively, before reaching the nearshore zone [Tanski et al., 2017]. Abbott and Jones describe similar processes for RTSs in upland areas: after RTSs develop, 51% of organic-layer SOC and 21 kg m^2 of mineral-layer SOC is removed [Abbott and Jones, 2015]. Following headwall erosion, water transports melted ground ice and most sediments to the nearshore zone. Without enough viscous flow, the remaining part of the sediments accumulates and settles on the RTS floor, as indicated by higher bulk densities in samples from RTS floors [Tanski et al., 2017, Lantuit et al., 2012b]. The OC in the sediments is released to the atmosphere as CO_2 [Cassidy et al., 2016], buried in the RTS floor, or transported to the nearshore zone [Tanski et al., 2017].

RTSs are transient phenomena in coastal settings; coastal retreat eventually erodes and transports 45% of the material reworked by RTSs alongshore. However, as explained above, RTSs affect the OC release process and alter the OC budget of the nearshore zone.

4.7 Conclusion

The number of RTSs along the Yukon Coast increased by 73% between 1952 and 2011, and the total areal coverage of RTSs increased by 14%. We observed disparities between geomorphic units: the largest increase was on ice-thrust moraines, where the number of RTSs increased at an annual rate of 1.2 RTSs yr^{-1}. Many RTSs are polycyclic and were reactivated between 1972 and 2011. RTSs reworked at least 16.6×10^6 m^3 of material within a 190 km portion of the coastal fringe. The majority of the material came from

erosion of the headwall (53%), and 3% remained in the RTS floors.
A large amount of the material from RTSs was eroded and transported alongshore due to coastal processes (45%). The OC flux from 17% of the RTSs identified in 2011 was 1.3 $\times 10^3$ kg km^{-1} yr^{-1} and represented 0.6% of the annual OC fluxes from coastal retreat in the study area.
Not all the OC mobilized by RTSs is immediately transported to the nearshore zone; an important part is mobilized in the RTS floors. Therefore, RTSs alter the amount of OC that enters he nearshore zone by affecting the OC release process. Our results show that the contribution of RTSs to the nearshore OC budget is non-negligible and should be included when estimating the quantity of OC released from the Arctic coasts to the ocean.

5 Dissecting valleys: Snapshot of carbon and nitrogen distribution in Arctic valleys

5.1 Abstract

Thermokarst is a dominant process along hillslopes of valleys in lowland permafrost regions. Increasing permafrost thaw in the Arctic alter the biogeochemical cycling in the Arctic by reworking soil material and redistributing organic carbon and nitrogen along hillslopes.

Estimating the impact of this redistribution is key to better estimating both the storage of Soil Organic Carbon (SOC) in permafrost terrains and further implications on the release of Greenhouse gases. However, there are insufficient studies quantifying long-term impacts of thaw processes on the distribution of SOC and Total Nitrogen (TN) along hillslopes. We address these uncertainties by providing estimates of SOC and TN stocks along the hillslopes of three Arctic valleys located on Herschel Island (Yukon, Canada). In this study, we interrogate the spatial distribution of SOC and TN stocks and discuss the impact of hillslope geomorphology on their distribution.

We found that the average SOC and TN 0-100 cm stocks in the valleys were 26.4 ± 8.9 kg C m^{-2} and 2.1 ± 0.6 kg N m^{-2}, with large differences across the landscape. We highlight the high variability in the soils physical and chemical properties within geomorphic units, distance to the shore and slope orientation. The average carbon-to-nitrogen ratio in the valleys was 12.9, ranging from 9.7 to 18.9, and was significantly higher in the uplands compared to the hilltoes, suggesting a degradation of SOC to downhill. Our results showed that lateral redistribution of SOC and TN due to soil erosion has important implications not only for the storage but also the stability of SOC in dynamic landscapes.

5.2 Introduction

Near-surface permafrost in the High Arctic has warmed by more than 0.5°C between 2007–2009 and 2017 [AMAP, 2017]. In Ice-rich permafrost areas, thawing permafrost leads to land surface changes, which affects both soil physical properties and hydrology [Schaefer et al., 2014]. Increasing permafrost disturbance in Arctic catchments [Lamoureux and Lafrenière, 2009, Lantz and Kokelj, 2008, Rudy et al., 2013] alter the biogeochemical cycling by reworking soil material and redistributing Organic Carbon (OC) and nutrients along hillslopes [Kokelj et al., 2013, Lamoureux and Lafrenière, 2014, Larouche et al., 2015, Woods et al., 2011]. There are increasing evidence of the impact of permafrost disturbances on adjacent lakes and streams [Dvornikov et al., 2018, Grewer et al., 2016, Kokelj et al., 2009a, Woods et al., 2011], yet there is a lack of studies focusing on understanding the evolution of hillslopes in lowland permafrost, and measuring their impact on soils and Soil Organic Carbon (SOC) redistribution along hillslopes. We address this gap by assessing the distribution and degradation of SOC and TN along hillslopes in Arctic valleys.
Hydrologic pathways erode and transport material and nutrients from land to the ocean [Aufdenkampe et al., 2011]. Arctic watersheds exhibit nival flow regimes, where snowmelt is the main hydrologic event of the year [Peel, 1990, Woo, 1986]. The magnitude of exported material and nutrients depends on the interaction between the hydrological flow and the erodible material in streambeds and on valley hillslopes. Environmental parameters characterizing draining valleys (e.g. topography, permafrost coverage, soil type, and water/ground ice content) are therefore key parameters determining the magnitude of terrestrial export to aquatic systems [Brierley et al., 2006, Vonk et al., 2015].

Permafrost thaw affects the stability of soils along hillslopes in the valleys; it impacts the active layer depth [Lamoureux and Lafrenière, 2009], enhances the development of water tracks [McNamara et al., 1999, Paquette et al., 2018], and causes soil collapse and subsidence, creating thermokarst and thermo-erosional landforms [Kokelj et al., 2017, Rudy et al., 2013]. A recent study estimated that hillslope thermokarst landscape coverage in the northern circumpolar permafrost region is below 5% [Olefeldt et al., 2016]. The incidence of hillslope thermokarst landforms (e.g. active layer detachment, thaw slumps and thermo-erosional gullies) is increasing [Fortier et al., 2007, Kokelj et al., 2017, Lantuit and Pollard, 2008, Ramage et al., 2017, Rudy et al., 2013, Segal et al., 2016]. Hillslopes thermokarst is a dominant process in V-shaped valleys in lowland permafrost regions [Kokelj and Jorgenson, 2013, Kokelj and Lewkowicz, 1998, Rudy et al., 2016]. It affects valley morphologies by reworking soils and transporting material downhill [Hinzman and Kane, 1992].
As a result of increased lateral transfer from the hillslopes, the quantities of material and nutrients in the adjacent streams increase [Dvornikov et al., 2018, Harms and Ludwig, 2016, Malone et al., 2013, Vonk et al., 2015]. Hillslope thermokarst landforms deliver large quantities of material, including SOC [Abbott et al., 2014, Kokelj et al., 2013],

and nutrients to streams [Bowden et al., 2008]. However, part of this material remains deposited along hillslopes or in the riparian zone [Larouche et al., 2015]. Due to persistent cold and saturated soil conditions, decomposition of Soil Organic Matter (SOM) is limited in permafrost soils. There, SOM turnover is related to soil forming factors such as temperature, moisture, oxygen and nutrient availability, parent material, and cryoturbation [Hobbie et al., 2000]. Changes affecting physical and chemical parameters as well as the quantity, quality, and availability of SOC in the soils influence the magnitude of SOM decomposition and mineralization.

The SOC storage in the upper 3 m of the northern circumpolar permafrost region is estimated to 1000 ± 150 Pg [Hugelius et al., 2014]. However, this estimate overlooks the spatial variability of SOC storage [Obu et al., 2017b, Palmtag et al., 2016, Siewert et al., 2015] and poorly accounts for SOC on hillslopes and in mountain regions [Hugelius et al., 2014, Mishra et al., 2013]. Slope processes contribute the accumulation of SOC downslope [Berhe et al., 2007, Rosenbloom et al., 2006]. This pattern was observed in the few studies that examined the spatial variability of SOC in permafrost terrains: thick soil deposits on hilltoe positions store large amount of SOC due to accumulation and burial of SOM following deposition [Michaelson et al., 1996, Shelef et al., 2017]. However SOC storage remains uncertain at hillslope scale: the fate of carbon along hillslopes depends on the rates of sediment forcing that acts on SOM turnover [Rosenbloom et al., 2006, Shelef et al., 2017]. There is a need to understand the slope processes acting on the redistribution of SOC in permafrost environments to better constrain the impact of permafrost thaw on the carbon cycle.

As a first step, we estimate the storage of SOC and TN along hillslopes in Arctic valleys, and discuss the impact of geomorphic changes on the variability of these stocks. We first describe the geomorphology of the valleys and hillslopes. Second, we relate SOC and TN stocks and carbon degradation (using C:N ratios) to spatial (e.g. hillslope position, valley position, and slope orientation) and soil variables (volumetric water content, cryoturbation, active layer depth, and topographic wetness index).

5.3 Study Area

Herschel Island (Qikiqtaruk Park Territory) is located in the western Canadian Arctic, 2 km off the Yukon Coastal plain (Fig. 5.1). The island of ca. 111 km^2 is characterized by rolling and hummocky moraines, modified by periglacial processes [MacKay, 1959]. Ridges and hills reach up to 178 m a.s.1 inland; steep cliffs up to 60 m high characterize the coasts. The coasts are actively receding: the mean rate of coastal retreat was 0.45 m yr^{-1} between 1970 and 2000 [Lantuit and Pollard, 2008], and 0.68 m yr^{-1} between 2000 and 2011 [Obu et al., 2017a]. The ground forming Herschel Island was thrust during the advance of the Laurentide Ice Sheet from the Herschel Basin to the margin of the glaciated area. Part of the permafrost on Herschel Island is therefore old, pre-dating

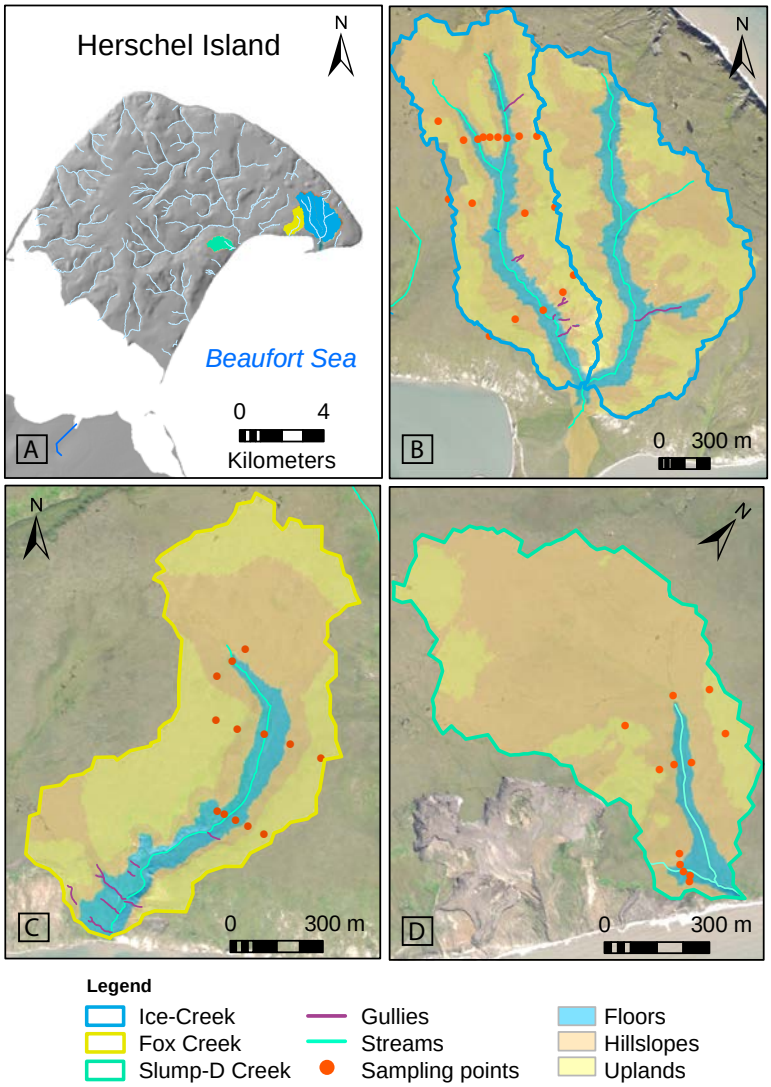

Figure 5.1 – Map of Herschel Island and of the three studied valleys (A): Ice Creek West (ICW) (B), Fox Creek (FC) (C), and Slump-D Creek (SLD) (D). The valleys are located on the eastern sector of the island and drain into the Beaufort Sea. Each basin is divided into three geomorphic sub-units; the uplands, the slopes and the valley floors. Sampling sites were distributed along transects located upstream, midstream, and downstream, intersecting the valleys perpendicularly.

the formation of the island [Burn, 2000]. Preglacial deposits are marine and terrestrial sediments. Glacial and postglacial deposits include till, erratic boulders, peat accumulation and alluvial deposits [Bouchard, 1974]. Most of the soils are Turbic Cryosols [Group, 1998], with well developed, but variable, organic surface horizons underlain by mineral clayey-silt soils [Bouchard, 1974]. Burial of surface organic horizons into the mineral subsoil through cryoturbation is prevalent [Bouchard, 1974]. Ground ice is present throughout the island except on beaches and spits: volumetric ground ice contents vary from 44% to 77% [Couture and Pollard, 2017] and mostly occur as pore and segregated ice lenses, ice wedges and massive icy beds [Pollard, 1990].

Burn and Zhang showed that the mean annual air temperature for the period 1971-2000 on Herschel Island was -9°C, while July and August daily average was ca. 5°C. Yearly precipitation for the same period was low, varying between 150 and 200 mm. The snow cover on Herschel Island is thin, as a result of low precipitation and strong winds. Late winter snow depth between 1999 and 2007 on the uplands was on average 17 cm, with a range of 10-26 cm. The snow is blown away from the uplands and accumulates in topographic depressions[Burn and Zhang, 2009].

The Island is divided into 40 main watersheds with mean drainage basins of 73.2 ha, ranging from 20.4 to 2697.7 ha [Ramage, 2017]. To the best of our knowledge, there is no published data on the origin of the valleys on Herschel Island.
The fieldwork took place along the eastern coast of Herschel Island, in three Arctic valleys. The valleys are representative in size of the valleys on the island (Figure 5.1) ([Ramage, 2017]. As many Arctic watersheds, which commonly exhibit a nival flow regime [Woo, 1986]. In summer, discharge is mostly controlled by rainfall, and occasional rainfall events may lead to high discharge [Coch, 2018; personal communication].

5.4 Methods

5.4.1 Spatial analyses

The streams and watersheds on Herschel Island were mapped using a high-resolution GeoEye-1 satellite image (1.8 m resolution in multi-spectral and 0.5 m in panchromatic view) acquired in July 2011 [Ramage et al., 2017]. Streams were manually mapped at a 1:2000 scale, from the source to the outlet in ArcMap (ESRI, 10.3). We used a Digital Elevation Model (DEM) from TandeM-X created in 2012 (12 m resolution) to delineate the watersheds and derive spatial information (slope gradient, elevation, aspect). The streams were classified as: large valley streams with permanent flow; valley streams with temporary flow; gullies; thermo-erosional gullies; and ravines. We divided the valleys into four geomorphic units using field observations and the topographic position index (TPI) tool with a threshold of 50 m. The TPI compares the elevation of each cell in a DEM to the mean elevation of a specified neighborhood around that cell. Positive (respectively, negative) TPI values define areas that are higher (respectively, lower) than the average of their surroundings. TPI values near zero are either flat or sloping areas [Guisan et al., 1999].

5.4.2 Sampling Scheme

We divided the valleys into four geomorphic units using field observations and the TPI (Fig. 5.2). The four units represent the valley uplands, midslopes, hilltoes, and floors.

The samples were collected between July 27^{th} and August 8^{th}, 2015. We defined three

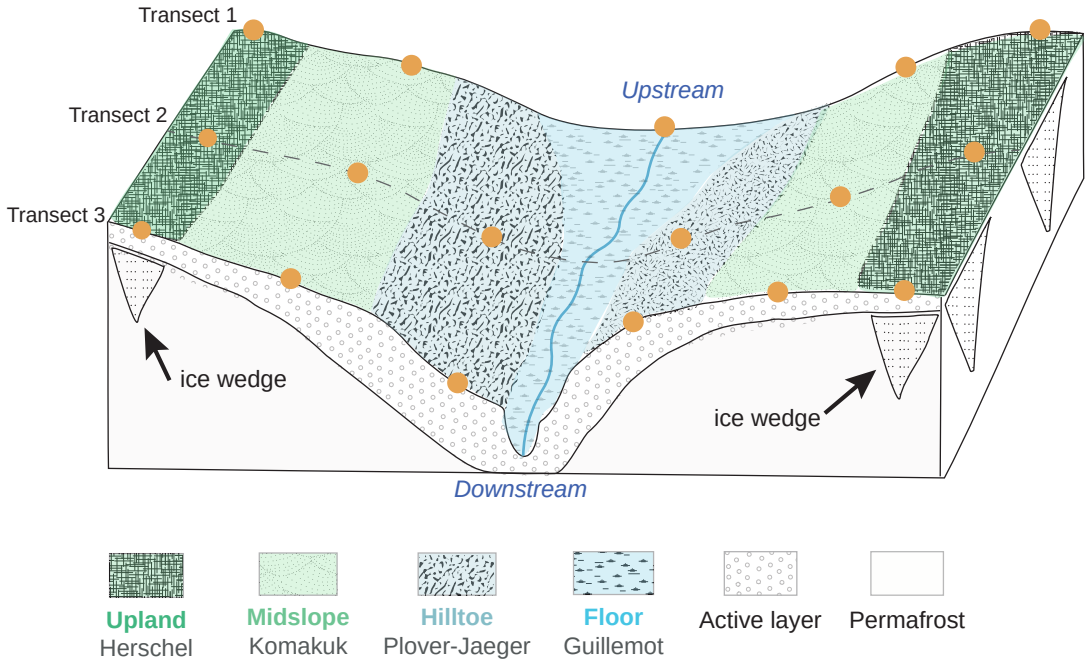

Figure 5.2 – Simplified sampling scheme. We sampled soil pits along and across each of the valleys. Soil pits were dug in each of the valley geomorphic unit: upland, midslope, hilltoe, and valley floor. Ecological classes associated to these units are indicated below each unit.

transects cutting each valley perpendicularly, in the upper, middle and lower parts of the valleys (Fig. 5.2). Along each transect we established three to five sampling sites, chosen to be representative of each geomorphic unit. We systematically described qualitatively the vegetation and the slope. Active layer depth was determined for each profile as the depth to the top of the permafrost on the sampling day. We assigned a relative level of cryoturbation (1 = low to 3 = high cryotubation) based on the observation of the pit profiles and descriptions of the permafrost samples (Appendix A.3, ds06). We sampled 43 sites and collected 316 samples.

At each site, we excavated soil pits down to the permafrost table, if reached before 1 m depth. We measured the depth of the active layer for each soil pit. We described the soil horizons in the active layer (e.g. sediment type, structure, color, texture) and sampled each soil genetic horizon using fixed volume cylinders (diameter = 3.4 cm, height = 3.8 cm). The organic surface horizon was cut out and measured for volume. To collect permafrost samples, we hammered a steel pipe (diameter = 4.2 cm) from the top of the permafrost to a depth of 1 m at 10 cm increments. For each sample, we qualitatively described the ice content, cryostructure [French and Shur, 2010] and degree of cryoturbation if applicable (Table 5.1). The samples were kept cool and were transported after

fieldwork to the laboratory for further analysis.

5.4.3 Geochemical analyses

The samples were freeze-dried for 72 hours at -20°C. We weighted the samples before and after freeze-drying to assess for volumetric water content. We estimated the dry bulk density (ρ_b) using Eq. (1), where dW_i is the dry-weight of a sample and V_i its volume.

(1) $\rho_b = dW_i / V_i$

The samples were separately analyzed for %C and %N in a carbon-nitrogen analyzer (Vario EL III elemental analyzer). The Total Organic Carbon (TOC) was measured using a Vario Max carbon analyzer (Elementar). SOC was then calculated using Eq. (2), where %TOC is the TOC content (wt%), ρ_b the bulk density, and L the length of a sample (cm).

(2) SOC = %TOC x ρ_b x L x 10

The C:N ratio was calculated using the ratio between %TOC and %N. The C:N ratio can be used as an index for the potential degradability of SOM stored in permafrost soils and the potential for carbon loss upon thaw [Schädel et al., 2014, Kuhry and Vitt, 1996]. Stable carbon isotopes ($\delta^{13}C$) values were analyzed with a DELTAplusXL Finnigan mass spectrometer (Thermo Fisher Scientific, Germany) coupled to a Carlo-Erba NC2500 elemental analyzer. Isotope signatures are reported in per mille (‰) against Vienna Pee Dee Belemnite (VPDB).

5.4.4 Environmental variables and statistical analyses

We tested the dependency of SOC, TN and C:N ratio against the environmental variables. Environmental variables are described in Table 5.1. The variables were either described in the field (hillslope position, distance to shore, active layer depth), derived from laboratory analyses (volumetric water content), or from GIS analyses using ArcGIS 10.3 (hillslope position, distance to shore, slope orientation and topographic wetess index). Hillslope positions were adjusted from direct field observations using the TPI with a threshold of 50 m. We defined the distance to shore as an ordinal number ranging from 1 to 3 and corresponding to the relative distance of each transect to the shore (1 downstream; 2 midstream and 3 upstream).

The impact of the spatial position (spatial variables) on the geochemical variables was assessed using the Kruskal-Wallis non-parametric test and Dunn's posthoc test. Linear correlations between soil and geochemical variables were assessed using student t-tests. All tests were performed using the R software (The R Foundation, version 3.3.1).

Table 5.1 – Environmental variables used in the statistical analyses.

Type	Abbreviation	Signification
Spatial	HSP	Hillslope position: upland, midslope, hilltoe, floor
Spatial	DS	Distance to shore: upper, middle, lower parts of the valley
Spatial	PAIR	Slope orientation: east- and west-facing slopes
Soil	ALD	Active layer depth (cm)
Soil	CRY	Level of cryoturbation (scale: 1, low to 3, high)
Soil	VWC	Volumetric water content (%)
Soil	TWI	Topographic weTNess index

5.5 Results

5.5.1 Geomorphology of the valleys

Longitudinal profiles

Table 5.2 – Geomorphic characteristics of the studied valleys on Herschel: Ice-Creek West (ICW), Fox-Creek (FC) and Slump-D Creek (SLD).

	ICW	FC	SLD
Drainage basin (km^2)	3.09	0.77	0.62
Stream number	4	5	6
Total stream length (m)	3569	1688	1786
Stream order 1	2	4	4
Stream order 2	1	1	1
Stream order 3	1	0	1
Drainage density (km^{-1})	1.15	2.19	2.88
Valley width upstream (m)	483	103	497
Valley width midstream (m)	456	312	484
Valley width downstream (m)	612	313	177
Differential elevation upstream E-facing slope (m)	11.35	4.04	8.19
Differential elevation upstream W-facing slope (m)	16.46	3.27	3.60
Differential elevation midstream E-facing slope (m)	21.55	12.49	9.59
Differential elevation midstream W-facing slope (m)	31.47	15.49	9.78
Differential elevation downstream E-facing slope (m)	33.65	6.14	2.11
Differential elevation downstream W-facing slope (m)	41.19	17.83	5.72
Main stream			
Length (m)	2511	1396	960
Gradient (°)	1.6	2.6	3.00
Elevation max (m)	81	67.9	55
Elevation min (m)	0	0	0

The drainage basins of the studied valleys – Slump-D Creek (SLD), Fox Creek (FC) and Ice Creek (IC) – are respectively 61.8 ha, 77.5 ha and 309.1 ha, ranging in elevation from 0 m to 80 m a.s.l. The valleys are oriented north-south and drain directly into the Herschel Basin in the Beaufort Sea (Fig. 5.1). Stream gradients range between 1.6° and 3.0° (Table 5.2). In the upper part of the valleys thermo-erosional processes create U-shaped beds, where ice wedge degradation and beaded streams occur. In the middle and lower parts of the valleys, water tracks, gullies, and mass wasting processes are common along hillslopes. The upper parts of the valleys are flat, characterized by polygonal fields (Fig. 5.3). Ice wedges, degrading during the summer months, are common at the source of the valleys. In the upper part, valley floors are covered by sedge-grass vegetation and have poorly drained soils and hygric conditions. The soils are fibric with a thick peat layer and high organic content. Due to the low stream gradient, ponds can form and develop further into beaded streams. In the middle part of the valleys, hillslope runoff through water tracks is a main supply for the widening streams (ca. 50 cm). The streams start eroding the valley floor and lower the water table (Fig. 5.3). On the segments where streamflow increases, knickpoints form, the vegetation is absent and pebbles and cobbles are visible. Streams become turbid as soon as they receive sediment input from streambed erosion. Mass movements occur in the lower part of the valley (Fig. 5.3). In late July 2015 the streams at the outlet were up to 100 cm wide and ca. 10 cm deep.

Transversal profile

Surface topography, including vegetation and patterned-ground reflect the dynamics of the valleys. The valley hillslopes are concavo-convex, with relatively smooth profiles and no abrupt breaks. The midslopes are concave, characterized by mass wasting processes; the hilltoes are convex, characterized by sediment accumulations deposited from uphill. The upper and middle parts of the valleys have gentle, stabilized, and vegetated hillslopes with increasing slope gradient downstream (Table 5.2). Periglacial processes are active on the hillslopes; solifluction, creeping and stripes were observed in the valleys. In the middle and lower parts of the valleys, active layer detachments, thaw slumps, and gullies are common. In their lower parts, the valleys evolve as ravines, with steep, non-vegetated, and asymmetric hillslopes. Slope asymmetries are present in the valleys: west-facing slopes have lower gradients and are more vegetated than east-facing slopes (Fig. 5.3, Table 5.2).

The uplands cover stable and mostly flat surfaces where little erosion has occurred. They are characterized by hummocky surfaces covered by cottongrass and moss vegetation. Ecological conditions are relatively uniform on this unit: a dense vegetation cover allows a shallow active layer with no erosion. The most common type of soil is Turbic Cryosol [Group, 1998], with silty-clays. The soils are moist or moderately well drained and weathered within the active layer. Non-sorted patterned-ground can be

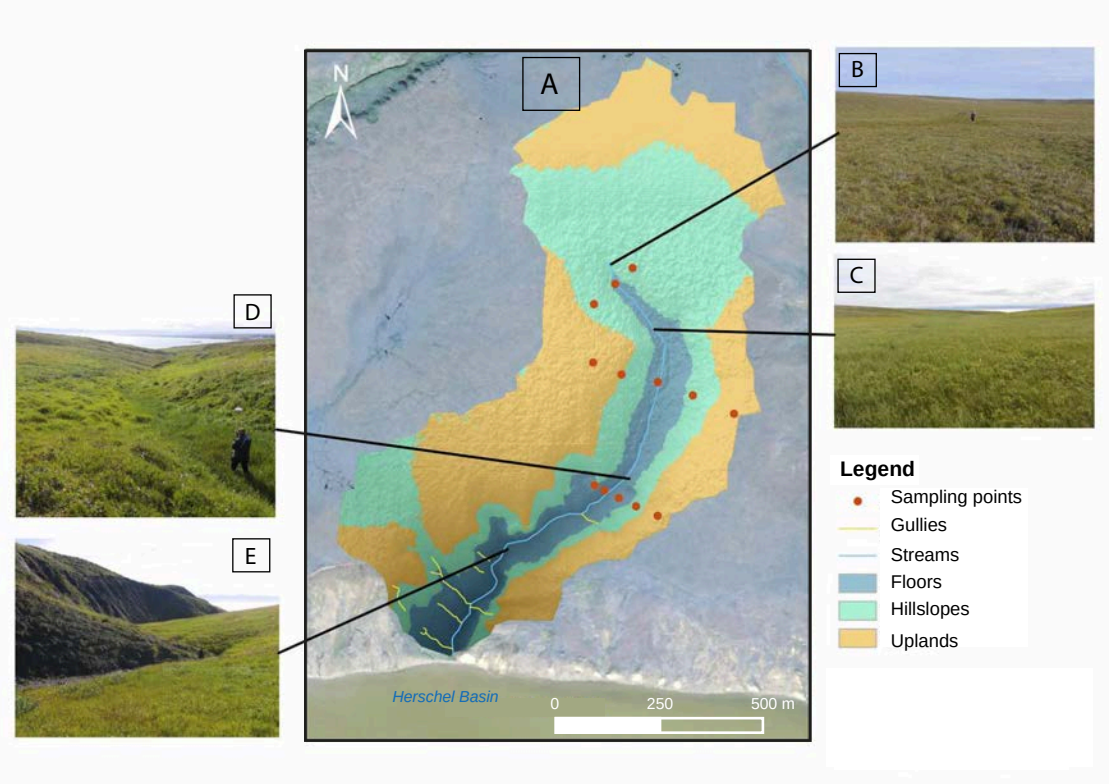

Figure 5.3 – Morphology of a valley, Fox Creek (FC). (A) The map shows the different valley units (defined using the Topographic Position Index (TPI)) and the sampling locations. The underlying image is a World-View satellite image from August 8^{th} 2015. The photographs were taken on August 4^{th} 2015 and show the valley in the (B) upstream, (C) midstream up, (D) midstream down, and (E) downstream. Person for scale (Photos by S. Stettner).

present and cryoturbation is common. Uplands are associated with the Herschel and Komakuk ecological units defined by [Smith et al., 1989]. The Herschel ecological unit, characterizing hummocky tussock tundra, is the climax vegetation community of the island. The Komakuk ecological unit describes slightly disturbed upland tundra with patterned-ground closer to the crests [Smith et al., 1989]. Uplands covers ca. 44% of the Island. The midslopes comprise terrains on complex slopes undergoing moderate erosion. Gully erosion, mass movements (active layer detachments and retrogressive thaw slumps) and patterned-ground (stripes, earth-hummocks and frost-boils) are present on both east- and west-facing slopes. The above processes contribute to creating heterogeneous conditions: as a consequence, soils are reworked and soil-forming processes are interrupted in some areas, forming Static Cryosols [Group, 1998] that lack developed horizons. The common ecological unit on mid-slopes is Plover-Jaeger with Arctic willows covering non-eroded soils [Smith et al., 1989]. The hilltoes correspond to the terrains downslope, bordering the valley floors. Hilltoes represent zones of soil accumulation being reworked from the mid-slopes by mass movements to downhill. Soils are composed of a thin organic layer (<5 cm) and a thick uniform mineral horizon (>70 cm). Static Cryosol [Group, 1998] is the most common soil of this unit. Hilltoes are as-

sociated with the Thrasher vegetation class, characterized by Arctic willow and early successional grass vegetation on more recently disturbed surfaces [Smith et al., 1989]. Valley floors represent areas from the upper and middle valley floors, characterized by depressions formed by degradation of polygonal terrains. They evolve as alluvium in the middle part of the valley. The soils are mostly Organic Cryosols [Group, 1998]: a thick organic peat layer (>20 cm) overlays mineral horizons. The soils are hygric with a high water table located a few centimetres under the surface. The main vegetation type is sedges and grasses.

5.5.2 Spatial distribution of carbon and nitrogen

Distribution at depth

Table 5.3 – Summary of soil geochemical variables at different depths averaged for the 3 valleys (0-30 cm; 0-50 cm; 0-100 cm ; active layer (AL), permafrost (PF)). Mean values are reported with ± one standard deviation.

	SOC (kg C m^2)	TN (kg N m^2)	C content (%)	N content (%)	C:N	δ^{13}C (‰)
0-30 cm	11.4 ± 3.7	0.8 ± 0.3	15.4 ± 11.9	0.9 ± 0.4	17.7 ± 6.4	-28.0 ± 1.2
0-50 cm	17.9 ± 4.9	1.4 ± 0.4	14.9 ± 11.8	0.8 ± 0.4	15.9 ± 5.9	-27.7 ± 1.2
0-100 cm	26.4 ± 8.9	2.1 ± 0.6	8.3 ± 3.5	0.5 ± 0.2	12.9 ± 2.2	-27.1 ± 0.6
AL	16.2 ± 4.6	1.3 ± 0.4	13.4 ± 11.9	0.7 ± 0.5	15.1 ± 6.0	-27.6 ± 1.1
PF	11.2 ± 1.8	0.9 ± 0.1	6.8 ± 5.0	0.4 ± 0.3	12.1 ± 2.9	-26.9 ± 0.7

The mean active layer depth in the valleys was 52 cm, ranging between 26 to <100 cm. The C and N contents decreased with increasing depth and were higher in the active layer than in the permafrost (Table 5.3, Appendix A.3, ds07). The average C:N ratio in the valleys was 12.9, ranging from 9.7 to 18.9. Individual pits showed a decrease in C:N ratios with increasing depth. The C:N ratio in the active layer was significantly higher than in the permafrost (Table 5.3). The δ^{13}C values were similar between sites and typical of a C3-plant dominant ecosystem, ranging between -28.9 and -26.3‰.

Differences between valleys

Active layer depths varied between valleys; the mean active layer depth in SLD valley was thinner (42 ± 14 cm) than in the FC and ICW valleys (55 ± 20 and 57 ± 22 cm, respectively). Larger stocks of SOC were found in the SLD valley compared to FC and ICW valleys (Table 5.4). We found similar patterns in the spatial distribution of TN stocks between valleys. TN stocks were higher in the SLD valley compared to the FC and ICW valleys. The C:N ratios were on average higher in the SLD valley compared to FC and ICW valleys.

Table 5.4 – Summary of the geochemical variables in each of the three valleys (Ice-Creek West, ICW; Fox-Creek, FC; and Slump-D Creek, SLD). Mean values are reported with ± one standard deviation and reported for 0-100 cm depth.

	SOC (kg C m^2)	TN (kg N m^2)	C content (%)	N content (%)	C:N
ICW	23.6 ± 8.2	2.1 ± 0.5	7.2 ± 3.2	0.5 ± 0.1	11.9 ± 2.4
FC	26.9 ± 10.3	2.1 ± 0.7	7.9 ± 4.2	0.5 ± 0.2	12.9 ± 2.1
SLD	30.1 ± 7.1	2.3 ± 0.6	10.3 ± 2.1	0.7 ± 0.1	14.1±1.3

Differences between transects

Table 5.5 – Summary of geochemical parameters for each transect averaged for the three valleys. Mean values are reported with ± one standard deviation. The mean values are given for the whole soil depths in bold, and below for each depth category (0-30 cm; 0-50 cm; 0-100 cm; active layer (AL), Permafrost (PF)). The red color indicates significant differences ($p<0.05$).

	AL mean (cm)	SOC (kg C m^2)	TN (kg N m^2)	C content (%)	N content (%)	C:N
Downstream	58.5 ± 22.6					
0-30 cm		8.4 ± 4.5	0.7 ± 0.3	11.0 ± 4.7	0.7 ± 0.2	14.4 ± 2.3
0-50 cm		14.7 ± 7.1	1.2 ± 0.5	9.3 ± 5.0	0.6 ± 0.2	13.6 ± 2.7
0-100 cm		25.1 ± 10.3	2.1 ± 0.7	7.1 ± 4.1	0.4 ± 0.2	12.5 ± 2.5
AL		15.7 ± 6.0	1.3 ± 0.4	10.2 ± 10.6	0.6 ± 0.4	14.0 ± 5.4
PF		10.7 ± 7.1	0.9 ± 0.5	6.5 ± 4.9	0.5 ± 0.3	12.1 ± 3.1
Mid-stream	51.6 ± 19.7					
0-30 cm		10.3 ± 3.2	0.8 ± 0.2	14.8 ± 4.7	0.8 ± 0.2	15.3 ± 2.1
0-50 cm		15.8 ± 6.3	1.3 ± 0.4	12.7 ± 5.1	0.7 ± 0.2	14.5 ± 2.2
0-100 cm		26.3 ± 8.8	2.2 ± 0.5	8.2 ± 2.8	0.5 ± 0.2	12.6 ± 1.9
AL		16.9 ± 6.0	1.4 ± 0.5	13.4 ± 12.4	0.7 ± 0.5	14.9 ± 5.9
PF		10.3 ± 8.6	0.8 ± 0.5	5.4 ± 5.2	0.4 ± 0.3	11.6 ± 3.1
Upstream	38.7 ± 6.0					
0-30 cm		10.9 ± 3.6	0.8 ± 0.2	20.3 ± 1.9	1.0 ± 0.2	18.6 ± 2.7
0-50 cm		13.9 ± 9.1	1.0 ± 0.6	13.5 ± 6.3	0.7 ± 0.3	16.0 ± 3.2
0-100 cm		30.2 ± 4.0	2.2 ± 0.3	11.4 ± 2.5	0.7 ± 0.2	14.9 ± 1.6
AL		15.1 ± 5.6	1.1 ± 0.5	18.8 ± 13.5	0.9 ± 0.4	18.1 ± 7.3
PF		15.1 ± 6.4	1.1 ± 0.4	8.0 ± 4.7	0.6 ± 0.3	13.4 ± 2.0

The mean active layer depth decreased with increasing the distance from the shore. In the upper part of the valley, the mean active layer depth was on average 38.7 ± 6.0 cm while it was 58.5 ± 22.6 cm on the downstream transect (Table 5.5). The C content was significantly higher on the upstream transects compared to the downstream transects. This difference was also found in the top 30 cm and the active layer. The C:N ratios were

significantly higher on the upstream transect compared to the mid and downstream transects (Table 5.5).

Differences between geomorphic units

Table 5.6 – Summary of geochemical parameters for each geomorphic unit averaged for the three valleys. Mean values are reported with ± one standard deviation. The mean values are given for the whole soil depths in bold, and below for each depth category (0-30 cm; 0-50 cm; 0-100 cm; active layer (AL), permafrost (PF)). The red color indicates significant differences ($p<0.05$).

	AL mean (cm)	SOC (kg C m^2)	TN (kg N m^2)	C content (%)	N content (%)	C:N
Floors	41.2 ± 9.3					
0-30 cm		9.2 ± 3.8	0.6 ± 0.3	18.9 ± 3.2	1.1 ± 0.2	17.2 ± 3.3
0-50 cm		17.6 ± 3.9	1.2 ± 0.3	13.6 ± 2.7	0.8 ± 0.1	15.5 ± 2.4
0-100 cm		33.8 ± 9.1	2.5 ± 0.8	11.3 ± 3.0	0.8 ± 0.2	14.1 ± 2.1
AL		15.2 ± 4.8	1.0 ± 0.3	16.2 ± 4.6	0.9 ± 0.1	16.5 ± 3.8
PF		18.6 ± 1.6	1.4 ± 0.1	9.3 ± 2.9	0.7 ± 0.2	13.1 ± 1.9
Hilltoes	94.5 ± 11.0					
0-30 cm		6.6 ± 3.2	0.6 ± 0.3	8.2 ± 5.9	0.5 ± 0.2	13.0 ± 3.2
0-50 cm		9.3 ± 3.2	0.9 ± 0.4	7.2 ± 5.3	0.5 ± 0.2	12.1 ± 2.8
0-100 cm		18.5 ± 6.3	1.9 ± 0.7	5.0 ± 3.3	0.4 ± 0.2	11.0 ± 1.5
AL		17.3 ± 4.9	1.7 ± 0.6	5.6 ± 3.0	0.4 ± 0.1	11.6 ± 1.6
PF		3.8 ± NA	0.4 ± NA	1.2 ± NA	0.1 ± NA	8.3 ± NA
Midslopes	57.6 ± 17.7					
0-30 cm		9.8 ± 7.7	0.8 ± 0.3	13.8 ± 5.0	0.8 ± 0.2	14.6 ± 2.0
0-50 cm		14.8 ± 6.3	1.2 ± 0.5	12.4 ± 6.4	0.7 ± 0.3	14.0 ± 2.7
0-100 cm		25.3 ± 10.4	2.2 ± 0.6	6.9 ± 2.8	0.5 ± 0.2	11.8 ± 1.5
AL		17.0 ± 4.9	1.5 ± 0.4	14.8 ± 5.4	0.7 ± 0.2	13.8 ± 2.2
PF		8.8 ± 1.6	0.8 ± 0.1	4.1 ± 3.4	0.3 ± 0.2	10.7 ± 2.3
Uplands	41.1 ± 8.8					
0-30 cm		10.6 ± 2.7	0.8 ± 0.2	19.4 ± 4.7	0.8 ± 0.2	16.3 ± 2.1
0-50 cm		16.2 ± 7.2	1.2 ± 0.5	11.9 ± 5.0	0.7 ± 0.2	15.1 ± 2.3
0-100 cm		27.1 ± 6.3	2.1 ± 0.4	9.3 ± 3.3	0.6 ± 0.2	13.9 ± 2.2
AL		15.5 ± 4.1	1.2 ± 0.4	15.0 ± 5.0	0.8 ± 0.2	16.5 ± 2.2
PF		11.6 ± 1.9	0.9 ± 0.1	6.6 ± 4.9	0.5 ± 0.3	12.6 ± 3.0

As shown in Table 5.6, the deepest active layers were found on the hilltoes. The valley floors and uplands had similar active layer depths of ca. 41 cm. The largest C, N contents and SOC, TN stocks were found in the valleys floors (Table 5.6).

Figure 5.4 illustrates the significant differences in the C contents and C:N ratios between

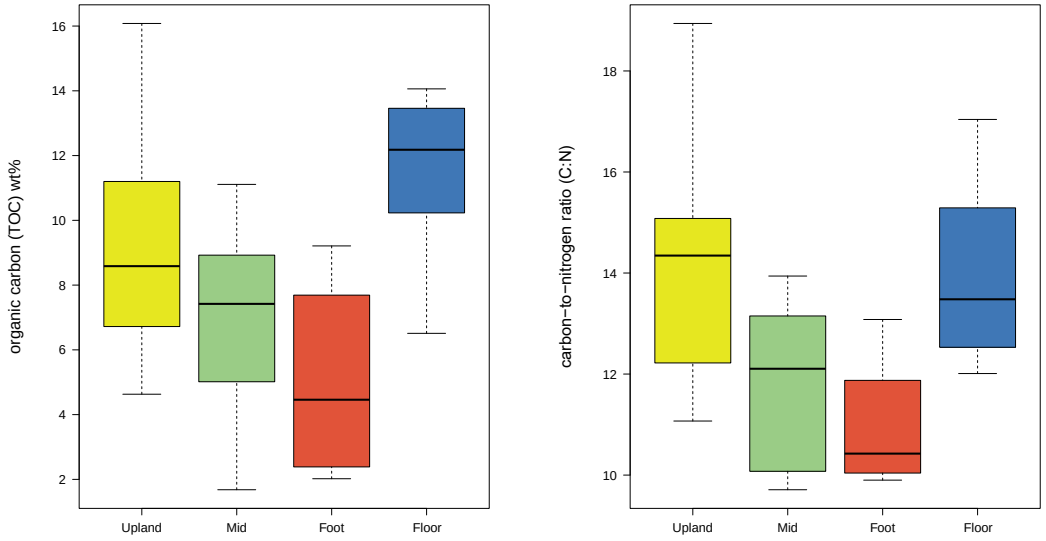

Figure 5.4 – Boxplots summarizing significant spatial variability of a) carbon content and b) Carbon-to-nitrogen ratios between geomorphic units in the valleys.

geomorphic units. The C content was significantly higher in the valley floors compared to the hilltoes and the N content significantly higher on the floors compared to the slopes. The valley floors are characterized by peat accumulation and water saturated soils. On the contrary, significantly low C and N contents were found in the hilltoes that are characterized by deposition of material from the uplands. The C:N ratios were significantly higher in the uplands compared to the slopes, however, there was no significant difference in C:N ratios between sites located in the valley floor and other units (Table 5.6).

Differences between paired slopes

The active layer depths were similar on the east and west-facing slopes, with the thinnest active layers at 26-28 cm, the deepest >100 cm (Table 5.7). The TN stocks and N contents were significantly higher on the east-facing slopes compared to the west-facing slopes (Table 5.7). In the permafrost, SOC, TN, C and N contents were significantly higher on the east-facing slopes compared to the west-facing slopes.

Table 5.7 – Summary of geochemical parameters for the paired slopes averaged for the three valleys. Mean values are reported with ± one standard deviation. The mean values are given for the whole soil depths in bold, and below for each depth category (0-30 cm; 0-50 cm; 0-100 cm; active layer (AL), permafrost (PF)). The red color indicates significant differences ($p<0.05$).

	AL mean (cm)	SOC (kg C m^2)	TN (kg N m^2)	C content (%)	N content (%)	C:N
East	53.1 ± 23.6					
0-30 cm		10.2 ± 4.0	0.8 ± 0.3	12.8 ± 5.1	0.7 ± 0.2	15.2 ± 2.8
0-50 cm		15.9 ± 6.7	1.3 ± 0.4	11.1 ± 5.4	0.7 ± 0.2	14.2 ± 2.8
0-100 cm		28.3 ± 9.2	2.3 ± 0.6	8.9 ± 3.8	0.6 ± 0.2	13.3 ± 2.5
AL		17.0 ± 6.3	1.4 ± 0.5	12.0 ± 5.3	0.7 ± 0.2	14.8 ± 2.9
PF		13.5 ± 8.7	1.0 ± 0.5	7.5 ± 4.9	0.5 ± 0.3	12.8 ± 3.1
West	54.2 ± 18.5					
0-30 cm		9.4 ± 3.6	0.7 ± 0.2	14.6 ± 5.3	0.8 ± 0.2	15.3 ± 2.0
0-50 cm		13.7 ± 7.8	1.1 ± 0.6	12.0 ± 6.1	0.7 ± 0.3	14.6 ± 2.5
0-100 cm		22.5 ± 6.8	1.9 ± 0.4	6.9 ± 2.6	0.4 ± 0.1	12.1 ± 1.7
AL		15.7 ± 5.6	1.3 ± 0.4	13.1 ± 6.3	0.7 ± 0.3	14.8 ± 2.6
PF		7.1 ± 5.0	0.6 ± 0.3	3.3 ± 2.8	0.3 ± 0.2	10.6 ± 2.3

5.5.3 Correlations between soil characteristics and geochemical variables

The volumetric water contents and level of cryoturbation decreased and the bulk densities increased from up to downhill. Similarly, the volumetric water contents decreased and the bulk density increased from up- to downstream (Appendix A.3, ds07). Geochemical variables were well correlated to the soil characteristics (Table 5.8). Among all soil characteristics, the level of cryoturbation was the most correlated to the geochemical variables (Table 5.8). Moist and strongly cryoturbated sites had higher SOC and TN stocks, C and N contents and C:N ratios. The C and N content as well as C:N ratio were negatively correlated to the depth of the active layer; sites with thin active lay-

Table 5.8 – Pearson correlation coefficients between geochemical parameters and soil variables (ALD, active layer depth; CRY, cryoturbation; VWC, volumetric water content; TWI, topographic weTNess index). The means were averaged for the three valleys. Significant relations are indicated in bold and marked according to their significance level: ***$p<0.001$; **$p<0.05$;*$p<0.1$.

	AL (r^2)	CRY (r^2)	VWC (r^2)	TWI (r^2)
SOC (kg C m^2)	-0.40*	0.55***	0.49*	0.21*
TN (kg N m^2)	-0.12*	0.37**	0.37*	0.07*
C (%)	-0.51***	0.71***	0.44***	0.30**
N (%)	-0.49***	0.79***	0.52	0.36***
C:N	-0.53***	0.66***	0.36***	0.29***

ers had the highest C, N contents and C:N ratios. The C:N ratio was positively correlated to the volumetric water content and the topographic wetness index (Table 5.8).

5.6 Discussion

5.6.1 Variability in soil and geochemical properties in Arctic valleys

Our study based on the analysis of 43 sites located in three valleys on Herschel Island highlights the high variability in soil characteristics between and within the valleys. We found strong heterogeneity in the soils physical and chemical properties within geomorphic units, distance to the shore and slope orientation. Similar heterogeneity in soil profiles and SOC storage pattern on Herschel Island and in other Arctic areas were related to geomorphic processes acting at different scales such as disturbances, patterned-ground, ground-ice and soil characteristics [Pautler et al., 2010, Siewert, 2016, Michaelson et al., 1996]. We associate the strong variability of active layer depth on the hillslopes to differences in mass wasting processes. Midslopes, which comprise terrains on complex slopes undergoing moderate erosion, was the most heterogeneous unit: active layer depths varied between 34 cm and over 100 cm, soils were reworked and soil-forming processes were interrupted at some depth. On the hilltoes, characterized by accumulation of material from uphill, thaw consolidation produced deep active layers with thin organic layers and compacted homogenous mineral layers. These mineral layers record previous thaw events; rapid thaw of ice-rich clayey sediments often lead to soft sediment deformation [Harris et al., 2000]. At this position, the main difference between soils was in the thickness of the organic layer, which reflects differences in the stability of the slopes.

The average SOC and TN 0-100 cm stocks in the valleys on Herschel Island were 26.4 ± 8.9 kg C m^2 and 2.1 ± 0.6 kg N m^2 . These values are lower than previous estimates of mean SOC and TN 0-100 cm stocks for Herschel Island; 34.8 kg C m^2 and 3.4 kg N m^2 , respectively [Obu et al., 2017b]. SOC stocks in the valleys are in the same range as the stocks found in the geomorphic unit defined by Obu et al. as strongly disturbed terrain (20.9 kg C m^2) [Obu et al., 2017b]. Siewert also reported higher SOC stocks for several sites on Herschel Island [Siewert, 2016]. However, the latter study shows a similar spatial pattern: SOC stocks are higher on the uplands compared to the slopes, but with a strong heterogeneity between sites. Heterogeneity in SOC and TN stocks on hillslopes was also reported by Shelef et al. for a site in Alaska [Shelef et al., 2017]. They related this variability to spatiotemporal heterogeneity in topography, hydrology, permafrost condition, and glacial history.
We showed that differences in soil properties explained the variability in SOC and TN stocks. Differences in cryoturbation and volumetric water content were the factors most correlated to the SOC and TN stocks. Cryoturbation was previously identified as a major component in explaining the strong contrast in SOC density at meter to decame-

ter scale on Herschel Island [Siewert, 2016].

The δ^{13}C values in the valleys on Herschel were homogeneous and typical of a C3-plant dominant ecosystem, ranging between -28.9‰ and -26.3‰. The C:N ratios and δ^{13}C values were negatively correlated (r^2 = -0.58, $p<0.05$), indicating that sediments in the valleys are predominantly of terrigenous origin. The average C:N ratio in the valleys was 12.9, ranging from 9.7 to 18.9. The C:N ratios on the upstream transects were significantly higher than on the mid- and downstream transects, reflecting the differences in soil processes in these areas. Upstreams are characterized by peat with impeded drainage and thick vegetation cover, which facilitate accumulation of fresh SOM. In contrast, downstream transects were characterized by greater erosion and decomposition of SOM. The C:N ratios were significantly higher in the uplands and lower on the hillslopes, suggesting that OC was more degraded downhill. Similar results were found in temperate environments where soil erosion has important implications on the storage of SOM and on its stability in dynamic landscapes [Berhe et al., 2012].

5.6.2 Hillslope Processes

Depending on the slope gradient, hillslopes are affected by erosion, including mass movements. Soil erosion includes three processes: detachment, transport and deposition of soil particles [Berhe et al., 2007]. As a result of downslope soil transport through soil creep, slump and fluvial processes, as well as accumulation of locally produced organic material; hillslopes commonly accumulate thick soil deposits at hilltoe position [Berhe et al., 2007, Shelef et al., 2017, Yoo et al., 2005].

Geomorphic processes are driving soil thickness and provide fundamental mechanisms that control the spatial SOM decomposition and SOC patterns on vegetated hillslopes [Yoo et al., 2005]. Soil thickness is a key control on the SOC storage [Yoo et al., 2005]. On hilltoes, SOM decomposition is slowed down due to wetter and less oxygenated environments. As a result, SOM in depositional areas is better preserved than in eroding landform positions [Berhe et al., 2012]. However, this pattern is not straightforward; the redistribution of SOM by soil erosion can both increase and decrease accessibility of SOM to decomposition depending on the environment in which the OM is redeposited [Berhe et al., 2012]. The quantity of accumulated SOC on the hilltoes strongly depends on the rate of SOM decomposition during transport and within buried deposits [Berhe et al., 2012, Berhe et al., 2007, Yoo et al., 2005].

In permafrost terrains, hillslope thermokarst is the major process through which large quantities of material are abruptly transported downhill. Detachment and slumping erode large quantities of material, leaving barren scar zones on hillslopes. Following erosion, the exposed mineral soils, which contain older and labile-rich OM, become prone to decomposition by soil microorganisms [Grewer et al., 2016, Pautler et al., 2010].

Stimulated biogeochemical cycling rates of SOM enhance the mineralization of stored SOC. Tanski et al. show that, following slump initiation, SOM rapidly decomposes and SOC storage decreases by 77% in the impacted areas [Tanski et al., 2017]. Decrease in SOC storage is related to increasing soil temperature and associated to dilution with melted ice, leaching and mineralization [Abbott et al., 2014, Abbott and Jones, 2015, Tanski et al., 2017]. On the disturbed midslopes, thermokarst alters SOM composition with depth and enhances erosion of labile-rich SOM [Grewer et al., 2016]. As a result of erosion and increased SOM decomposition, there is a decrease in the stocks of SOC on the midslopes affected by thermokarst [Abbott and Jones, 2015, Cassidy et al., 2016, Grewer et al., 2016, Tanski et al., 2017]. Between 6% and 51% of the initial organic-layer SOC is displaced by hillslope thermokarst and partly accumulates downhill [Abbott and Jones, 2015].
In our study site, hilltoes were characterized by thick (> 1 m) material deposited from upslope and soils had high bulk densities and no cryoturbation. Hilltoes stored low amount of SOC compared to other geomorphic units (18.5 ± 6.3 kg C m^3). This suggests that a large part of the SOM and SOC transported from uphill either decomposed during its transport to the hilltoes or in situ, or was transported further to the riverine ecosystem.

Lateral redistribution of SOC due to soil erosion has important implications not only for the storage but also the stability of SOC in dynamic landscapes. Hilltoes exhibit deep active layers with finer soil particles and impeded drainage. These conditions hinder the decomposition of SOM, and partly explain the large quantities of SOC stored on hilltoes [Berhe et al., 2012, Shelef et al., 2017]. In our study sites, C:N ratios were significantly lower on the hilltoes compared to the uplands, especially in the active layers, suggesting that SOM degraded in situ on hilltoes. It contradicts previous research done on hillslope landscapes, which show that along with the burial of SOC in accumulation areas, these areas may favor SOM stabilization [Berhe et al., 2012, Grewer et al., 2016, Grewer et al., 2015]. However, Berhe et al. pointed out that SOM stabilization in accumulation zones differs across landscapes due to heterogeneous geomorphology and environmental conditions that affect the stability of buried SOM [Berhe et al., 2012]. In some situations, disturbances take away the physical and chemical mechanisms of SOM protection, exposing the soils to decomposition [Abbott et al., 2014, Berhe et al., 2012]. Our study reflects complex processes acting on the decomposition of SOC and accumulation of SOC along hillslopes. We recommend further research at landform scale to reveal these processes.

5.7 Conclusion

This study is a snapshot of the distribution and degradation of SOC in three Arctic valleys located on Herschel Island, Yukon Territory, Canada. The average SOC and TN 0-100 cm stocks in the valleys on Herschel Island were 26.4 ± 8.9 kg C m^2 and 2.1 ± 0.6

kg N m^2. We highlight the strong spatial variability in SOC and TN storage within Arctic valleys. There was no correlation between the mean SOC and TN stocks and spatial variables. We associate this variability to the diversity of geomorphic processes acting on hillslopes that redistribute soils from up- to downhill. As a result of different hillslope thermokarst processes, surface topography and soil profiles are irregular, which impacts the decomposition of SOM and storage of SOC and TN. As shown by Abbott and Jones, the interaction between landform morphology and landscape characteristics determines both the initial displacement of organic matter and subsequent carbon and nitrogen storage [Abbott and Jones, 2015]. The C:N ratios indicated significant degradation of carbon downstream and downhill, suggesting again the important role of hillslope processes on the SOM quality in permafrost terrains. There is a need to look into specific processes that drive the heterogeneous distribution of SOC and TN along hillslopes in order to better constrain the partitioning of these stocks at a landscape scale.

6 Eidesstattliche Erklärung

Hiermit versichere ich, dass ich die vorliegende Arbeit selbstständig verfasst und keine anderen als die angegebenen Quellen und Hilfsmittel verwendet habe.
Ich habe diese kumulative Dissertation am Alfred-Wegener-Institut Helmholtz Zentrum für Polar und Meeresforschung in Potsdam erarbeitet und in englischer Sprache angefertigt. Diese Dissertation wird erstmalig und ausschließlich an der Universität Potsdam eingereicht.
Die dem Promotionsverfahren zugrundeliegende Promotionsordnung vom 17.09.2014 ist mir bekannt.

Potsdam, den 16. April 2018

A Appendix

A.1 Chapter 3

The supplementary dataset in Chapter 3 contains one shapefile (ds01), two .csv tables (ds02 and ds03), and one .xls table (ds05). The files are described below and can be downloaded here: https://agupubs.onlinelibrary.wiley.com/doi/abs/10.1002/2017JF004231

1. Data Set **S1** is a shapefile created in 2015. It contains 287 polygons and associated geographic information. Each polygon represents a Retrogressive Thaw Slump (RTS).

2. The Data Set **ds02** and **ds03** are .csv tables. They contain RTS characteristics (ds02) and morphological and spatial information for each coastal segment (ds03).

3. The Data Set **ds05** is a .csv table: The Table contains the metadata of the 21 aerial photographs used in the study.

A.2 Chapter 4

The supplementary dataset in Chapter 4 contains one .xls table. The file is described below and can be downloaded here: https://www.biogeosciences.net/15/1483/2018/

1. The Table contains the whole dataset used to measure volumes of eroded material from retrogressive thaw slumps (RTSs). Each row represent one RTS and the columns describe the

A.3 Chapter 5

The supplementary dataset in Chapter 5 contains one .xls table, one .csv file, and a shapefile. The files are described below and can be downloaded here:

1. The dataset **ds06** is a .xls table. It contains observations for each soil pit. The observations were taken during the fieldwork that took place between July 27^{th} and August 8^{th}, 2015 on Herschel Island.
2. The dataset **ds07** is a .csv file. It contains the results of the laboratory analyses for each of the samples collected on Herschel Island between July 27^{th} and August 8^{th}, 2015.
3. The shapefile stores the waypoints and coordinates for the sites sampled on Herschel Island between July 27^{th} and August 8^{th}, 2015.

Bibliography

[Abbott and Jones, 2015] Abbott, B. W. and Jones, J. B. (2015). Permafrost collapse alters soil carbon stocks, respiration, CH_4, and N_2O in upland tundra. Global Change Biology, 21:4570–4587.

[Abbott et al., 2016] Abbott, B. W., Jones, J. B., Schuur, E. A. G., III, F. S. C., Bowden, W. B., Bret-Harte, M. S., Epstein, H. E., Flannigan, M. D., Harms, T. K., Hollingsworth, T. N., Mack, M. C., McGuire, A. D., Natali, S. M., Rocha, A. V., Tank, S. E., Turetsky, M. R., Vonk, J. E., Wickland, K. P., Aiken, G. R., Alexander, H. D., Amon, R. M. W., Benscoter, B. W., Bergeron, Y., Bishop, K., Blarquez, O., Bond-Lamberty, B., Breen, A. L., Buffam, I., Cai, Y., Carcaillet, C., Carey, S. K., Chen, J. M., Chen, H. Y. H., Christensen, T. R., Cooper, L. W., Cornelissen, J. H. C., de Groot, W. J., DeLuca, T. H., Dorrepaal, E., Fetcher, N., Finlay, J. C., Forbes, B. C., French, N. H. F., Gauthier, S., Girardin, M. P., Goetz, S. J., Goldammer, J. G., Gough, L., Grogan, P., Guo, L., Higuera, P. E., Hinzman, L., Hu, F. S., Hugelius, G., Jafarov, E. E., Jandt, R., Johnstone, J. F., Karlsson, J., Kasischke, E. S., Kattner, G., Kelly, R., Keuper, F. E., Kling, G. W., Kortelainen, P., Kouki, J., Kuhry, P., Laudon, H., Laurion, I., Macdonald, R. W., Mann, P. J., Martikainen, P. J., McClelland, J. W., Molau, U., Oberbauer, S. F., Olefeldt, D., Paré, D., Parisien, M.-A., Payette, S., Peng, C., Pokrovsky, O. S., Rastetter, E. B., Raymond, P. A., Raynolds, M. K., Rein, G., Reynolds, J. F., Robards, M., Rogers, B. M., Schädel, C., Schaefer, K., Schmidt, I. K., Shvidenko, A., Sky, J., Spencer, R. G. M., Starr, G., Striegl, R. G., Teisserenc, R., Tranvik, L. J., Virtanen, T., Welker, J. M., and Zimov, S. (2016). Biomass offsets little or none of permafrost carbon release from soils, streams, and wildfire: an expert assessment. Environmental Research Letters, 11(3):34014.

[Abbott et al., 2014] Abbott, B. W., Larouche, J. R., Jones, J. B., Bowden, W., and Balser, A. W. (2014). Elevated dissolved organic carbon biodegradability from thawing and collapsing permafrost. Journal of Geophysical Research: Biogeosciences, 119:2049–2063.

[AMAP, 2017] AMAP (2017). Snow, Water, Ice and Permafrost in the Arctic (SWIPA). Oslo.

[Are et al., 2008] Are, F., Reimnitz, E., Grigoriev, M., Hubberten, H.-W., and Rachold, V. (2008). The influence of cryogenic processes on the erosional arctic shoreface. Journal of Coastal Research, pages 110–121.

[Aré, 1988] Aré, F. E. (1988). Thermal abrasion of sea coasts (part I). Polar Geography and Geology, 12(1):1.

[Aré, 1999] Aré, F. E. (1999). The role of coastal retreat for sedimentation in the Laptev Sea, pages 288–295. Springer Berlin Heidelberg, Berlin, Heidelberg.

[Atkinson, 2005] Atkinson, D. E. (2005). Observed storminess patterns and trends in the circum-arctic coastal regime. Geo-Marine Letters, 25(2-3):98–109.

[Aufdenkampe et al., 2011] Aufdenkampe, A. K., Mayorga, E., Raymond, P. A., Melack, J. M., Doney, S. C., Alin, S. R., Aalto, R. E., and Yoo, K. (2011). Riverine coupling of biogeochemical cycles between land, oceans, and atmosphere. front Eol Environ, 9(1):53–60.

[Balser et al., 2014] Balser, A. W., Jones, J. B., and Gens, R. (2014). Timing of retrogressive thaw slump initiation in the Noatak Basin, northwest Alaska, USA. Journal of Geophysical Research: Earth Surface, 119(5):1106–1120.

[Barnhart et al., 2014] Barnhart, K. R., Overeem, I., and Anderson, R. S. (2014). The effect of changing sea ice on the physical vulnerability of Arctic coasts. The Cryosphere, 8(5):1777–1799.

[Berhe et al., 2012] Berhe, A. A., Harden, J. W., Torn, M. S., Kleber, M., Burton, S. D., and Harte, J. (2012). Persistence of soil organic matter in eroding versus depositional landform positions. Journal of Geophysical Research, 117:1–16.

[Berhe et al., 2007] Berhe, A. A., Harte, J., Harden, J. W., and Torn, M. S. (2007). The Significance of the erosion-induced terrestrial carbon sink. BioScience, 57(4):337–346.

[Bouchard, 1974] Bouchard, M. (1974). Surficial Geology of Herschel Island, Yukon Territory. PhD thesis, University of Montreal.

[Bowden et al., 2008] Bowden, W. B., Gooseff, M. N., Balser, A., Green, A., Peterson, B. J., and Bradford, J. (2008). Sediment and nutrient delivery from thermokarst features in the foothills of the North Slope, Alaska: Potential impacts on headwater stream ecosystems. Journal of Geophysical Research: Biogeosciences, 113.

[Breiman et al., 1984] Breiman, L., Friedman, J., Stone, C. J., and Olshen, R. A. (1984). Classification and Regression Trees. Routledge, crc press edition.

[Brierley et al., 2006] Brierley, G., Fryirs, K., and Jain, V. (2006). Landscape connectivity : the geographic basis of geomorphic applications. Area, 38(2):165–174.

[Brooker et al., 2014] Brooker, A., Fraser, R. H., Olthof, I., Kokelj, S. V., and Lacelle, D. (2014). Mapping the activity and evolution of retrogressive thaw slumps by Tasselled Cap trend analysis of a Landsat satellite image stack. Permafrost and Periglacial Processes, 25(4):243–256.

[Brown et al., 1997] Brown, J., Ferrians Jr, O., Heginbottom, J., and Melnikov, E. (1997). Circum-Arctic map of permafrost and ground-ice conditions. US Geological Survey Reston.

[Burke et al., 2012] Burke, E. J., Hartley, I. P., and Jones, C. D. (2012). Uncertainties in the global temperature change caused by carbon release from permafrost thawing. The Cryosphere, 6(5):1063–1076.

[Burn, 2000] Burn, C. R. (2000). The thermal regime of a retrogressive thaw slump near Mayo, Yukon Territory. Canadian Journal of Earth Sciences, 37(7):967–981.

[Burn and Lewkowicz, 1990] Burn, C. R. and Lewkowicz, A. G. (1990). Canadian landform examples - 17 retrogressive thaw slumps. The Canadian Geographer / Le Géographe canadien, 34(3):273–276.

[Burn and Zhang, 2009] Burn, C. R. and Zhang, Y. (2009). Permafrost and climate change at Herschel Island (Qikiqtaruq), Yukon Territory, Canada. Journal of Geophysical Research: Earth Surface, 114(F2):1–16.

[Cannone et al., 2010] Cannone, N., Lewkowicz, A. G., and Guglielmin, M. (2010). Vegetation colonization of permafrost-related landslides, Ellesmere Island, Canadian High Arctic. Journal of Geophysical Research: Biogeosciences, 115.

[Cassidy et al., 2016] Cassidy, A. E., Christen, A., and Henry, G. H. R. (2016). The effect of a permafrost disturbance on growing-season carbon-dioxide fluxes in a high Arctic tundra ecosystem. Biogeosciences, 13(8):2291–2303.

[CAVM, 2003] CAVM (2003). Circumpolar Arctic vegetation map. Scale 1: 7,500,000. Conservation of Arctic Flora and Fauna (CAFF) Map No. 1. Technical report, US Fish and Wildlife Service, Anchorage, Alaska.

[Chin et al., 2016] Chin, K. S., Lento, J., Culp, J. M., Lacelle, D., and Kokelj, S. V. (2016). Permafrost thaw and intense thermokarst activity decreases abundance of stream benthic macroinvertebrates. Global Change Biology, 22(8):2715–2728.

[Chipman et al., 2016] Chipman, M. L., Kling, G. W., Lundstrom, C. C., and Hu, F. S. (2016). Multiple thermo-erosional episodes during the past six millennia: Implications for the response of Arctic permafrost to climate change. Geology, 44(6):439.

[Couture et al., 2018] Couture, N., Irrgang, A. M., Pollard, W., Lantuit, H., and Fritz, M. (2018). Coastal Erosion of Permafrost Soils Along the Yukon Coastal Plain and Fluxes of Organic Carbon to the Canadian Beaufort Sea. Journal of Geophysical Research: Biogeosciences, 123:406–422.

[Couture, 2010] Couture, N. J. (2010). Fluxes of Soil Organic Carbon from Eroding Permafrost Coasts, Canadian Beaufort Sea. PhD thesis, McGill Univ., Montreal, Canada.

[Couture and Pollard, 2017] Couture, N. J. and Pollard, W. H. (2017). A Model for quantifying ground-ice volume, Yukon Coast, western Arctic Canada. Permafrost and Periglacial Processes, 28(3):534–542.

[Cray and Pollard, 2015] Cray, H. A. and Pollard, W. H. (2015). Vegetation recovery patterns following permafrost disturbance in a low Arctic setting: case study of Herschel Island, Yukon, Canada. Arctic, Antarctic, and Alpine Research, 47(1):99–113.

[Dallimore et al., 1996] Dallimore, S. R., Wolfe, S. A., and Solomon, S. M. (1996). Influence of ground ice and permafrost on coastal evolution, Richards Island, Beaufort Sea coast, N.W.T. Canadian Journal of Earth Sciences, 33(5):664–675.

[De'ath and Fabricius, 2000] De'ath, G. and Fabricius, K. E. (2000). Classification and regression trees: a powerful yet simple technique for ecological data analysis. Ecology, 81(11):3178–3192.

[Dunton et al., 2006] Dunton, K. H., Weingartner, T., and Carmack, E. C. (2006). The nearshore western beaufort sea ecosystem: circulation and importance of terrestrial carbon in arctic coastal food webs. Progress in Oceanography, 71(2-4):362–378.

[Dvornikov et al., 2018] Dvornikov, Y., Leibman, M., Heim, B., Bartsch, A., Herzschuh, U., Skorospekhova, T., Fedorova, I., Khomutov, A., Widhalm, B., Gubarkov, A., et al. (2018). Terrestrial cdom in lakes of yamal peninsula: Connection to lake and lake catchment properties. Remote Sensing, 10(2):167.

[Dyke and Prest, 1987] Dyke, A. and Prest, V. (1987). Late Wisconsinan and Holocene History of the Laurentide Ice Sheet. Géographie physique et Quaternaire, 41(2):237–263.

[Forbes, 2011] Forbes, D. L. (2011). State of the Arctic coast 2010: scientific review and outlook. Land-Ocean Interactions in the Coastal Zone, Institute of Coastal Research.

[Fortier et al., 2007] Fortier, D., Allard, M., and Shur, Y. (2007). Observation of rapid drainage system development by thermal erosion of ice wedges on Bylot Island , Canadian Arctic Archipelago. Permafrost and Periglacial Processes, 18(August 2006):229–243.

[French, 2007] French, H. (2007). The Periglacial Environment, Wiley. Chichester.

[French and Shur, 2010] French, H. and Shur, Y. (2010). The principles of cryostratigraphy. Earth-Science Reviews, 101(3-4):190–206.

[Fritz et al., 2017] Fritz, M., Vonk, J. E., and Lantuit, H. (2017). Collapsing Arctic coastlines. Nature Climate Change, 7:6.

[Fritz et al., 2012] Fritz, M., Wetterich, S., Schirrmeister, L., Meyer, H., Lantuit, H., Preusser, F., and Pollard, W. H. (2012). Eastern Beringia and beyond: Late Wisconsinan and Holocene landscape dynamics along the Yukon Coastal Plain, Canada. Palaeogeography, Palaeoclimatology, Palaeoecology, 319-320:28–45.

[Godin and Fortier, 2012] Godin, E. and Fortier, D. (2012). Geomorphology of a thermo-erosion gully , Bylot. Canadian Journal of Earth Sciences, 49:979–986.

[Grewer et al., 2016] Grewer, D., Lafrenière, M. J., Lamoureux, S. F., and Simpson, M. J. (2016). Redistribution of soil organic matter by permafrost disturbance in the Canadian High Arctic. Biogeochemistry, 128:397–415.

[Grewer et al., 2015] Grewer, D. M., Lafrenière, M. J., Lamoureux, S. F., and Simpson, M. J. (2015). Potential shifts in Canadian High Arctic sedimentary organic matter composition with permafrost active layer detachments. Organic Geochemistry, 79:1–13.

[Grosse et al., 2006] Grosse, G., Schirrmeister, L., and Malthus, T. J. (2006). Application of Landsat-7 satellite data and a DEM for the quantification of thermokarst-affected terrain types in the periglacial Lena – Anabar coastal lowland. Polar Research, 25(1):51–67.

[Group, 1998] Group, S. C. W. (1998). The Canadian system of soil classification. NRC Research press.

[Guisan et al., 1999] Guisan, A., Weiss, S. B., and Weiss, A. D. (1999). Glm versus cca spatial modeling of plant species distribution. Plant Ecology, 143(1):107–122.

[Günther et al., 2015] Günther, F., Grosse, G., Wetterich, S., Jones, B. M., Kunitsky, V. V., Kienast, F., and Schirrmeister, L. (2015). The Batagay mega thaw slump, Yana Uplands, Yakutia, Russia: permafrost thaw dynamics on decadal time scale. In PAST Gateways - Palaeo-Arctic Spatial and Temporal Gateways - Third International Conference and Workshop, Potsdam. TERRA NOSTRA - Schriften der GeoUnion Alfred-Wegener-Stiftung.

[Günther et al., 2013] Günther, F., Overduin, P. P., Sandakov, A. V., Grosse, G., and Grigoriev, M. N. (2013). Short-and long-term thermo-erosion of ice-rich permafrost coasts in the laptev sea region. Biogeosciences, 10(6):4297–4318.

[Harms and Ludwig, 2016] Harms, T. K. and Ludwig, S. M. (2016). Retention and removal of nitrogen and phosphorus in saturated soils of arctic hillslopes. Biogeochemistry, 127(2):291–304.

[Harper, 1990] Harper, J. R. (1990). Morphology of the Canadian Beaufort Sea coast. Marine Geology, 91(1-2):75–91.

[Harris et al., 2000] Harris, C., Urton, J. M., and Davies, M. C. R. (2000). Soft-sediment deformation during thawing of ice-rich frozen soils : results of scaled centrifuge modelling experiments. Sedimentology, 47:687–700.

[Hinzman and Kane, 1992] Hinzman, L. D. and Kane, D. L. (1992). Potential repsonse of an Arctic watershed during a period of global warming. Journal of Geophysical Research: Atmospheres, 97(D3):2811–2820.

[Hobbie et al., 2000] Hobbie, S. E., Schimel, J. P., Trumbore, S., and Randerson, J. R. (2000). Controls over carbon storage and turnover in high-latitude soils. Global Change Biology, 6:196–210.

[Holmes et al., 2012] Holmes, R. M., McClelland, J. W., Peterson, B. J., Tank, S. E., Bulygina, E., Eglinton, T. I., Gordeev, V. V., Gurtovaya, T. Y., Raymond, P. A., Repeta, D. J., Staples, R., Striegl, R. G., Zhulidov, A. V., and Zimov, S. A. (2012). Seasonal and annual fluxes of nutrients and organic matter from large rivers to the arctic ocean and surrounding seas. Estuaries and Coasts, 35(2):369–382.

[Houben et al., 2016] Houben, A. J., French, T. D., Kokelj, S., Wang, X., Smol, J., and Blais, J. M. (2016). The impacts of permafrost thaw slump events on limnological variables in upland tundra lakes, Mackenzie Delta region. Fund. Appl. Limnol., 189(1):11–35.

[Huang et al., 2017] Huang, J., Zhang, X., Zhang, Q., Lin, Y., Hao, M., Luo, Y., Zhao, Z., Yao, Y., Chen, X., Wang, L., Nie, S., Yin, Y., and Xu, Y. (2017). Recently amplified arctic warming has contributed to a continual global warming trend. Nature Climate Change, 7:875–880.

[Hugelius et al., 2014] Hugelius, G., Strauss, J., Zubrzycki, S., Harden, J. W., Schuur, E. A. G., Ping, C. L., Schirrmeister, L., Grosse, G., Michaelson, G. J., Koven, C. D., O'Donnell, J. A., Elberling, B., Mishra, U., Camill, P., Yu, Z., Palmtag, J., and Kuhry, P. (2014). Estimated stocks of circumpolar permafrost carbon with quantified uncertainty ranges and identified data gaps. Biogeosciences, 23(11).

[Irrgang et al., 2018] Irrgang, A. M., Lantuit, H., Manson, G. K., Günther, F., Grosse, G., and Overduin, P. P. (2018). Variability in rates of coastal change along the Yukon coast, 1951-2015. Journal of Geophysical Research: Earth Surface.

[Jensen et al., 2014] Jensen, A. E., Lohse, K. A., Crosby, B. T., and Mora, C. I. (2014). Variations in soil carbon dioxide efflux across a thaw slump chronosequence in northwestern Alaska. Environmental Research Letters, 9(2):25001.

[Jones et al., 2009] Jones, B. M., Arp, C. D., Jorgenson, M. T., Hinkel, K. M., Schmutz, J. A., and Flint, P. L. (2009). Increase in the rate and uniformity of coastline erosion in Arctic Alaska. Geophysical Research Letters, 36(3).

[Jones et al., 2008] Jones, B. M., Hinkel, K. M., Arp, C. D., and Eisner, W. R. (2008). Modern erosion rates and loss of coastal features and sites, Beaufort Sea coastline, Alaska. Arctic, 61(4):361–372.

[Kessler, 2017] Kessler, L. (2017). Estimating the economic impact of the permafrost carbon feedback. Climate Change Economics, 08(02):1750008.

[Kizyakov et al., 2013] Kizyakov, A. I., Zimin, M. V., Leibman, M. O., and Pravikova, N. V. (2013). Thermal denudation, thermal abrasion of sea shores, thermocirques. Earth, 17(4):36–47.

[Kohnert et al., 2014] Kohnert, K., Serafimovich, J., Hartmann, and Sachs, T. (2014). Airborne measurements of methane fluxes in Alaskan and Canadian tundra with the research aircraft Polar 5. Technical report, Berichte zur Polar-und Meeresforschung= Reports on Polar and Marine Research, 673.

[Kokelj and Jorgenson, 2013] Kokelj, S. V. and Jorgenson, M. T. (2013). Advances in Thermokarst Research. Permafrost and Periglacial Processes, 24(2):108–119.

[Kokelj et al., 2013] Kokelj, S. V., Lacelle, D., Lantz, T. C., Tunnicliffe, J., Malone, L., Clark, I. D., and Chin, K. S. (2013). Thawing of massive ground ice in mega slumps drives increases in stream sediment and solute flux across a range of watershed scales. Journal of Geophysical Research: Earth Surface, 118(2):681–692.

[Kokelj et al., 2009a] Kokelj, S. V., Lantz, T. C., Kanigan, J., Smith, S. L., and Coutts, R. (2009a). Origin and polycyclic behaviour of tundra thaw slumps, Mackenzie Delta region, Northwest Territories, Canada. Permafrost and Periglacial Processes, 20(2):173–184.

[Kokelj et al., 2017] Kokelj, S. V., Lantz, T. C., Tunnicliffe, J., Segal, R., and Lacelle, D. (2017). Climate-driven thaw of permafrost preserved glacial landscapes, northwestern Canada. Geology, 45(4):371.

[Kokelj and Lewkowicz, 1998] Kokelj, S. V. and Lewkowicz, A. G. (1998). Long-term influence of active-layer detachment sliding on permafrost slope hydrology, Hot Weather Creek, Ellesmere Island, Canada. In Nordicana, editor, PERMAFROST - Seventh International Conference, number 55, pages 583–589, Yellowknife.

[Kokelj et al., 2015a] Kokelj, S. V., Tunnicliffe, D., Lacelle, T. C., Lantz, T. C., and Fraser, R. H. (2015a). Retrogressive thaw slumps: From slope process to the landscape sensitivity of northwestern Canada. In GeoQuebec, Proceedings of 7th Canadian Permafrost Conference, Sept. 20–23,, Quebec City.

[Kokelj et al., 2015b] Kokelj, S. V., Tunnicliffe, J., Lacelle, D., Lantz, T. C., Chin, K. S., and Fraser, R. (2015b). Increased precipitation drives mega slump development and destabilization of ice-rich permafrost terrain, northwestern Canada. Global and Planetary Change, 129:56–68.

[Kokelj et al., 2009b] Kokelj, S. V., Zajdlik, B., and Thompson, M. S. (2009b). The impacts of thawing permafrost on the chemistry of lakes across the subarctic boreal-tundra transition, Mackenzie Delta region, Canada. Permafrost and Periglacial Processes, 20(2):185–199.

[Konopczak et al., 2014] Konopczak, A. M., Manson, G. K., and Couture, N. J. (2014). Variability of coastal change along the western Yukon coast. Technical report, Geol. Surv. of Canada Open File, 7516, 81.

[Koven et al., 2015] Koven, C., Schuur, E., Schädel, C., Bohn, T. J., Burke, E., Chen, G., Chen, X., Ciais, P., Grosse, G., Harden, J., Hayes, D., Hugelius, G., Jafarov, E., Krinner, G., Kuhry, P., Lawrence, D., MacDougall, A., Marchenko, S., McGuire, A., Natali, S., Nicolsky, D. J., Olefeldt, D., Peng, S., Romanovsky, V. E., Schaefer, K., Strauss, J., Treat, C., and Turetsky, M. (2015). A simplified, data-constrained approach to estimate the permafrost carbon–climate feedback. Philosophical Transactions of the Royal Society A: Mathematical, Physical and Engineering Sciences.

[Koven et al., 2011] Koven, C. D., Ringeval, B., Friedlingstein, P., Ciais, P., Cadule, P., Khvorostyanov, D., Krinner, G., and Tarnocai, C. (2011). Permafrost carbon-climate feedbacks accelerate global warming. Proceedings of the National Academy of Sciences, 108(36):14769–14774.

[Kuhry and Vitt, 1996] Kuhry, P. and Vitt, D. H. (1996). Fossil carbon / nitrogen ratios as a measure of peat decomposition. Ecology, 77(1):271–275.

[Lacelle et al., 2010] Lacelle, D., Bjornson, J., and Lauriol, B. (2010). Climatic and geomorphic factors affecting contemporary (1950–2004) activity of retrogressive thaw slumps on the Aklavik Plateau, Richardson Mountains, NWT, Canada. Permafrost and Periglacial Processes, 21(1):1–15.

[Lacelle et al., 2015] Lacelle, D., Brooker, A., Fraser, R. H., and Kokelj, S. V. (2015). Distribution and growth of thaw slumps in the Richardson Mountains–Peel Plateau region, northwestern Canada. Geomorphology, 235:40–51.

[Lamoureux and Lafrenière, 2009] Lamoureux, S. F. and Lafrenière, M. J. (2009). Fluvial Impact of Extensive Active Layer Detachments, Cape Bounty, Melville Island, Canada. Arctic, Antarctic, and Alpine Research, 41(1):59–68.

[Lamoureux and Lafrenière, 2014] Lamoureux, S. F. and Lafrenière, M. J. (2014). Seasonal fluxes and age of particulate organic carbon exported from arctic catchments impacted by localized permafrost slope disturbances. Environmental Research Letters, 9(4):045002.

[Lantuit et al., 2011] Lantuit, H., Atkinson, D., Overduin, P. P., Grigoriev, M., Rachold, V., Grosse, G., and Hubberten, H.-W. (2011). Coastal erosion dynamics on the permafrost-dominated Bykovsky Peninsula, north Siberia, 1951–2006. Polar Research, 30(1):7341.

[Lantuit et al., 2012a] Lantuit, H., Overduin, P. P., Couture, N., Wetterich, S., Aré, F., Atkinson, D., Brown, J., Cherkashov, G., Drozdov, D., Donald Forbes, L., Graves-Gaylord, A., Grigoriev, M., Hubberten, H. W., Jordan, J., Jorgenson, T., Ødegård, R. S., Ogorodov, S., Pollard, W. H., Rachold, V., Sedenko, S., Solomon, S., Steenhuisen, F., Streletskaya, I., and Vasiliev, A. (2012a). The Arctic Coastal Dynamics database: a new classification scheme and statistics on Arctic permafrost coastlines. Estuaries and Coasts, 35(2):383–400.

[Lantuit and Pollard, 2005] Lantuit, H. and Pollard, W. (2005). Temporal stereophotogrammetric analysis of retrogressive thaw slumps on Herschel Island, Yukon Territory. Natural Hazards and Earth System Science, 5(3):413–423.

[Lantuit and Pollard, 2008] Lantuit, H. and Pollard, W. H. (2008). Fifty years of coastal erosion and retrogressive thaw slump activity on Herschel Island, southern Beaufort Sea, Yukon Territory, Canada. Geomorphology, 95(1):84–102.

[Lantuit et al., 2012b] Lantuit, H., Pollard, W. H., Couture, N., Fritz, M., Schirrmeister, L., Meyer, H., and Hubberten, H. (2012b). Modern and late Holocene retrogressive thaw slump activity on the Yukon Coastal Plain and Herschel Island, Yukon Territory, Canada. Permafrost and Periglacial Processes, 23(1):39–51.

[Lantz and Kokelj, 2008] Lantz, T. C. and Kokelj, S. V. (2008). Increasing rates of retrogressive thaw slump activity in the Mackenzie Delta region, N.W.T., Canada. Geophysical Research Letters, 35(6).

[Lantz et al., 2009] Lantz, T. C., Kokelj, S. V., Gergel, S. E., and Henry, G. H. R. (2009). Relative impacts of disturbance and temperature: persistent changes in microenvironment and vegetation in retrogressive thaw slumps. Global Change Biology, 15(7):1664–1675.

[Larouche et al., 2015] Larouche, J. R., Abbott, B. W., Bowden, W. B., and Jones, J. B. (2015). The role of watershed characteristics , permafrost thaw , and wildfire on dissolved organic carbon biodegradability and water chemistry in Arctic headwater streams. Biogeosciences, 12:4221–4233.

[Leibman et al., 2008] Leibman, M., Gubarkov, A., Khomutov, A., Kizyakov, A., and Vanshtein, B. (2008). Coastal processes at the tabular-ground-ice-bearing area, Yugorsky Peninsula, Russia. In Proceedings of the Ninth International Conference on Permafrost, pages 1037–1042.

[Lewkowicz, 1987a] Lewkowicz, A. G. (1987a). Headwall retreat of ground-ice slumps, Banks Island, Northwest Territories. Canadian Journal of Earth Sciences, 24(6):1077–1085.

[Lewkowicz, 1987b] Lewkowicz, A. G. (1987b). Nature and Importance of Thermokarst Processes, Sand Hills Moraine, Banks Island, Canada. Geografiska Annaler: Series A, Physical Geography, 69(2):321–327.

[Lewkowicz, 1988] Lewkowicz, A. G. (1988). Ablation of massive ground ice, Mackenzie Delta. In Proceedings, 5th International Conference on Permafrost, pages 605–610.

[Lewkowicz, 2007] Lewkowicz, A. G. (2007). Dynamics of active-layer detachment failures, fosheim peninsula, ellesmere island, nunavut, canada. Permafrost and Periglacial Processes, 18(1):89–103.

[MacDougall et al., 2012] MacDougall, A. H., Avis, C. A., and Weaver, A. J. (2012). Significant contribution to climate warming from the permafrost carbon feedback. Nature Geoscience, 5:719.

[MacKay, 1959] MacKay, J. R. (1959). Glacier ice thrust features of the Yukon coast. Geographic Bulletin, 13:5–21.

[Mackelprang et al., 2011] Mackelprang, R., Waldrop, M. P., DeAngelis, K. M., David, M. M., Chavarria, K. L., Blazewicz, S. J., Rubin, E. M., and Jansson, J. K. (2011). Metagenomic analysis of a permafrost microbial community reveals a rapid response to thaw. Nature, 480(7377):368–371.

[Malone et al., 2013] Malone, L., Lacelle, D., Kokelj, S., and Clark, I. D. (2013). Impacts of hillslope thaw slumps on the geochemistry of permafrost catchments (Stony Creek watershed, NWT, Canada). Chemical Geology, 356:38–49.

[Manson et al., 2005] Manson, G., Solomon, S. M., Forbes, D. L., Atkinson, D., and Craymer, M. (2005). Spatial variability of factors influencing coastal change in the western canadian arctic. Geo-Marine Letters, 25(2-3):138–145.

[Mars and Houseknecht, 2007] Mars, J. C. and Houseknecht, D. W. (2007). Quantitative remote sensing study indicates doubling of coastal erosion rate in past 50 yr along a segment of the Arctic coast of Alaska. Geology, 35:583–586.

[McGuire et al., 2016] McGuire, A. D., Koven, C., Lawrence, D. M., Clein, J. S., Xia, J., Beer, C., Burke, E., Chen, G., Chen, X., Delire, C., Jafarov, E., MacDougall, A. H., Marchenko, S., Nicolsky, D., Peng, S., Rinke, A., Saito, K., Zhang, W., Alkama, R., Bohn, T. J., Ciais, P., Decharme, B., Ekici, A., Gouttevin, I., Hajima, T., Hayes, D. J., Ji, D., Krinner, G., Lettenmaier, D. P., Luo, Y., Miller, P. A., Moore, J. C., Romanovsky, V., Schädel, C., Schaefer, K., Schuur, E. A. G., Smith, B., Sueyoshi, T., and Zhuang, Q. (2016). Variability in the sensitivity among model simulations of permafrost and carbon dynamics in the permafrost region between 1960 and 2009. Global Biogeochemical Cycles, 30(7):1015–1037.

[McNamara et al., 1999] McNamara, J. P., Kane, D. L., and Hinzman, L. D. (1999). An analysis of an arctic channel network using a digital elevation model. Geomorphology, 29(3-4):339–353.

[Michaelson et al., 1996] Michaelson, G. J., Ping, C., and Kimble, J. (1996). Carbon storage and distribution in tundra soils of arctic alaska, usa. Arctic and Alpine Research, pages 414–424.

[Mishra et al., 2013] Mishra, U., Jastrow, J. D., Matamala, R., Hugelius, G., Koven, C. D., Harden, J. W., Ping, C.-L., Michaelson, G. J., Fan, Z., Miller, R., McGuire, a. D., Tarnocai, C., Kuhry, P., Riley, W. J., Schaefer, K., Schuur, E. A. G., Jorgenson, M. T., and Hinzman, L. D. (2013). Empirical estimates to reduce modeling uncertainties of soil organic carbon in permafrost regions : a review of recent progress and remaining challenges. Environmental Research Letters, 8.

[Naidu et al., 2000] Naidu, A., Cooper, L., Finney, B., Macdonald, R., Alexander, C., and Semiletov, I. P. (2000). Organic carbon isotope ratios (δ13c) of arctic amerasian continental shelf sediments. International Journal of Earth Sciences, 89(3):522–532.

[Obu et al., 2017a] Obu, J., Lantuit, H., Grosse, G., Günther, F., Sachs, T., Helm, V., and Fritz, M. (2017a). Coastal erosion and mass wasting along the Canadian Beaufort Sea based on annual airborne LiDAR elevation data. Geomorphology, 293:331–346.

[Obu et al., 2017b] Obu, J., Lantuit, H., Heim, B., Wolter, J., and Fritz, M. (2017b). Effect of terrain characteristics on soil organic carbon and total nitrogen stocks in soils of Herschel Island, western Canadian Arctic. Permafrost and Periglacial Processes, 28:92–107.

[Olefeldt et al., 2016] Olefeldt, D., Goswami, S., Grosse, G., Hayes, D., Hugelius, G., McGuire, a. D., Romanovsky, V. E., Sannel, A. B. K., Schuur, E. A. G., Turetsky, M. R., Kuhry, P., McGuire, a. D., Romanovsky, V. E., Sannel, A. B. K., Schuur, E. A. G., and Turetsky, M. R. (2016). Circumpolar distribution and carbon storage of thermokarst landscapes. Nature Communications, 7:13043.

[Overduin et al., 2014] Overduin, P. P., Strzelecki, M. C., Grigoriev, M. N., Couture, N., Lantuit, H., St-Hilaire-Gravel, D., Günther, F., and Wetterich, S. (2014). Coastal changes in the Arctic. Geological Society, London, Special Publications.

[Overeem et al., 2011] Overeem, I., Anderson, R. S., Wobus, C. W., Clow, G. D., Urban, F. E., and Matell, N. (2011). Sea ice loss enhances wave action at the Arctic coast. Geophysical Research Letters, 38(September):1–6.

[Palmtag et al., 2016] Palmtag, J., Ramage, J., Hugelius, G., Gentsch, N., Laschinskiy, N., Richter, A., and Kuhry, P. (2016). Controls on the storage of organic carbon in permafrost soil in northern Siberia. European Journal of Soil Science, 67:478–491.

[Paquette et al., 2018] Paquette, M., Fortier, D., and Vincent, W. F. (2018). Hillslope water tracks in the high arctic: Seasonal flow dynamics with changing water sources in preferential flow paths. Hydrological Processes.

[Pautler et al., 2010] Pautler, B. G., Simpson, J., Mcnally, D. J., and Lamoureux, S. F. (2010). Arctic permafrost active layer detachments stimulate microbial activity and degradation of soil organic matter. Environmental Science and Technology, 44(11):4076–4082.

[Peel, 1990] Peel, D. (1990). Elsevier's dictionary of glaciology Compiled by V.M. Kotlyakov and N.A. Smolyarova. Antarctic Science, 3(3):341–342.

[Ping et al., 2011] Ping, C., Michaelson, G. J., Guo, L., Jorgenson, M. T., Kanevskiy, M., Shur, Y., Dou, F., and Liang, J. (2011). Soil carbon and material fluxes across the eroding Alaska Beaufort Sea coastline. Journal of Geophysical Research: Biogeosciences, 116(G2).

[Pizano et al., 2014] Pizano, C., Barón, A. F., Schuur, E. A. G., Crummer, K. G., and Mack, M. C. (2014). Effects of thermo-erosional disturbance on surface soil carbon and nitrogen dynamics in upland arctic tundra. Environmental Research Letters, 9(7):75006.

[Pollard, 1990] Pollard, W. H. (1990). The Nature and Origin of Ground ice in the Herschel Island Area, Yukon Territory. In Proceedings, Fifth Canadian Permafrost Conference, Quebec, Quebec.

[Rachold et al., 2000] Rachold, V., Grigoriev, M. N., Are, F. E., Solomon, S., Reimnitz, E., Kassens, H., and Antonow, M. (2000). Coastal erosion vs riverine sediment discharge in the arctic shelf seas. International Journal of Earth Sciences, 89(3):450–460.

[Ramage, 2017] Ramage, J. L. (2017). Valleys of Herschel Island, Yukon, Canada. https://doi.org/10.1594/PANGAEA.883524. Technical report.

[Ramage et al., 2017] Ramage, J. L., Irrgang, A. M., Herzschuh, U., Morgenstern, A., Couture, N., and Lantuit, H. (2017). Terrain controls on the occurrence of coastal retrogressive thaw slumps along the Yukon Coast, Canada. Journal of Geophysical Research: Earth Surface, 122(9):1619–1634.

[Rampton, 1982] Rampton, V. N. (1982). Quaternary Geology of the Yukon Coastal Plain. Technical report, Geological Survey of Canada, Canada.

[Romanovskii and Hubberten, 2001] Romanovskii, N. N. and Hubberten, H.-W. (2001). Results of permafrost modelling of the lowlands and shelf of the laptev sea region, russia. Permafrost and periglacial processes, 12(2):191–202.

[Rosenbloom et al., 2001] Rosenbloom, N. A., Doney, S. C., and Schimel, D. S. (2001). Geomorphic evolution of soil texture and organic matter in eroding landscapes. Global Biogeochemical Cycles, 15(2):365–381.

[Rosenbloom et al., 2006] Rosenbloom, N. A., Harden, J. W., Neff, J. C., and Schimel, D. S. (2006). Geomorphic control of landscape carbon accumulation. Journal of Geophysical Research: Biogeosciences, 111(G1).

[Rudy et al., 2013] Rudy, A. C., Lamoureux, S. F., Treitz, P., and Collingwood, A. (2013). Identifying permafrost slope disturbance using multi-temporal optical satellite images and change detection techniques. Cold Regions Science and Technology, 88:37–49.

[Rudy et al., 2016] Rudy, A. C., Lamoureux, S. F., Treitz, P., and Van Ewijk, K. Y. (2016). Transferability of regional permafrost disturbance susceptibility modelling using generalized linear and generalized additive models. Geomorphology, 264:95–108.

[Schädel et al., 2014] Schädel, C., Schuur, E. A. G., Bracho, R., Elberling, B., Knoblauch, C., Lee, H., Luo, Y., Shaver, G. R., and Turetsky, M. R. (2014). Circumpolar assessment of permafrost C quality and its vulnerability over time using long-term incubation data. Global Change Biology, 20(2):641–652.

[Schaefer et al., 2014] Schaefer, K., Lantuit, H., Romanovsky, V. E., Schuur, E. a. G., and Witt, R. (2014). The impact of the permafrost carbon feedback on global climate. Environmental Research Letters, 9:085003.

[Schuur et al., 2008] Schuur, E. A. G., Bockheim, J., Canadell, J. G., Euskirchen, E., Field, C. B., Goryachkin, S. V., Hagemann, S., Kuhry, P., Lafleur, P. M., Lee, H., Mazhitova, G., Nelson, F. E., Rinke, A., Romanovsky, V. E., Shiklomanov, N., Tarnocai, C., Venevsky, S., Vogel, J. G., and Zimov, S. A. (2008). Vulnerability of permafrost carbon to climate change: implications for the global carbon cycle. BioScience, 58(8):701–714.

[Schuur et al., 2015] Schuur, E. a. G., McGuire, a. D., Schädel, C., Grosse, G., Harden, J. W., Hayes, D. J., Hugelius, G., Koven, C. D., Kuhry, P., Lawrence, D. M., Natali, S. M., Olefeldt, D., Romanovsky, V. E., Schaefer, K., Turetsky, M. R., Treat, C. C., and Vonk, J. E. (2015). Climate change and the permafrost carbon feedback. Nature, 520:171–179.

[Segal et al., 2016] Segal, R. A., Lantz, T. C., and Kokelj, S. V. (2016). Acceleration of thaw slump activity in glaciated landscapes of the Western Canadian Arctic. Environmental Research Letters, 11(3):34025.

[Serreze et al., 2009] Serreze, M., Barrett, A., Stroeve, J., Kindig, D., and Holland, M. (2009). The emergence of surface-based arctic amplification. The Cryosphere, 3(1):11.

[Shelef et al., 2017] Shelef, E., Rowland, J. C., and Wilson, C. J. (2017). Large uncertainty in permafrost carbon stocks due to hillslope soil deposits. Geophysical Research Letters, 44:1–11.

[Shur et al., 2005] Shur, Y., Hinkel, K. M., and Nelson, F. E. (2005). The transient layer: implications for geocryology and climate-change science. Permafrost and Periglacial Processes, 16(1):5–17.

[Siewert et al., 2015] Siewert, M., Hanisch, J., Weiss, N., Kuhry, P., Maximov, T., and Hugelius, G. (2015). Comparing carbon storage of Siberian tundra and taiga permafrost ecosystems at very high spatial resolution. Journal of Geophysical Research: Biogeosciences, 120:1973–1994.

[Siewert, 2016] Siewert, M. B. (2016). High-resolution mapping and spatial variability of soil organic carbon storage in permafrost environments. PhD thesis, Stockholm University, Department of Physical Geography.

[Smith et al., 1989] Smith, C., Kennedy, C., Hargrave, A., and McKenna, K. (1989). Soil and vegetation of Herschel Island, Yukon territory - Yukon Soil Survey Report. Technical report, Land Resource Research Centre, Agriculture Canada, Ottawa.

[Solomon, 2005] Solomon, S. M. (2005). Spatial and temporal variability of shoreline change in the Beaufort-Mackenzie region, northwest territories, Canada. Geo-Marine Letters, 25(2):127–137.

[Tanski et al., 2016] Tanski, G., Couture, N., Lantuit, H., Eulenburg, A., and Fritz, M. (2016). Eroding permafrost coasts release low amounts of dissolved organic carbon (DOC) from ground ice into the nearshore zone of the Arctic Ocean. Global Biogeochemical Cycles, 30(7):1054–1068.

[Tanski et al., 2017] Tanski, G., Lantuit, H., Ruttor, S., Knoblauch, C., Radosavljevic, B., Strauss, J., Wolter, J., Irrgang, A. M., Ramage, J., and Fritz, M. (2017). Transformation of terrestrial organic matter along thermokarst-affected permafrost coasts in the Arctic. Science of The Total Environment, 581–582:434–447.

[Thieler et al., 2009] Thieler, E. R., Himmelstoss, E. A., Zichichi, J. L., and Ergul, A. (2009). The digital shoreline analysis system (dsas) version 4.0-an arcgis extension for calculating shoreline change. Technical report, US Geological Survey.

[Van Everdingen, 2005] Van Everdingen, R. (2005). Multi-language glossary of permafrost and related ground-ice terms: National snow and ice data center. Data Center for Glaciology.

[von Deimling et al., 2012] von Deimling, T., Meinshausen, M., Levermann, A., Huber, V., Frieler, K., Lawrence, D. M., and Brovkin, V. (2012). Estimating the near-surface permafrost-carbon feedback on global warming. Biogeosciences, 9(2):649–665.

[Vonk et al., 2012] Vonk, J. E., Sánchez-García, L., van Dongen, B. E., Alling, V., Kosmach, D., Charkin, a., Semiletov, I. P., Dudarev, O. V., Shakhova, N., Roos, P., Eglinton, T. I., Andersson, a., and Gustafsson, Ö. (2012). Activation of old carbon by erosion of coastal and subsea permafrost in Arctic Siberia. Nature, 489:137–140.

[Vonk et al., 2015] Vonk, J. E., Tank, S. E., Bowden, W. B., Laurion, I., Vincent, W. F., Alekseychik, P., Amyot, M., and Billet, M. F. (2015). Reviews and syntheses : Effects of permafrost thaw on Arctic aquatic. Biogeosciences, 12:7129–7167.

[Wegner et al., 2015] Wegner, C., Bennett, K. E., de Vernal, A., Forwick, M., Fritz, M., Heikkilä, M., Łącka, M., Lantuit, H., Laska, M., Moskalik, M., et al. (2015). Variability in transport of terrigenous material on the shelves and the deep arctic ocean during the holocene. Polar Research, 34(1):24964.

[Wolfe et al., 2001] Wolfe, S. A., Kotler, E., and Dallimore, S. (2001). Surficial characteristics and the distribution of thaw landforms (1970 to 1999), Shingle Point to Kay Point, Yukon Territory. Technical report, Geological Survey of Canada, Open File.

[Woo, 1986] Woo, M.-k. (1986). Permafrost hydrology in North America. Atmosphere-Ocean, 24(3):201–234.

[Woods et al., 2011] Woods, G. C., Simpson, M. J., Pautler, B. G., Simpson, J., Lamoureux, S. F., and Lafrenie, M. J. (2011). Evidence for the enhanced lability of dissolved organic matter following permafrost slope disturbance in the Canadian High Arctic. Geochimica et Cosmochimica Acta, 75:7226–7241.

[Wu and Hung, 2016] Wu, Y.-H. E. and Hung, M.-C. (2016). Comparison of spatial interpolation techniques using visualization and quantitative assessment. In Hung, M.-C., editor, Applications of Spatial Statistics, chapter 02. InTech, Rijeka.

[Yoo et al., 2005] Yoo, K., Amundson, R., Heimsath, A. M., and Dietrich, W. E. (2005). Erosion of upland hillslope soil organic carbon : Coupling field measurements with a sediment transport model. Global Biogeochemical Cycles, 19.

[Zuur et al., 2007] Zuur, A., Ieno, E. N., and Smith, G. M. (2007). Analyzing ecological data. Springer Science & Business Media.